THE STRUCTURE OF THE KUROSHIO WEST OF KYUSHU

by

Changsheng Chen

M.S. Qingdao University of Oceanography
(1983)

Submitted in partial fulfillment of the
requirements for the degree of

Master of Science

at the

MASSACHUSETTS INSTITUTE OF TECHNOLOGY

and the

WOODS HOLE OCEANOGRAPHIC INSTITUTION

September 1989

Signature of Author .....

Joint Program in Physical Oceanography
Massachusetts Institute of Technology
Woods Hole Oceanographic Institution
August 8, 1989

Certified by .....

Robert Beardsley
Senior Scientist
Thesis Supervisor

Accepted by .....

Carl Wunsch
Chairman, Joint Committee for Physical Oceanography
Massachusetts Institute of Technology
Woods Hole Oceanographic Institution

THE STRUCTURE OF THE KUROSHIO WEST OF KYUSHU

by
Changsheng Chen

Submitted in partial fulfillment of the requirements for the degree of
Master of Science at the Massachusetts Institute of Technology
and the Woods Hole Oceanographic Institution
August 8, 1989

Abstract

A triangular CTD/ADCP survey was made across the Kuroshio west of Kyushu aboard the R/V Thompson during January, 1986 in order to investigate the water properties and flow field in the Kuroshio. A similar CTD survey was made in July, 1986 aboard the R/V Washington to study the seasonal variability in the Kuroshio.

The Kuroshio in this region exhibited a marked seasonal change in its near-surface stratification and water properties. In January, the Kuroshio water was separated from the vertically well-mixed coastal water over the shelf by a strong front located near the shelf break. Horizontal mixing between the Kuroshio and coastal water was observed but was limited near the shelf break. In July, surface coastal water extended far past the shelf break over the Kuroshio region near the surface, and in turn, Kuroshio water intruded onto the shelf near the bottom. Mixing between the Kuroshio and coastal water was found over much of the mid and outer shelf and upper slope, spanning a cross-stream distance of 75 km. In addition, evidence of deep vertical mixing within the Kuroshio itself was found near 32.0°N and 128.2°E., most likely due to internal tidal mixing over the slope.

Since Loran C navigation coverage in the study region was poor during the R/V Thompson cruise, a simple averaging technique has been used to convert the ADCP data into an absolute velocity. An error analysis shows that the total error in the absolute ADCP velocity was about ± 5 cm/s. The absolute geostrophic velocity using the absolute Doppler velocity at 60 m as the reference velocity was then calculated for the sides of the triangle. The results show that the ADCP velocity shear was in good agreement with the geostrophic shear in the Kuroshio. The Kuroshio flowed through the western section as a coherent current, then split into two streams around a tall seamount as it left through the eastern section. Some recirculation also occurred between the core of the Kuroshio and the slope as well as near the seamount. The geostrophic velocity field calculated relative to the bottom missed some of the important features of the true flow field such as splitting of the Kuroshio and the recirculation in the slope region.

The volume, salt and heat transports of the Kuroshio during the January 1986 survey have been calculated using the absolute geostrophic velocity and CTD data. The volume transport of the Kuroshio west of Kyushu in January 1986 was 31.7±2.0 Sv, which is comparable to that of the Gulf Stream in the Florida Strait. The volume transport through the triangle was conserved within measurement uncertainty, so that a streamfuction field can be defined by the transport. The resulting streamlines clearly show the structure of the flow field in the Kuroshio and its adjacent currents during the survey. The advective heat transport of the Kuroshio west of Kyushu in January 1986 was $28.2 \pm 1.8 \times 10^{14}\ W$. The salt transport in January 1986 was about $108.0 \pm 7.3 \times 10^{10}\ kg/s$, and the net salt flux was zero within measurement error.

Analysis of the potential vorticity based on the January 1986 absolute geostrophic velocity field shows that the total potential vorticity in the Kuroshio may be approximately given by the product of the vertical gradient of the potential density and the sum of the planetary and relative vorticities. The distribution of relative vorticity plays a significant role in determining the structure of the potential vorticity in the Kuroshio. The path of the Kuroshio can be traced in the field of potential vorticity. Facing in the direction of the current, the axis of the maximum velocity is located to the right of the core of maximum potential vorticity. Finally, the Kuroshio was potentially unstable since the gradient of potential vorticity changed its sign on potential density surfaces across the Kuroshio.

Thesis Supervisor:
Dr. Robert Beardsley , Senior Scientist
Woods Hole Oceanographic Institution

Contents

Acknowledgments

I would first of all like to thank my advisor Robert Beardsley for his patient guidance and encouragement, for many valuable discussions and for his constructive criticisms of this work. Also, I would like to thank him for his efforts in editing my early, poorly written thesis drafts. His deep insight into a wide range of ocean sciences and his imagination have been a great help to me.

I want to thank the members of my thesis committee, Dave Chapman, Glenn Flierl, John Toole and Paola Rizzoli, for their helpful comments and suggestions. Also, I wish to thank Carl Wunsch for his friendly help and encouragment. Discussions with him made me more confident with my work.

Conversations with John Toole, Richard Limeburner, Robert Weller and Terry Joyce, in particular, helped my understanding of the treatment of Acoustic Doppler Current Profiler data which has been discussed in this thesis. Robert Weller generously supplied me with a Fortran program, which was used to calculate the ship's positions from Loran C data. Richard Limeburner processed the CTD data and also gave me a great deal of help in the data analysis.

My thanks also go to Melinda Hall, who kindly provided many valuable references relating to potential vorticity analysis, and made useful suggestions about my analysis of the potential vorticity distribution in the Kuroshio. Discussion with Larry Pratt helped me to understand the dynamical processes associated with the potential vorticity field.

I thank Veta Green for her help in typing the first draft of my thesis. Ann-Marie Michael taught me how to use LaTex. The fancy format and good organization of my thesis would be impossible without her kind help.

The friendship and support of my fellow Joint Program students have been invaluable. Talking with my classmates David Walsh, David Chester and Kurt Polzin improved my command of the English language.

Finally, I thank my darling wife Huichan Lin for her patient support during the last three years, and for the promise of continued love and happiness in the future.

Chapter 1

Introduction

The Kuroshio is a strong current along the western boundary of the North Pacific Ocean, which originates along the east coast of the Philippines as the continuation of the North Equatorial Current and finally leaves the edge of the continental shelf at 35°N to become the North Pacific Current or the Kuroshio Extension (Nitani, 1972). As a part of the general circulation, the Kuroshio is responsible for the large poleward mass and heat transports which are essential to the mass conservation and the global heat balance in the North Pacific Ocean, as well as the dissipation of the large input of energy and vorticity due to the surface wind and heat fluxes. Therefore, in order to understand the general circulation of the North Pacific, it is important to know the structure of the Kuroshio and its quantitative contribution to the meridional mass and heat transports.

Study of the Kuroshio can be divided into two main aspects; observation and theoretical explanation. Much of the observational knowledge of the Kuroshio has been derived from hydrographic and direct current measurements. The first hydrographic measurements of the Kuroshio were carried out south of Japan by Kitaharo (1910) in which several sections were made to determine the structure of the water properties in the Kuroshio (Teramoto, 1972). Since then, a large number of systematic hydrographic surveys have been made from the beginning of the Kuroshio to the region of the Kuroshio Extension which have identified many important features such as the ba-

sic structure of the Kuroshio and its water properties (Stommel, 1972), the Kuroshio front near the shelf break (Nakao ,1977) and the mixing between the Kuroshio and coastal water (Nagata,1981). The first direct current measurements in the Kuroshio were made by Wada (1814) who used drift bottles to reveal the surface current pattern in the Kuroshio. The introduction of Geomagnetic Electro - Kinematography (GEK) in the 1950's allowed the first extensive measurement of the Kuroshio surface velocity field and its time variation, by which the bimodel behavior of the Kuroshio path, i.e., the existence of small and large meander states, was discovered south of Japan (Taft, 1972). Moored current observations obtained in the late 1970's and 1980's are beginning to describe the local time variability of the Kuroshio at several sites (Takemetsu et al., 1986). However, the combined use of the Acoustic Doppler Current Profiler (ADCP), accurate navigation and Conductivity-Temperature -Depth (CTD) data provides the best approach for mapping the Kuroshio velocity field. This technique has been successfully used in the Gulf Stream since 1979 (Pinkel, 1979; Joyce et al., 1982; Joyce et al., 1986), and first used in the Kuroshio in 1985 by Bryden et al (1987).

Few direct measurements of absolute mass transport have been made in the Kuroshio. In 1985, measurements of the Kuroshio transport were made southeast of Ryukyu Islands and in Tokara Strait with the ADCP by Bryden et al (1987). However, they failed to calculate the absolute geostrophic mass transport of the Kuroshio in the Tokara Strait because of poor navigation coverage. As a part of the World Ocean Circulation Experiment (WOCE), a program was proposed by Taira (1986) to measure the transport of the Kuroshio in Tokara Strait, Ize Ridge and off Cape Shionomisaki. It has been accepted as an important part of the Core-I program in WOCE. In addition, another program called the Kuroshio Exploration and Utilization Research (KER) was started in 1986 by Japan and China to study the seasonal and interannual variabilities of absolute transport of the Kuroshio. However, no papers have been published except one data report (see 1986 data report of KER).

Theoretical study of the Kuroshio has focused on explanations of its existence as a western boundary current and the mechanism causing the bimodality of the Kuroshio. Stommel (1948) first demonstrated that the western intensification depends crucially on the planetary vorticity gradient , while the bottom friction in the western boundary plays an important role in dissipating the input of momentum by the wind in the interior ocean (for a comprehensive discussion, see Pedlosky, 1979). Munk (1950) then developed a model of the western boundary layer in which the contribution of lateral friction to western intensification was emphasized. Despite the different forms of dissipation, both Stommel and Munk solutions emphasize the important role of friction in dissipating the input of vorticity by the curl of the wind stress. Fofonoff (1954) discovered a family of unforced, steady, undamped flow patterns based on the conservation of potential vorticity in which the inertial boundary layer was found. However , Fofonoff's free mode is not able to dissipate the input of vorticity which has been accumulated in the interior due to the wind stress, so that a closed contour of wind-driven circulation could not be obtained with his model. A combined viscous nonlinear model of a western boundary layer was numerically treated by Bryan (1963). He found that as the Reynold number is increased the center of the gyre migrates northward, the south western boundary current broadens, the north western boundary current intensifies, and then recirculation streamlines occur in the northern corner. Consequently, the transport increases from south to north to compensate for the countercurrents produced by nonlinearity. Similar results were also found by Veronis (1966a, 1966b) and Hendershott (1987). Even though these theories are not complete in many aspects, they indeed provided a simple explanation for the pattern of the general circulation, particularly in the western boundary layer.

Bimodality of the Kuroshio south of Japan, a large meander and a small meander states of the mean path of the Kuroshio, was first described by Taft (1972). Robinson and Taft (1972) attributed the bimodal behavior of the Kuroshio to the combined effects of the β-plane and the continental slope, and used an inviscid numerical model

to show these two types of steady current paths. White and McCreary (1976) suggested that the large meander state was a Rossby lee wave excited by the Kyushu coastal perturbation. Charney and Flierl (1981) suggested that the bimodality of the Kuroshio may be a case of multiple equilibria because a nonlinear eastward flow over multiple bottom topographies can produce non-unique steady solutions. The idea of Charney and Flierl was examined numerically by Chao and McCreary (1982) who simulated a bimodal model Kuroshio using the Kyushu coastal perturbation and the Izu Ridge topography. Their model results demonstrated that the dynamics of meander formation involve the interaction of a Rossby lee wave generated by the Kyushu Peninsula and a westward propagating disturbance forced by the Izu Ridge. The model Kuroshio, however, deviated considerably from the observed paths. Chao (1984) developed a barotropic model in which the combined effects of the β-plane, the Kyushu coastal perturbation, the Izu Ridge and the SW - NE coastline orientation were taken into account. Chao found that this model successfully simulated the bimodality of the Kuroshio in good agreement with the observed paths. In addition, the numerical models mentioned above show that the meander of the Kuroshio was related to the upstream transport, such that the large meander occurred at the time of low transport.

However, despite recent progress in observational and theoretical studies, there still exist many unanswered questions about the Kuroshio. What is the absolute volume transport of the Kuroshio and how does it change seasonally? Where does the mixing between the Kuroshio and coastal water occur and how does it change with time? Is there vertical mixing within the Kuroshio? What does the three dimensional structure of the Kuroshio look like? How does the topography affect the path of the Kuroshio? Is the geostrophic approximation good in the Kuroshio? What does the potential vorticity field look like? Is potential vorticity conserved in the Kuroshio?

This thesis describes the results of two hydrographic surveys of the Kuroshio conducted in 1986. The first survey conducted January 8 to February 1 1986 aboard

the R/V Thompson covered the Yellow and East China Seas including the Kuroshio region west of Kyushu (see Figure 1.1). Both the CTD and ADCP data were recorded during this survey. The salinity data obtained on this survey exhibited some scatter and horizontal deviation from station to station in the Kuroshio attributable to conductivity noise and sensor drift. To correct these problems, the salinity data were smoothed at each station as a function of depth with a low pass filter, and then the smoothed salinity data were compared with concurrent Japanese Meteorological Agency bottle data to minimize the horizontal deviation error (a full discussion of this procedure is found in Appendix A). The resulting CTD and ADCP data have been used to examine the water property field and compute absolute geostrophic velocities. The second survey conducted July 4 to 20 1986 aboard the R/V Washington repeated many of the Thompson sections (see Figure 1.2), however, only CTD data were obtained.

Our primary interest here is to describe and understand the structure of the Kuroshio west of Kyushu. Thus, most of this work will focus on the two triangle sections made across the Kuroshio centered near 31°N, 128°E. This is an interesting and dynamically important oceanographic region in many respects. First, the Kuroshio enters the Tokara Strait through this region and then increases significantly in its transport south of Japan. Thus, from the dynamical point of view, this region is most similar to the Florida Strait in the Gulf Stream system. Second, past theoretical studies suggest that the Kyushu coast is one perturbation source for the bimodality of the Kuroshio south of Japan so that knowledge of the detailed structure of the Kuroshio in this region may be helpful to understand better the meandering of the Kuroshio. Third, the study region is connected to the wide shelf region of the East China Sea so that the interaction between coastal and Kuroshio water may be significant. Finally, the bottom topography west of Kyushu is quite complex and may have a strong influence on the pattern of flow in the Kuroshio.

This thesis consists of five chapters. In Chapter 2, the horizontal and vertical structure of water properties in the Kuroshio and the adjacent East China Sea shelf region are described. The Kuroshio in the study region exhibited a significant seasonal change in its near-surface stratification and water properties between January and July, 1986. In January, the Kuroshio was separated from the vertically well mixed coastal water on the shelf by a strong front located at the shelf break. Horizontal mixing between the coastal and Kuroshio water was observed but was limited to near the shelf break. In July, the coastal water extended far past the shelf break over the Kuroshio region near the surface, and, in turn, Kuroshio water intruded onto the shelf near the bottom. As a result, mixing between the Kuroshio and coastal water was found from the shelf to the Kuroshio. In addition, evidence of deep vertical mixing within the Kuroshio itself was found near 32.0°N, 128.2°E. Some suggestions are made to explain the existence of such intense mixing.

In Chapter 3, I first calculate the geostrophic velocity field relative to the bottom to estimate seasonal variability in the current structure of the Kuroshio and the coastal flow from winter to summer. Then, since Loran C navigation errors were large in the study region during the winter cruise, a simple averaging technique has been developed to estimate the absolute ADCP velocity normal to the CTD transect, and an analysis of the corresponding errors show the total uncertainty in the absolute ADCP velocity to be about ± 5 cm/s. The absolute ADCP velocity at 60 m between station pairs was then used as the reference level velocity to compute the absolute geostrophic velocity for all sides of the triangle except in the inner shelf region where 10 m was chosen as the reference level. The results show that the ADCP velocity shear was in good agreement with the geostrophic shear. The Kuroshio flowed through the western section as a coherent current, then split into two streams around a tall seamount as it left through the eastern section. Some countercurrents also occurred between the core of the Kuroshio and the slope as well as near the seamount. The geostrophic velocity

calculated relative to the bottom missed some of the important features of the true flow field such as the splitting of the Kuroshio and the recirculation in the slope region.

In Chapter 4, the winter CTD data and computed absolute geostrophic velocity fields allow the direct calculation of the volume, salt and heat transports in the Kuroshio during January 1986. The resulting poleward volume, salt, and heat transports were 31.7± 2.0 Sv, $108.0 \pm 7.3 \times 10^{10} kg/s$, and $28.2 \pm 1.8 \times 10^{14}\ W$. The volume transport through the triangular domain was conserved within measurement uncertainty, so that a streamfuction field can be defined by the transport. The resulting streamlines clearly show the structure of the flow field in the Kuroshio and its adjacent currents.

In Chapter 5, the structure of the potential vorticity of the Kuroshio as a dynamical quantity is described using the January R/V Thompson data. A scale analysis is first presented to find the dominant contribution to potential vorticity in the Kuroshio. Then three potential vorticity sections are presented. The results show that the total potential vorticity in the Kuroshio may be approximately given by the product of the vertical gradient of the potential density and the sum of the planetary and relative vorticities. The distribution of relative vorticity played a significant role in determining the structure of potential vorticity in the Kuroshio. The path of the Kuroshio in the study triangle could be traced with the core of maximum potential vorticity. Finally, the Kuroshio was potentially unstable since the gradient of potential vorticity changed sign on a potential density surface across the Kuroshio.

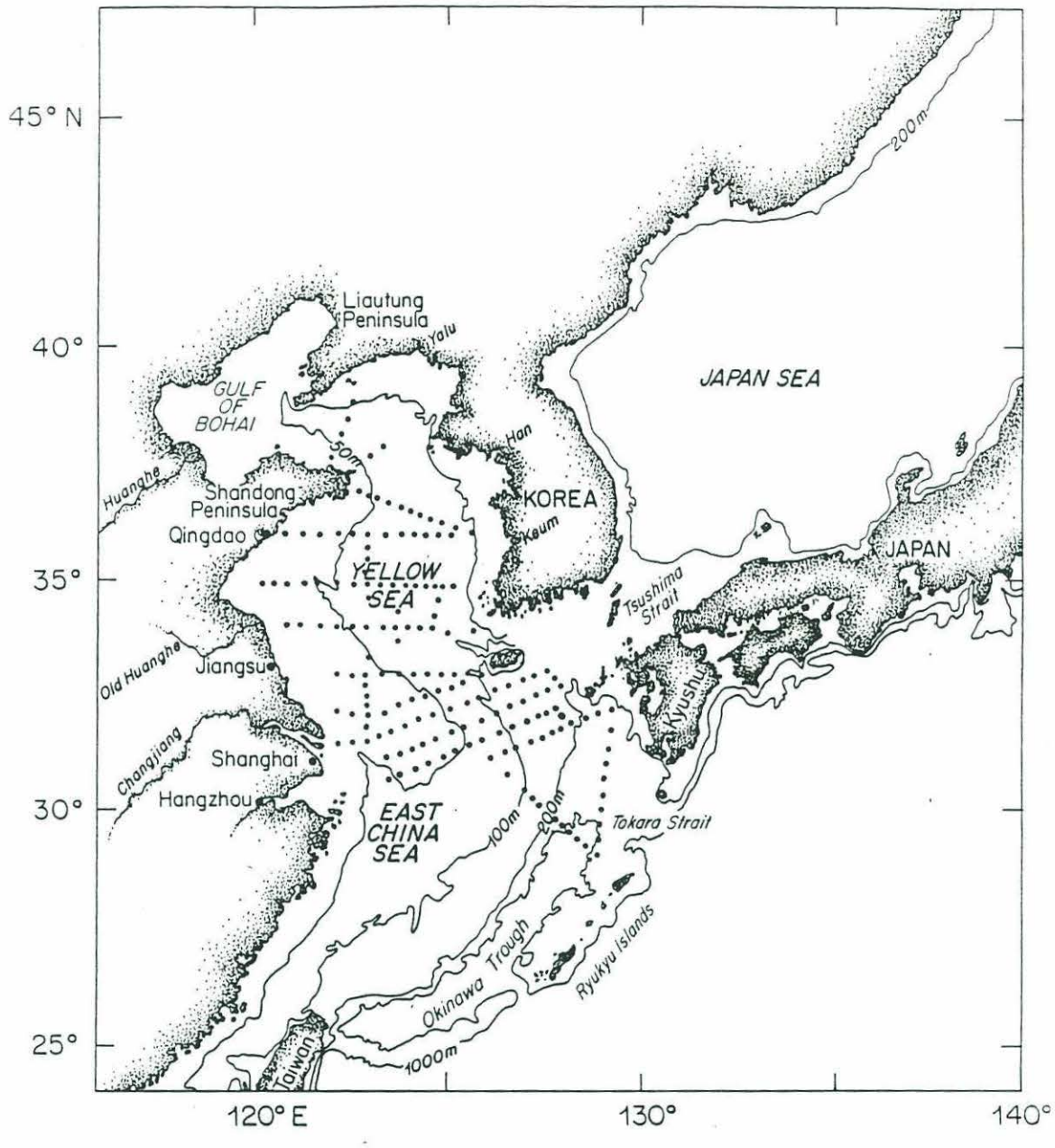

Figure 1.1: CTD stations during the R/V Thompson cruise, January 8 to February 1, 1986.

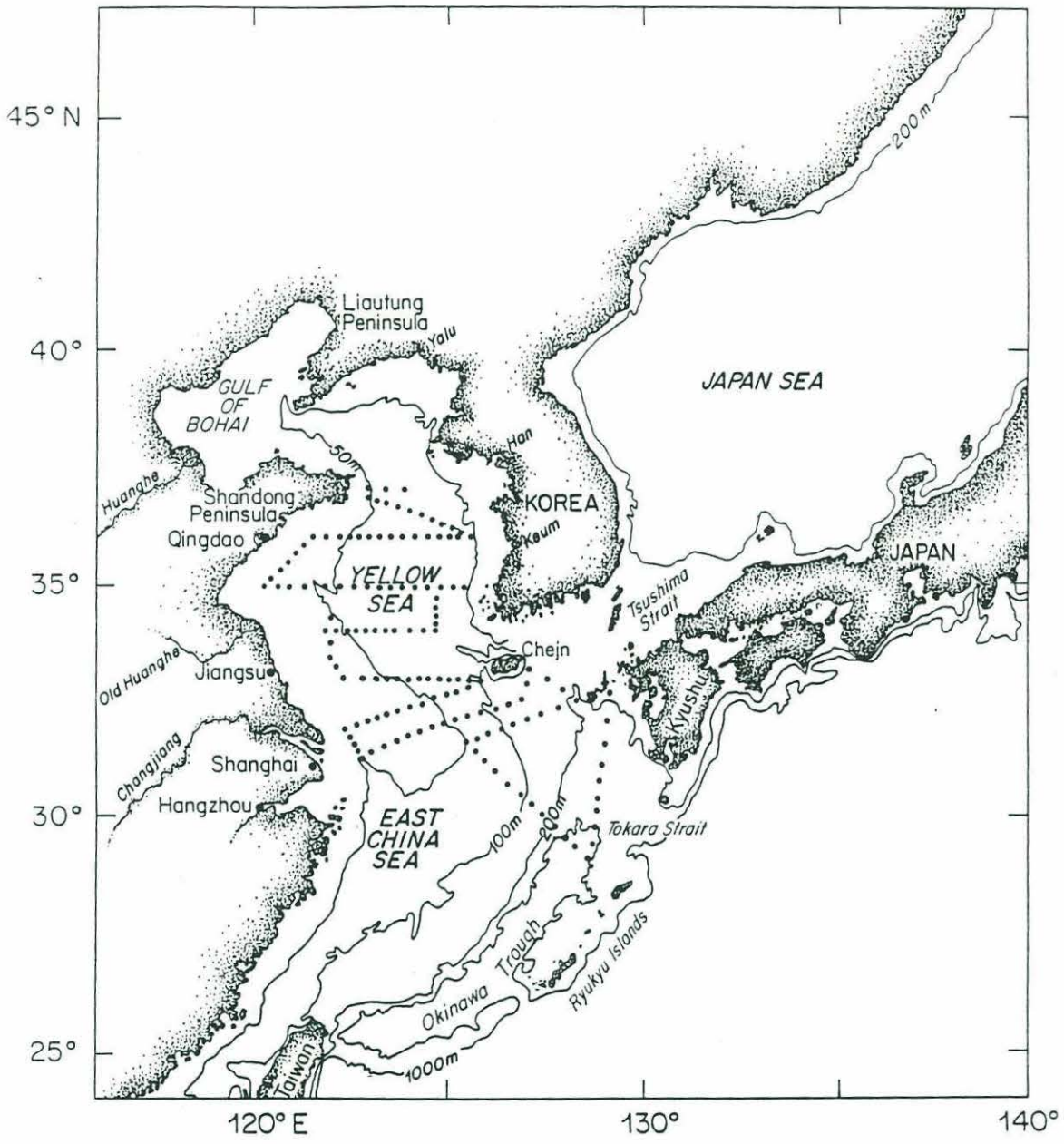

Figure 1.2: CTD stations during the R/V Washington cruise July 4- 20, 1986.

Chapter 2

The Seasonal Structure of Water Properties in the Kuroshio and Adjacent East China Sea

2.1 Introduction

It is well known that the Kuroshio enters the East China Sea from the east of Taiwan and flows northeastward along the edge of the continental shelf over the Okinawa Trough with a strong frontal zone between the warm high salinity Kuroshio water and the low salinity East China Sea water (Stommel, 1972). Miyazaki and Abe (1960) showed the existence of Kuroshio water over the bottom of the continental shelf west of Kyushu and low salinity coastal water on the surface of Kuroshio in summer. Nakao (1977) described the vertical structure of salinity in the summer of 1967 on a section north of Taiwan, indicating a front between Kuroshio water and Yellow Sea Cold Water. Nagata et al.(1981) found that coastal water in the bottom layer on the shelf flowed down along the isotherms between 17°to 18°C and spread into the Kuroshio around a depth of 250 m in May 1973, suggesting one mixing mechanism between Kuroshio and coastal water. Park (1985) discussed another possible mixing process at the front south of Cheju Island using 1977 summer hydrographic data, and suggested that the Asia monsoon winds, which are mainly southerly during the summer season, are responsible for the eastward advection of low salinity water in the East China Sea through Ekman transport. The mixing occurs when the East China Sea low salinity

water meets Kuroshio water on the slope region. The mechanism Park implied does not seem reasonable because eastward advection of the low salinity water still exists in winter during the winter northerly and northwesterly winds (Nakao, 1977). Beardsley et al (1983) described 1981 summer hydrographic measurements from the Changjiang River mouth to the Kuroshio and pointed out that water structure over the shelf in the East China Sea during early summer is dependent on three major influences, advection of warm, saline Taiwan Current Water from the southwest, advection of cooler, less saline Yellow Sea Cold Water from the north, and the fresh water discharge of the Changjiang River. Despite these earlier studies, the following questions remain unanswered. How does the Kuroshio water influence the water structure on the shelf? Where does the low salinity water near the Kuroshio surface come from? How is the front formed over the shelf break and what kind of mixing can happen there? Finally, is there a seasonal change in the interaction between Kuroshio and coastal water?

The hydrographic data from the two regional cruises undertaken in the winter and summer of 1986 aboard the R/V Thompson and the R/V Washington provide quasi-synoptic, high vertical and horizontal resolution snapshots of the distribution of water properties in the East China Sea and Kuroshio regions. Based on these two surveys plus some concurrent Japanese hydrographic data, the seasonal structure of the Kuroshio and coastal water properties will be discussed. To begin, the regional circulation and sources of fresh water are reviewed in Section 2.2. In Section 2.3, the horizontal distribution of water properties and their seasonal variation are described in more detail. Then the cross-stream water structures, including the classification of water masses, horizontal mixing near the Kuroshio front, and vertical mixing within the Kuroshio water, are discussed in Section 2.4. Finally, conclusions are given in Section 2.5.

2.2 Regional Circulation and Sources of Fresh Water

Circulation: A schematic of the surface circulation pattern in the Yellow and East China Seas is shown in Figure 2.1. The Kuroshio enters the East China Sea through the passage east of Taiwan at 24°30' N, 123 °20' E, and flows northeastward along the continental slope. It leaves the East China Sea southwest of Kyushu and subsequently flows along the south coast of Japan. Inshore of the Kuroshio, a warm saline current called the Taiwan Warm Current (TWC) also flows northeastward, but unlike the Kuroshio which flows offshore to the south of Japan, part of the TWC flows into the Japan Sea through the Tsushima Straits between Korea and Japan as the Tsushima Current. The other part of the TWC flows intermittently northward into the Yellow Sea along the Korean coast.

The semi-enclosed Yellow Sea is characterized by northward inflow of saline water along the Korea coast (the Yellow Sea Warm Current or YSWC) and outflow of less saline water along the northeast coast of China (the Yellow Sea Cold Current or YSCC). In winter, some southward-flowing coastal water along the coast of Jiangsu Province continues southward along the coast of Zhejiang Province, and some Jiangsu coastal water (the Jiangsu Coastal Current or JCC) flows offshore in a downwind, southeastward direction from a point just north of the mouth of the Changjiang. Between the nearshore southward-flowing and the offshore southeastward- flowing coastal waters, a northwestward inflow of the relatively saline TWC is found in the submerged river valley located just onshore of the Changjiang mouth (the relic river valley is defined primarily by the 40 m and 50 m isobaths; Butenko et al, 1985). This inflow is the source of the near bottom saline water found in the outer Changjiang estuary and is a dominant circulation feature of the East China Sea in both winter and summer.

The summer circulation pattern in the East China Sea is basically similar to the winter pattern except for the effect of the increasing Changjiang discharge. A detail discussion will be given next.

Sources of Fresh Water: Local sources of fresh water in the Yellow and East China Seas include the river discharge and the net precipitation over evaporation.

The Changjiang originates in the Tibetan high plateau and flows more than 6000 km through ten provinces of China before draining into the East China Sea near Shanghai. In terms of volume discharge, the Changjiang is the largest river in Asia and the fifth largest in the world, while the other major rivers which drain into the Yellow and East China Seas are one or two order of magnitude smaller (see Table 2.1). Therefore, the Changjiang is the single most important source of fresh water discharging into the Yellow and East China Seas.

Figure 2.2 shows the mean seasonal variation of river discharge measured at Datong, 400 km upstream from the Changjiang river mouth (Yang et al., 1982). The mean monthly Changjiang discharge ranges from about $1 \times 10^4\ m^3/s$ in winter to more than $5 \times 10^4\ m^3/s$ in summer. The peak monthly discharge occurs in July and minimum value is in January. Such an annual discharge variation is due to the monsoonal climate over eastern China where rainfall increases during the summer, and to a lesser degree to the spring melting of the winter snow pack.

The effect of the river discharge on the stratification and circulation in the East China Sea has been examined by Beardsley et al.(1983). They found that the spring and summer discharge of the Changjiang is large enough to form a surface plume of relatively fresh water which can extend at least 300 km out over the shelf. Part of this discharge flows south along the Chinese coast as the Changjiang Coastal Current. They also concluded that the buoyancy flux of the Changjiang is locally larger than the amount of vertical mixing due to tidal dissipation so that a stratified surface plume

exists even over the inner shelf where tidal currents are strongest. In winter, the much weaker Changjiang discharge flows primarily southward in a narrow band confined to the Chinese coast.

Table 2.1: Fresh water sources in the East China and Yellow Seas

rivers ($10^3\ m^3/s$)	annual mean	minimum	maximum	reference
Changjiang	20.0	10.0 (Jan)	50.0 (July)	Yang et al, 1983.
Yellow	0.9	0.5 (Feb)	2.0 (Sept)	Qin et al, 1983
Yalu	1.1	0.6 (April)	1.6 (July)	Schubel et al, 1984
Han	0.8	0.1 (Jan)	3.2 (July)	,, ,, ,,
Keum	0.2	0.03 (Jan)	0.5 (June)	,, ,, ,,

Estimate of net influx of fresh water due to rainfall can be made by subtracting evaporation from precipitation. Wyrtki (1966) calculated the mean heat exchange at the surface of the Pacific Ocean based on the climate data from ship's weather reports during 1947 to 1960. Using his monthly evaporation map, I roughly estimate the mean monthly evaporation rate in the East China Sea. The results show that the mean monthly evaporation ranged from about 2.6 cm/month in July to 23.4 cm/month in January. The mean annual evaporation is about 146.3 cm/year. There are few direct observations of precipitation in the East China Sea. However, since the percent frequency of rainfall is almost parallel to latitude in that region between the east Chinese coast and Kyushu[1], we can choose a land weather station on the east Chinese coast as a representative to estimate roughly the monthly precipitation over the sea. Shanghai, a weather station close to the East China Sea and with a rather large rainfall, was thus chosen to calculate roughly a maximum monthly precipitation rate. The 60 year data reports from 1912 to 1972 (Wernstedt,1972) show that the annual precipitation was

[1]U.S. Navy Marine Climatic Atlas of the World, Volume 11, North Pacific Ocean.

about 112.1 cm/year. The monthly maximum rainfall was about 17.8 cm/month in June, and the minimum value was 3.5 cm/month in December. Monthly variation of precipitation and evaporation is also shown in Figure 2.3. It indicates a large net influx of fresh water in summer from April to September which is approximately balanced by considerable evaporation in the rest of the months, so that there is no net fresh water flux into the East China Sea. Based on the above statistical analysis of over ten years, we could say that annual net influx of fresh water due to air-sea exchange rainfall is too small to provide a large fresh water in the East China Sea. The discharge of the Changjiang River is the single main source of fresh water there.

2.3 Horizontal Distribution of Water Properties

Long CTD sections covering much of the Yellow and East China Sea were made along the transects shown in Figures 2.4 and 2.5 in January and July, 1986 aboard the R/V Thompson and R/V Washington, respectively. Because our surveys did not cover the southwestern part of the East China Sea, bottle data[2] obtained on the Japanese R/V Chafu Maru and Royat Maru during January and July 1986 respectively have been used to extend our analysis and provide high quality hydrographic measurements in the Taiwain Warm Current and the Kuroshio upstream of our triangle study area. To illustrate the horizontal distributions of water properties, maps of properties at 4 m (called the surface) and at the bottom or 100 m, whichever is shallower, are described next. Since our primary interest here is to describe the seasonal variability of the Kuroshio, most of this section will focus on the triangle region.

January 1986: Figures 2.4 and 2.5 show the January surface (4 m) and bottom (100 m) distributions of temperature, salinity and sigma-t, respectively. The surface salinity and temperature distributions showed that the highest salinities and tempera-

[2]The Result of Marine Meterorological and Oceanographical Observation No. 78, January–December, 1986.

tures (greater than 34.4°/$_{oo}$ and 19°C which are characteristics of the Kuroshio water) were located in the southeast of the study area. The 34.4°/$_{oo}$ isohaline laid roughly along the 200 m isobath so that the inner boundary of the Kuroshio water at the surface was located near the shelf break. Intermediate salinity and temperature water types associated with the TWC and YSWC were found to the northwest of the Kuroshio and the west of Korea. Between the TWC and YSWC was the YSCC which was characterized by the relatively cool and less saline tongue flowing from northwest to southwest toward the shelf break. The very fresh and cool water ($S < 31°/_{oo}$ and $T < 6°C$) along the Chinese coast north of the Changjiang river mouth was associated with the JCC. The bottom (100 m) salinity and temperature distributions showed a very similar structure to the surface maps. This implies that the shelf water in this region during January is vertically well-mixed, due in part to strong wind and tidal mixing and surface cooling (Nakao, 1977; Beardsley et al, 1985).

Where did the mixed shelf water in January come from? Since the Changjiang discharge is too weak during winter to force fresh water directly to the shelf break (Yang et al, 1983), two possible sources of shelf water over the outer shelf were the YSCC and TWC. Nakao (1977) indicated that the YSCC was characterized by low salinity ($S < 33°/_{oo}$) and low temperature ($T < 8°\ C$ in winter, and $T < 11°\ C$ in summer). Beardsley (1983) showed that the YSCC was recognized by temperatures of 8°-17° C and salinity of 31-34°/$_{oo}$ in summer. Park (1985) also found that the YSCC in the summer of 1977 was defined by water of extremely low temperature ($T < 12°\ C$) and low salinity ($S < 33.5°/_{oo}$). Since the change of the salinity characteristic of YSCC is less than that of temperature in the different definitions, we may use a isohaline to define the boundary of the YSCC. If we regard the isohaline of 34°/$_{oo}$ as the boundary of YSCC in January, we can conclude on the basis of the horizontal distributions of salinity shown in Figures 2.4 and 2.5 that in January 1986 there was no direct intrusion of YSCC to the shelf break where the Kuroshio was located. Most of the shelf water in the triangle area must be the TWC water. Beardsley et al. (1983) discussed the T/S

characteristics of YSCC and TWC waters and found the existence of lateral mixing between these two water masses. Therefore, the well-mixed water located on the outer continental shelf was possibly a mixture of YSCC and TWC.

July 1986: Figures 2.6 and 2.7 show the July surface (4 m) and the bottom (100 m) distributions of temperature salinity and sigma-t , respectively. The seasonal increase in solar heating caused the high surface water temperature. The Kuroshio can be recognized by the maximum temperature core at the south corner of the triangle. Inshore of the Kuroshio, the TWC is traced in the southeast of the study area by the large temperature gradient.

Increasing discharge of the Changjiang causes less saline water to flow both northwest toward Cheju Island (which can be recognized as the bubble or lens of Changjiang dilute river water located near the west of Korea) and southward along the Chinese coast. It is thus latter flow which must in part be responsible for the very large layer of less saline water formed over the shelf and inner Kuroshio. A simple scaling analysis may help us to determine this. The total discharge of the Changjiang from January to the end of July from Figure 2.2 amounts to about $4.8 \times 10^{11}\ m^3$. If this is drained into the East China Sea, an area of about $2.9 \times 10^{11}\ m^2$, the sea would be covered with 1.7 m fresh water. This is a very big number. Similar calculation of net evaporation (E) and precipitation (P) based on the data from Wyrtki (1966) and Wernstedt (1972) shows that local precipitation is almost balanced by evaporation during these seven months. Therefore, we conclude that the increased discharge of Changjiang is responsible for the observed low salinity surface distribution over the shelf and in the Kuroshio.

Limeburner et al (1985) used July 1981 CTD data to describe the T/S characteristics in the East China Sea and found mixing between the Changjiang discharge, the TWC, and YSCW during summer. Since the hydrographic structure in this region of our July 1986 survey is similar to the 1981 July data, we suggest that the shelf

water formed in the triangle region consist of the mixed water of three currents. For convenience, we will refer to this mixed water as Coastal Water.

2.4 Cross-stream Water Structure

Water Properties of the Kuroshio

January 1986: The vertical distributions of temperature, salinity and sigma-t on three transects (two of them across the Kuroshio) are shown in Figures 2.8 - 2.10. The corresponding T/S diagrams for these transects are given in Figure 2.11. Near the surface is found the Kuroshio Surface Water (Nakao, 1977), which exhibits considerable scatter on the T/S diagram due to atmospheric variability. Tropical Water, characterized by a salinity maximum, formed at the surface of the Subtropical North Pacific by excess evaporation over precipitation in winter, and advected northward by the Kuroshio (Masuzawa, 1964), is found in both western and eastern sections. The maximum salinity at the core of the Tropical Water exceeds $34.8°/_{oo}$ at about 250 m depth on stations 126-127 on the western section, and 127-128 on the eastern section: the corresponding temperature is about 20°C. Defined by temperature 18°C-21°C and salinity more than $34.8°/_{oo}$ the thickness of the core of Tropical Water is about 100 m, covering the depth range from 200 m to 300 m. In the range from 18°C to 10°C and $34.4°/_{oo}$ to $34.8°/_{oo}$, the T/S relation is nearly linear, and temperature and salinity exhibit local maximums of vertical gradient. This water is called Central Water (Sverdrup et al., 1942) or Thermocline Water (Masuzawa, 1964). The average depth of the Central Water can be defined by the axis of maximum gradient of temperature which, in general, increases from the shelf break toward the open ocean. At stations 126-127, the Central Water is found from 300 m to 600 m with a average depth about 450 m. At station 123 on the upper slope, the average depth is about 150 m and the thickness ranges from 150 m to 350 m. Below the Central Water is found North Pacific

Intermediate Water, which is formed in subarctic regions (Reid, 1965) and is recognized by its vertical salinity minimum of about 34.36°/$_{oo}$ near 8°C. If we define this water by salinity less than 34.4°/$_{oo}$ and temperature between 6°and 10°C, then it is clear that Intermediate Water occupies much of the deep Kuroshio in the East China Sea. Near the bottom is the North Pacific Deep Water (Pickard, 1979), which is characterized by more uniform properties with depth (see Figures 2.8 and 2.9). As mentioned before, the large scatter in the deeper T/S relationship in the Central Water, Intermediate Water and Deep Water was due to conductivity noise in the CTD data. The original CTD data were smoothed and compared with concurrent Japanese bottle data and adjusted to minimize the salinity errors. A full discussion of this correction procedure is found in Appendix A.

July 1986: Figures 2.12 - 2.14 show vertical sections of temperature, salinity and sigma-t on the three July 1986 transects, and the T/S diagrams for these transects are shown in Figure 2.14. Seasonal increases in solar heating, Changjiang discharge and net precipitation result in the highly stratified structure of water properties in July 1986. The Surface Water of the Kuroshio had warmed 6°C from the Janaury survey and contained water of less than 34°/$_{oo}$. Tropical Water can be traced by the salinity maximum in the upper ocean at station 140 to the shelf break at station 136, with the salinity maximum decreasing from the trough to the shelf break. The core of the Tropical Water at station 140 with a salinity of 34.83°/$_{oo}$ and a temperature greater than 21°C was located at a depth of about 200 m, 50 m shallower than in January. At station 136 at the shelf break, the core was located at a depth of 100 m with a maximum salinity of only 34.75°/$_{oo}$ and a temperature of 18.8°C. The Central Water (Thermocline Water) defined by temperature between 10°C - 18°C and salinity from 34.36°/$_{oo}$ to 34.74°/$_{oo}$, had intruded onto the shelf. The 34.4°/$_{oo}$ isohaline, which was limited to the shelf break in January, reached station 134, 190 km northwest from the slope. Also the 18°C isotherm, which intersected the sea surface on the slope in January, had been overlaid everywhere by the seasonal thermocline water in July. The

25.5 isopycnal surface intersected the bottom on the slope rather than the sea surface as in January. In turn, the less saline Coastal Water extended from the shelf over into the Kuroshio near the surface, helping to create a highly stratified surface layer. There was little change in the Intermediate Water and Deep Water from January to July since both were too deep to be simply affected by the local atmospheric factors and intrusion of fresh water from the rivers.

Evidence of Mixing Processes Near the Kuroshio Front

January 1986: The January 1986 western transect (Figures 2.8 and 2.9) clearly showed near the shelf break the Kuroshio front between the relatively well-mixed cooler less saline shelf water and the warmer, more saline Central Water of the Kuroshio. Since the temperature and salinity gradients tended to compensate each other near the shelf break, the horizontal density gradient in this front was relatively weak (Figure 2.10). The T/S diagrams at the stations near the front (Figure 2.11) indicated the different mixing processes that occurred between these two water masses. At station 122 over the shelf break, the sharp bend in the T/S curve from the surface to bottom indicated mixing among three different water masses: 1) Kuroshio Surface Water with a salinity larger than 34.74°/$_{oo}$ and temperature of about 21.2°C; 2) Coastal Water with a salinity of 34.36°/$_{oo}$ and temperature of 16°C, and 3) Central Water with a salinity greater than 34.43°/$_{oo}$ and temperature of about 11.8°C. At station 123, 15 km offshore from the shelf break, mixing was observed between the Kuroshio Surface Water at the salinity of about 34.74°/$_{oo}$ near 21°C and Central Water with a salinity of 34.64°/$_{oo}$ near 15°C. A similar phenomenon was also seen at station 124, 45 km onto the shelf from the shelf break. Small scale bends in the T/S curves at stations 123 and 124 near 34.6°/$_{oo}$ and 18°C implied the influence of the mixed water over the shelf break (i.e., at station 122). At station 121, 30 km onto the shelf from the shelf break, the linear T/S curve indicated mixing between the coastal water with a salinity of 34.13°/$_{oo}$ and the temperature of 14.2° and the more saline and warmer mixed water at station 122. Over the mid and

inner shelf, the Coastal Water tended to be more well-mixed vertically, and there was no evidence to show any direct influence of the Kuroshio.

July 1986: The July 1986 western transect (Figures 2.12 and 2.13) clearly showed the spreading of coastal water over the Kuroshio at the surface and the intrusion of Kuroshio Central and Tropical Water over the shelf break in July. Evidence of mixing between these water masses was more obviously found in the T/S diagrams (Figure 2.15). The T/S curves at stations 136-138 from the shelf break to the center of Okinawa Trough indicated mixing between the less saline and warmer Surface Water ($S < 34°/_{oo}$ and $T > 28°C$) and the upper Tropical Water with a salinity less than $34.8°/_{oo}$ and the temperature greater than 20° C. As a result, the maximum salinity and the corresponding temperature of the Tropical Water were reduced to $34.7°/_{oo}$ and 19.6 °C, $0.12°/_{oo}$ fresher and 2° C cooler than those at stations 139-140. At the shelf station 135, 37 km onto the shelf from the shelf break, the T/S curve showed the minimum salinity core of $34.3°/_{oo}$and 19.6°C at the depth of about 80 m, and it went down linearly to $34.44°/_{oo}$ and 17.8°C, and up to $34.52°/_{oo}$ and 23°C, implying mixing among the less saline Coastal Water, Central Water and Kuroshio Surface Water. Mixing between Coastal and Central Waters was still observed on station 134, 75 km onto the shelf from the shelf break. The influence of Kuroshio water disappeared at station 133, 113 km inshore from the shelf break. There mixing was found between the TWCW with a salinity of $34.25°/_{oo}$ and temperature of 17°C and the YSBCW ($S < 33.7°/_{oo}$ and $T < 14.5°C$).

The T/S curves for the eastern transect were very similar to those on the western transect from station 134 to 140, implying that the less saline surface water comes from the mixed Kuroshio and Coastal Water. In other words, the relatively fresh Coastal Water over the mid and inner shelf (inshore of station 134) can not flow directly to the eastern section. However, the trace of this water can be found on the northern transect

through the similarities of the T/S curves on both the western and northern sections. This also meant that the mixed Coastal Water intruded further north in July 1986.

Vertical Mixing in the Kuroshio

Indirect evidence for vertical mixing within the deeper Kuroshio can be found in the T/S curves of stations 135-138 in January. These stations exhibited nearly straight T/S curves in the deep water , implying mixing of Central Water and Intermediate Water over the range of salinity 34.6°/$_{oo}$ and temperature 14.5°C to salinity 34.4°/$_{oo}$ and temperature less than 6°C such that water beneath about 200 m at these stations consists of this mixture. Similar T/S diagrams were found in the concurrent Japanese bottle data, strengthening our conclusion that vertical mixing was occurring at that time.

What mechanism do we think can be causing this vertical mixing? The map of streamfunction on an isopycnal surface (see Chapter 4) indicated that part of the Kuroshio water was recirculated toward the slope through the eastern section. The mixing occurred only when the recirculated water left the slope and turned anticyclonically to the interior ocean. The bottom topography must be expected to be important for the mixing. Wunsch (1969) discussed progressive internal waves on a slope and pointed out that internal waves could be reflected up, back or along the slope according to the relative magnitude of the wave trajectory angle and the slope of the boundary. Overturning associated with these processes could produce the mixed water which propagates into the interior along the slope. Since the process of vertical mixing in our case is very similar to that in Wunsch's theory, we can guess that small scale vertical mixing could be taking place over many depths due to internal wave reflection and finally a large mixing band could be formed vertically within the Kuroshio northeastern part of the triangle.

In addition, we can see from the topography map that there are some rough batymetric features in that region. Small scale eddies might be generated when the fluid passes these structure. Mixing associated with eddies is another possible mechanism for creating the mixed T/S curve in that area.

The Richardson number, $R_i = N^2/\ (\frac{dv}{dz})^2$, is a stability parameter for stratified shear flow. If the vertical shear of horizontal velocity is large enough to overcome the effects of stratification, the flow can be unstable and lead to the turbulence. Theoretically, the critical value is 0.25. When $R_i < 0.25$, turbulence may develop, and when $R_i > 0.25$, the flow is stable to infinitesimal perturbations. Using geostrophic velocities and density to estimate the shear instability in the study area, we found that R_i was much larger than 10. This means that the geostrophic flow was stable and the turbulence due to shear flow was very weak there. However, the mixing process associated with turburence in our case is a small scale problem which had already been filtered in the geostrophic field. Therefore, the vertical shear of mean flow estimated with geostrophic velocities does not reflect whether or not the small scale motion in the study region is unstable. The shear spectrum with respect to vertical wave number K is flat for wavelengths larger than 10 m and cascades like K^{-1} for smaller wavelengths. Therefore, root mean squared shear, which is given by the integral of the shear spectrum, is strongly affected by small scale shear.

We can crudely estimate the magnitude of salt eddy diffusion using a simple model. Let's model the salinity profile in the T/S curve as

$$S(z,t) = -C(t)\ \sin\frac{\pi z}{H} + S_o \qquad (2.1)$$

where $C(t) = \Delta S$ at $t = 0$ and zero at $t \rightarrow \infty$. H is the vertical scale. S_o is the constant background salinity (see Figure 2.16).

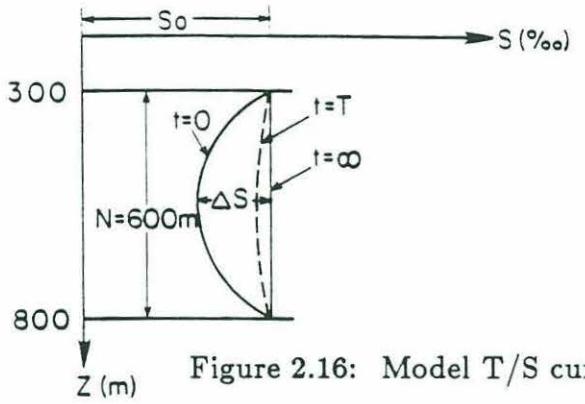

Figure 2.16: Model T/S curve.

In the absence of horizontal diffusion and advection, the salt diffusion equation can be given as

$$\frac{\partial S}{\partial t} = K_s \frac{\partial^2 S}{\partial z^2} \tag{2.2}$$

where K_s is the salt eddy diffusivity.

Substituting (2.1) into (2.2) yields,

$$\frac{\partial C(t)}{\partial t} = - K_s \frac{\pi^2}{H^2} C(t), \tag{2.3}$$

and then,

$$C(t) = \Delta S \; exp(-K_s \frac{\pi^2}{H^2} t). \tag{2.4}$$

Let $t = T$ be the time scale of vertical mixing. Then, the order of the salt eddy diffusivity can be estimated by

$$K_s \sim \frac{H^2}{T\,\pi^2}.$$

Since the mixed water comes from the countercurrent on the eastern section (see Chapter 4), one could roughly calculate the time scale using the velocity of the parcel to divide the distance between the countercurrent and the mixed water. Such a crude estimate gives

$$T \sim \frac{1.1 \times 10^5\ m}{0.3\ m/s} \sim 3.7 \times 10^5\ s.$$

And also H=600 m, so,

$$K_s \sim \frac{3.6 \times 10^5}{3.7 \times 10^5 \times 9.9} = 0.1\ (m^2/s)$$

Moreover, if we consider a curvature path of recirculated water, K_s can be reduced to $10^{-2}\ m^2 s^{-1}$ because of the increase of the time scale. This still is a big number (note: the acceptable maximum valve of K_s is about $10^{-1}\ m^2 s^{-1}$, Pond and Pickard, 1983) So, if this was true, the vertical mixing in the Kuroshio near northeastern part of the triangle was very intense during the measurement time. Otherwise, this model may not be right. The local change of salt may be caused by the horizontal advection, which carried the mixed water from the shelf to northeastern corner of the triangle.

2.5 Conclusion

Hydrographic data collected in the Yellow and East China Sea in January and July of 1986 have been used to describe the spatial structure of water properties in and near the Kuroshio west of Kyushu. Seasonal change in water structure occurred in this region due to increased solar heating and fresh water discharge onto the Chinese shelf during spring and summer. In January 1986, the Kuroshio front was located at the shelf break, separating the warmer, more saline Kuroshio water from the relatively well-mixed cooler, less saline Coastal Water. Mixing between these two water masses was observed but limited to near the shelf break. In July 1986, the Coastal Water from the Chinese shelf spread into the Kuroshio region near the surface and in turn, Kuroshio water intruded over the outer shelf near the bottom. Mixing between Kuroshio and Coastal water was found over much of the mid and outer shelf and upper slope, spanning across-stream distance of about 75 km. Finally, evidence for vertical mixing within the Kuroshio itself was found in the northeast corner of the study region, where the countercurrent occurred. This deep mixing may be due to enhanced internal tidal mixing and flow over steep topographic bottom.

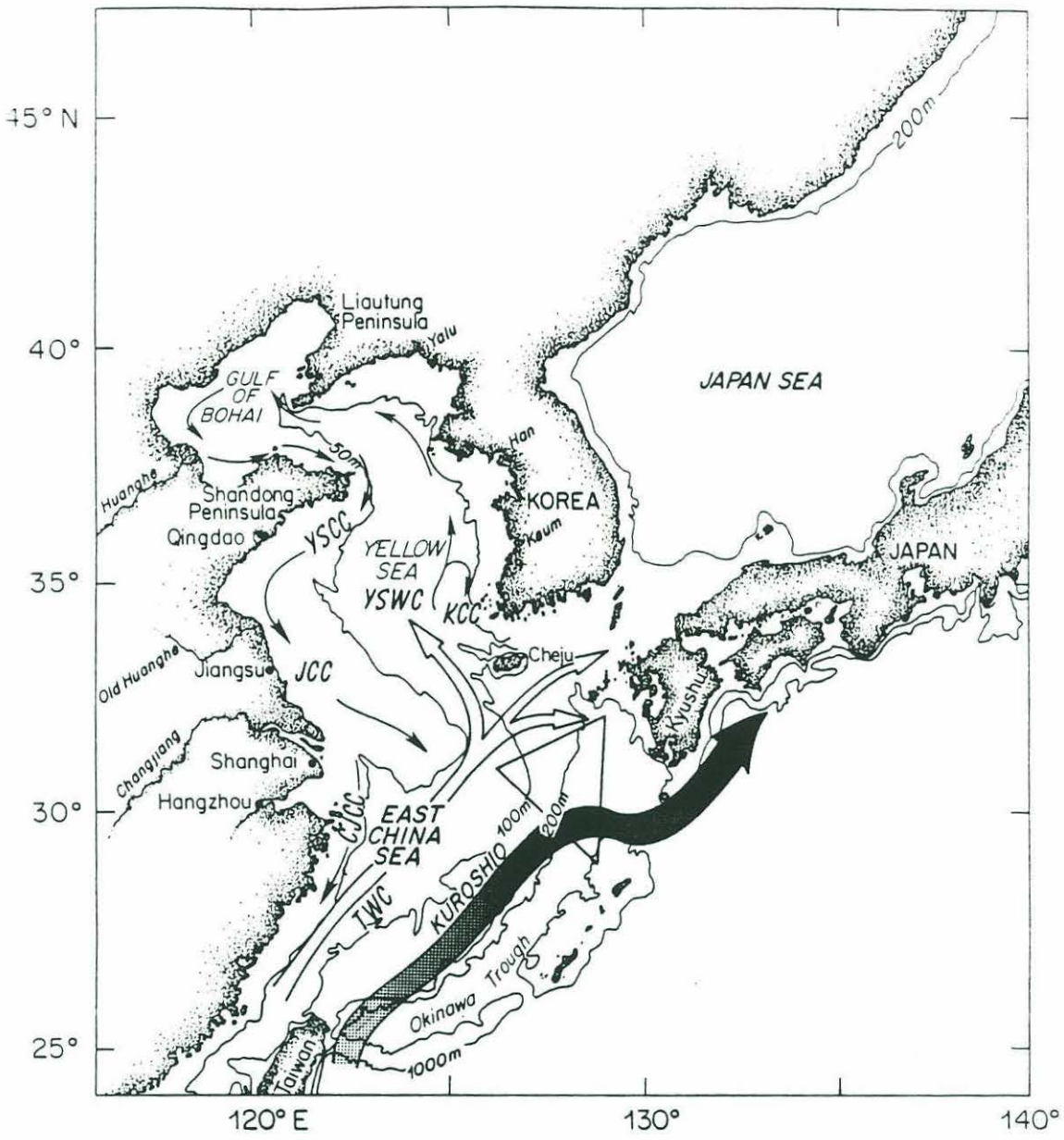

Figure 2.1: Regional circulation pattern in the Yellow and East China Sea.

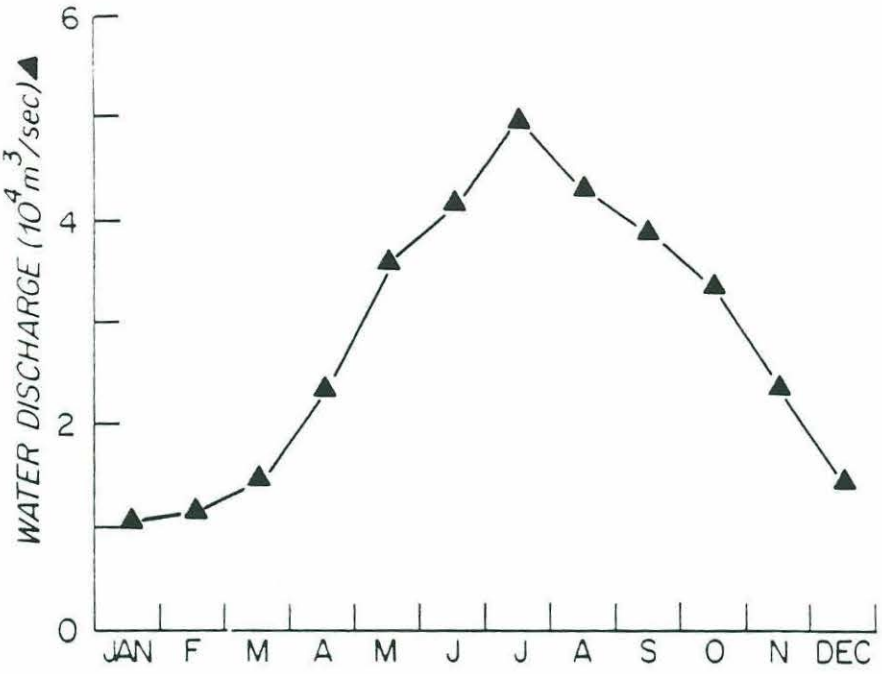

Figure 2.2: Average monthly discharge of Changjiang measured at Datong. (from Yang et al., 1983).

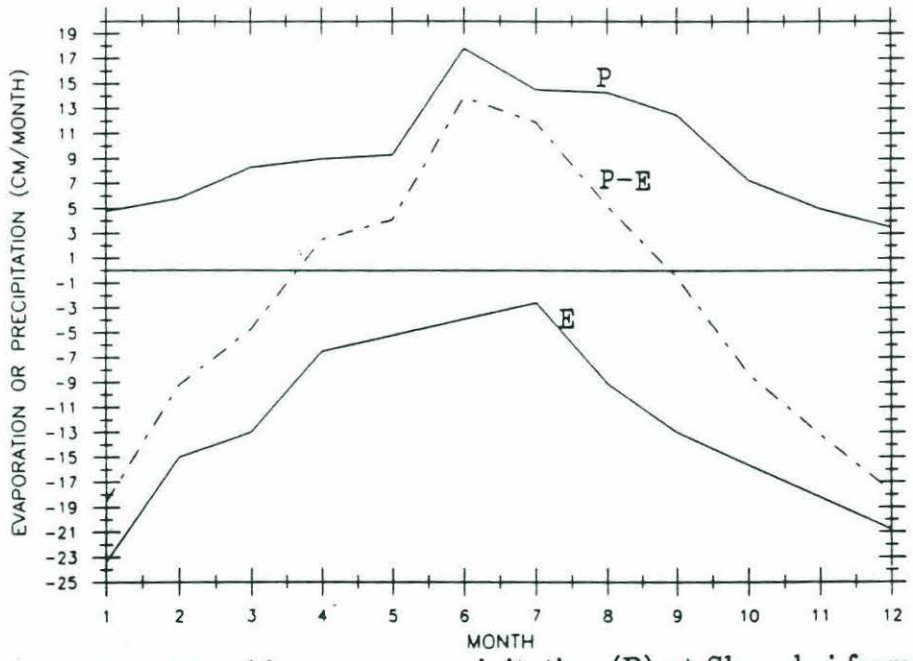

Figure 2.3: Monthly average precipitation (P) at Shanghai from 1912 to 1972 (taken from Wernstedt, 1972), evaporation (E) from 1947 to 1960 in the East China Sea (taken from Wyrtki, 1966) and P-E (dash line)

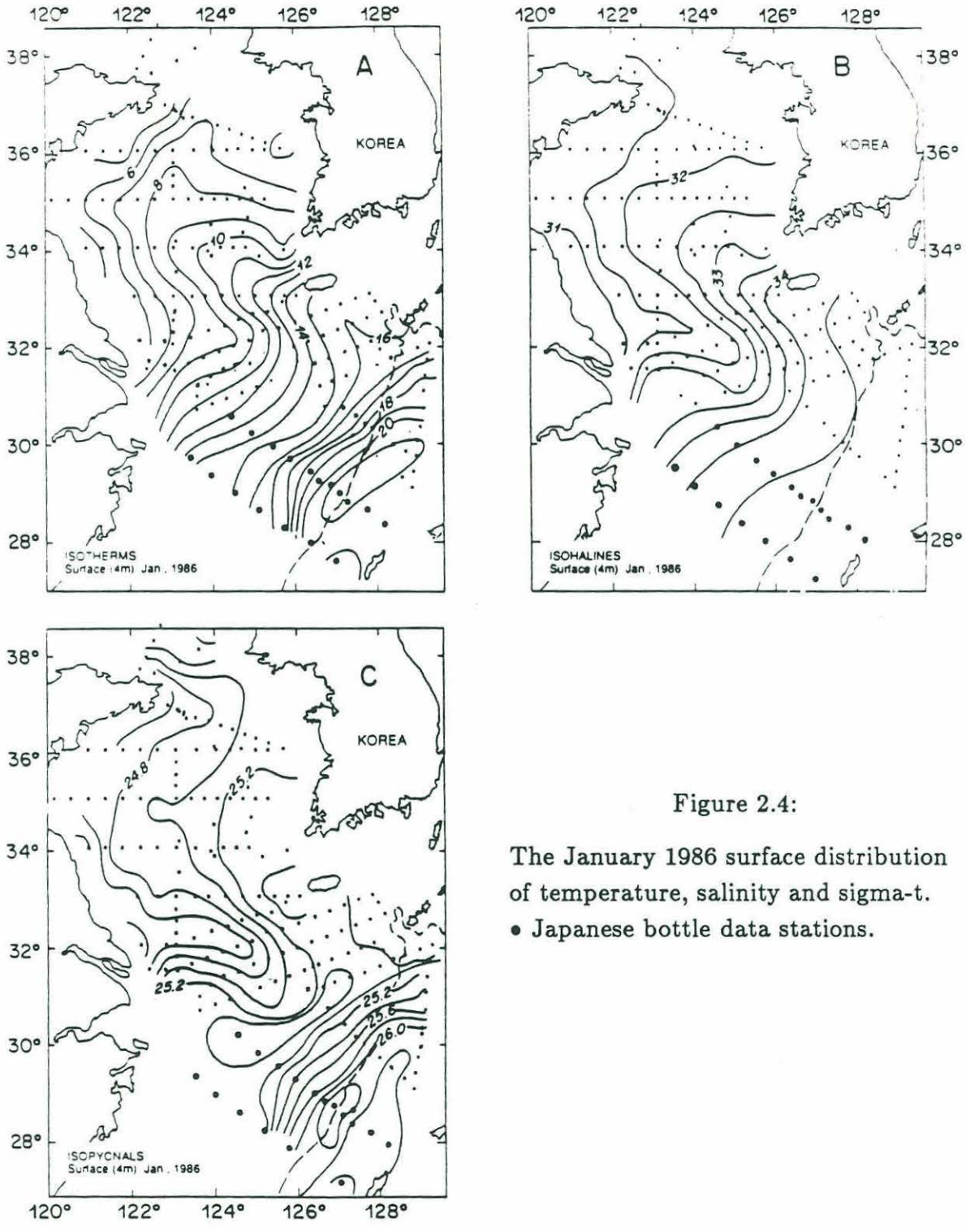

Figure 2.4:

The January 1986 surface distribution of temperature, salinity and sigma-t.
• Japanese bottle data stations.

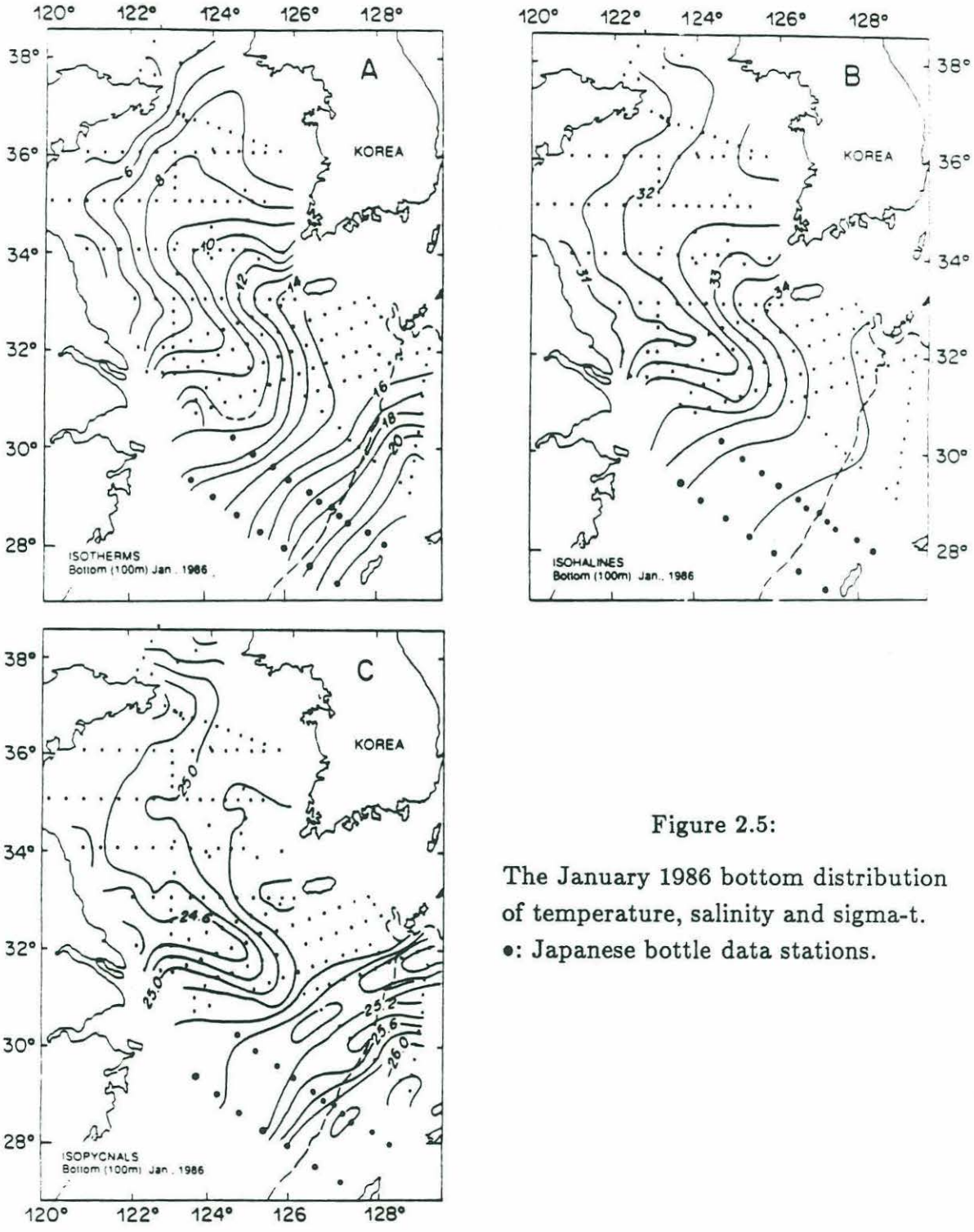

Figure 2.5:

The January 1986 bottom distribution of temperature, salinity and sigma-t.
•: Japanese bottle data stations.

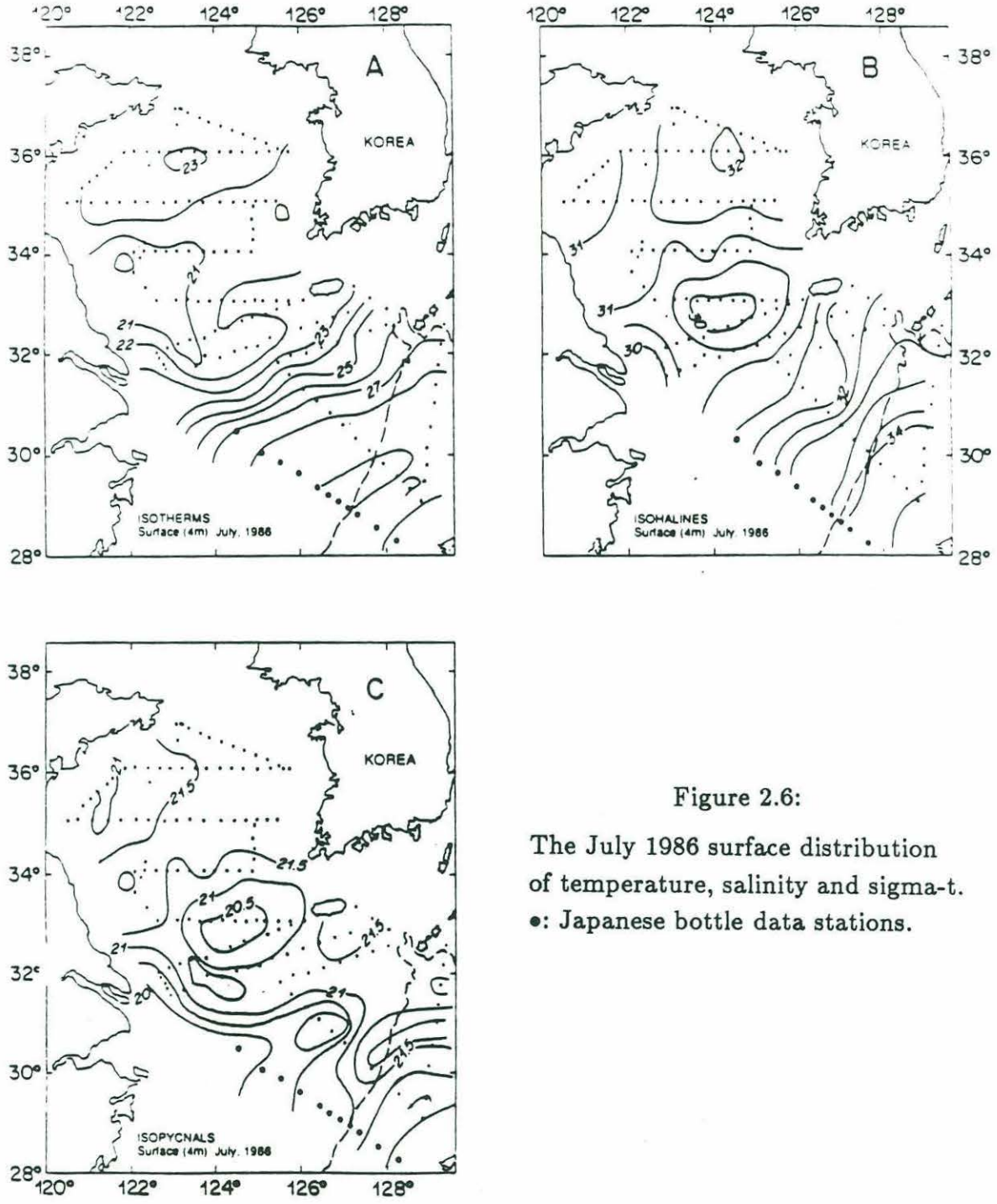

Figure 2.6:

The July 1986 surface distribution of temperature, salinity and sigma-t. •: Japanese bottle data stations.

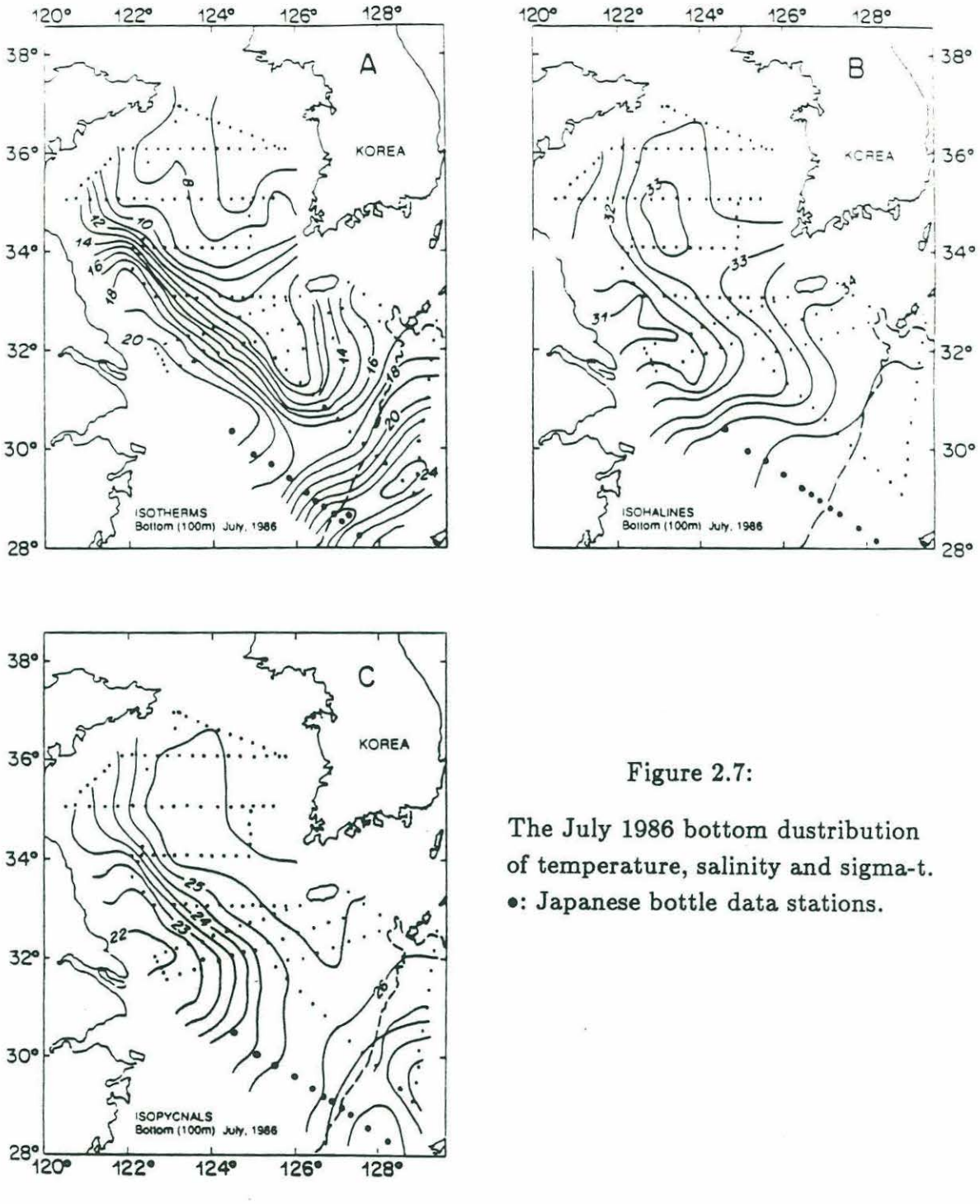

Figure 2.7:

The July 1986 bottom dustribution of temperature, salinity and sigma-t.
•: Japanese bottle data stations.

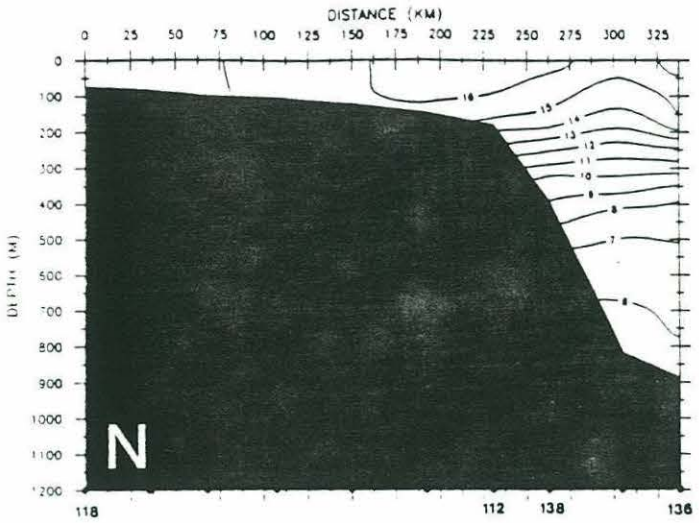

Figure 2.8:

The January 1986 vertical structure of temperature.
N: nothern section.
E: eastern section.
W: western section.

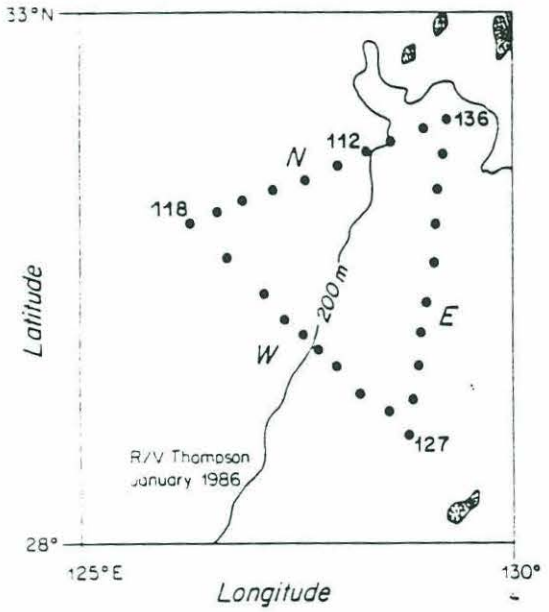

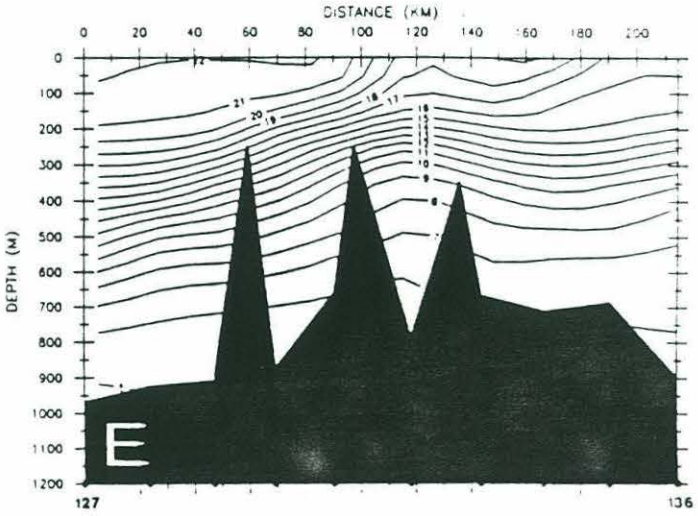

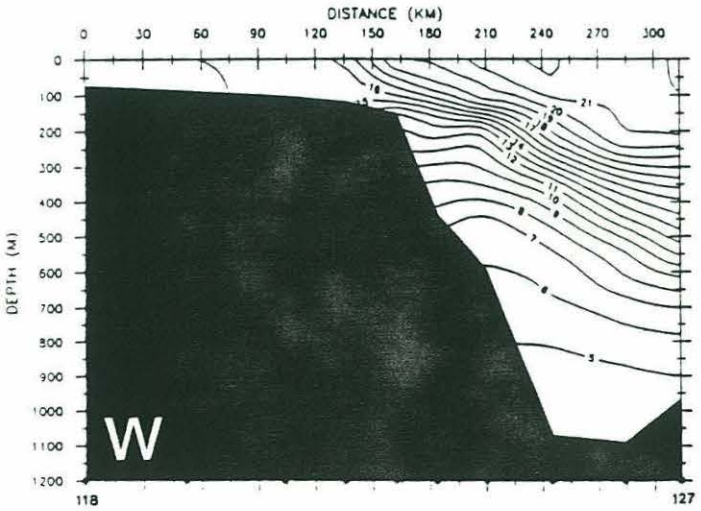

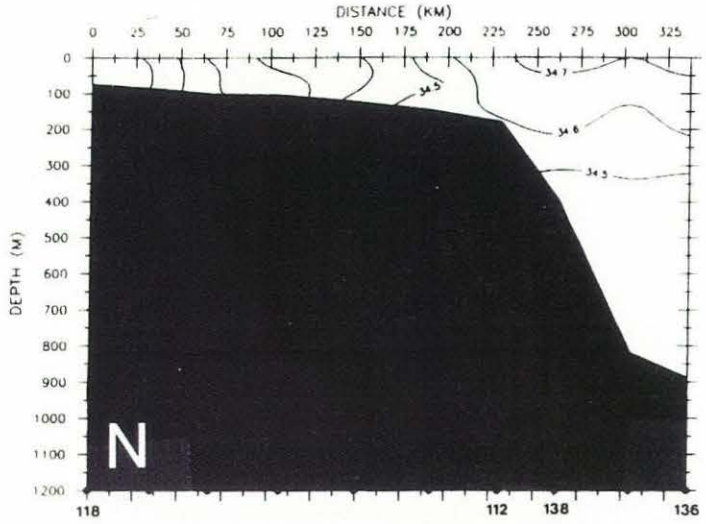

Figure 2.9:

The Junuary 1986 vertical structure of salinity.
N: northern section.
E: eastern section.
W: western section.

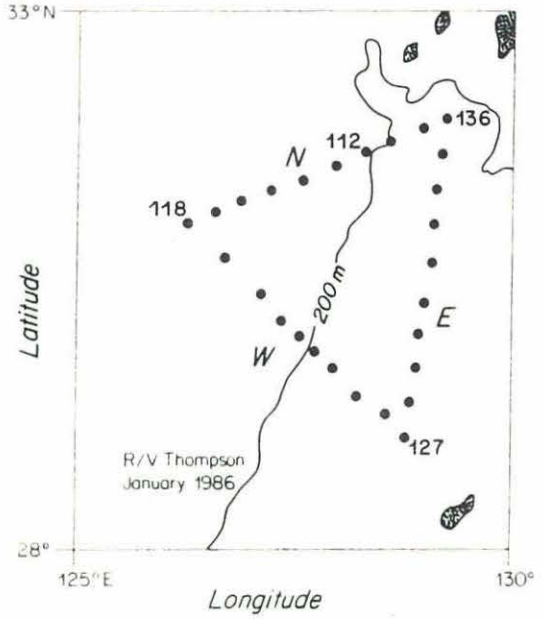

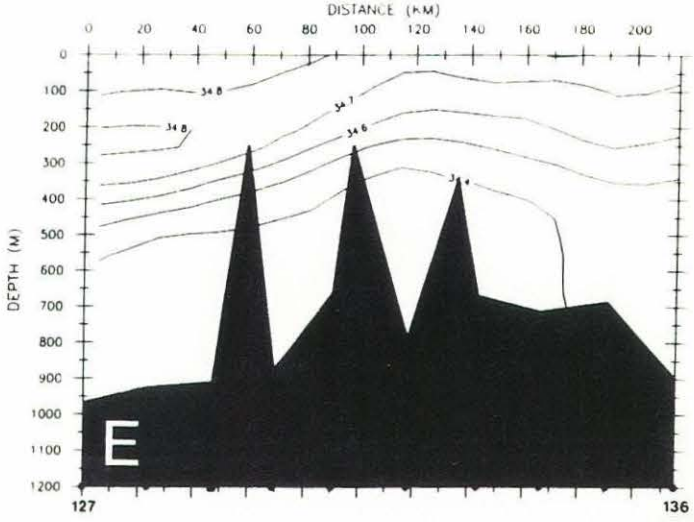

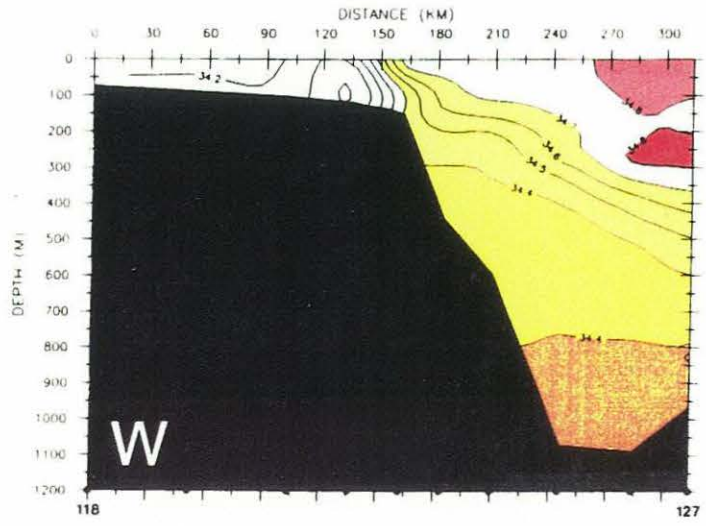

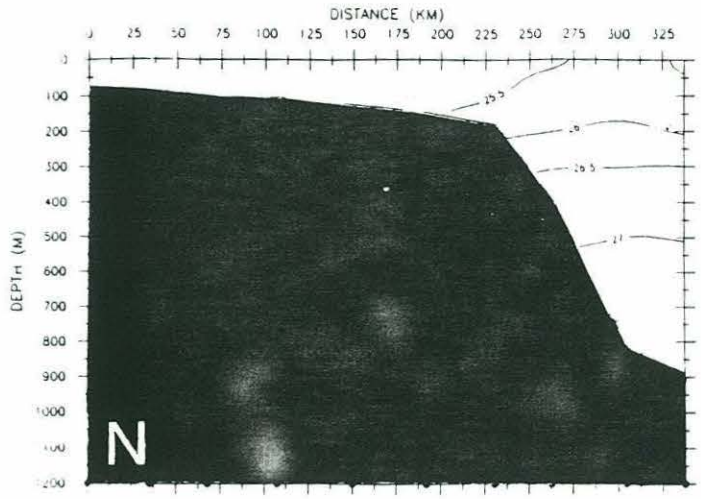

Figure 2.10:

The January 1986 vertical structure of sigma-t.

N: northern section.

E: eastern section.

W: western section.

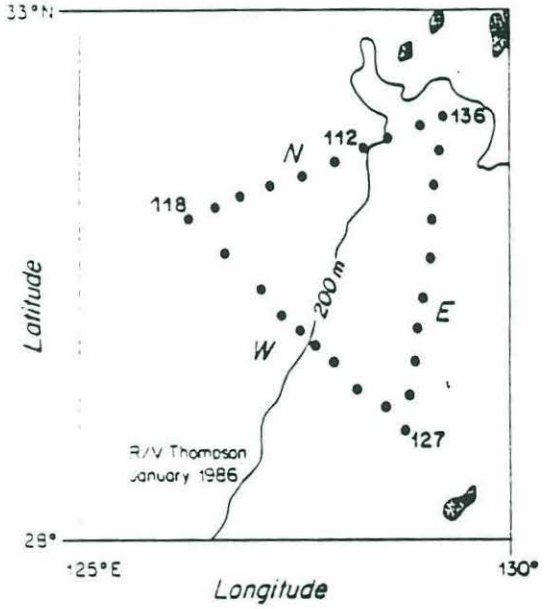

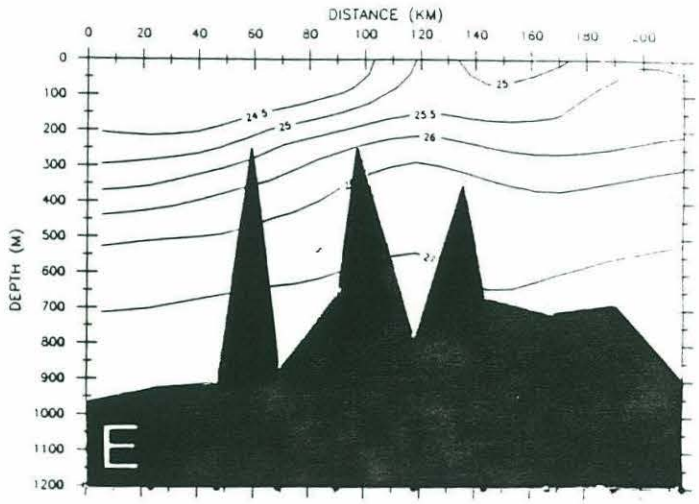

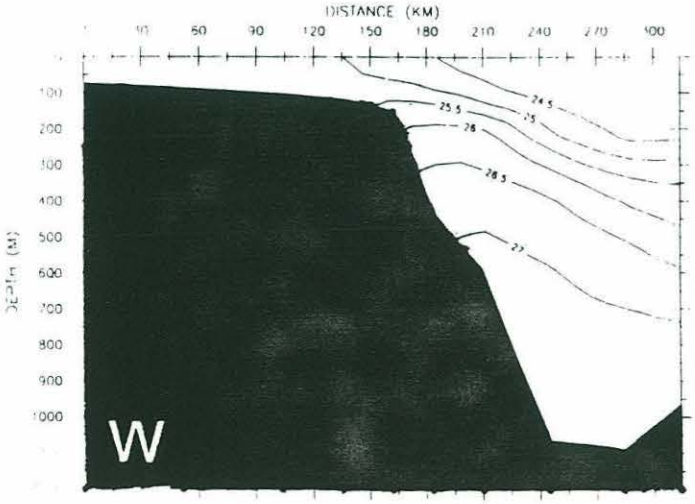

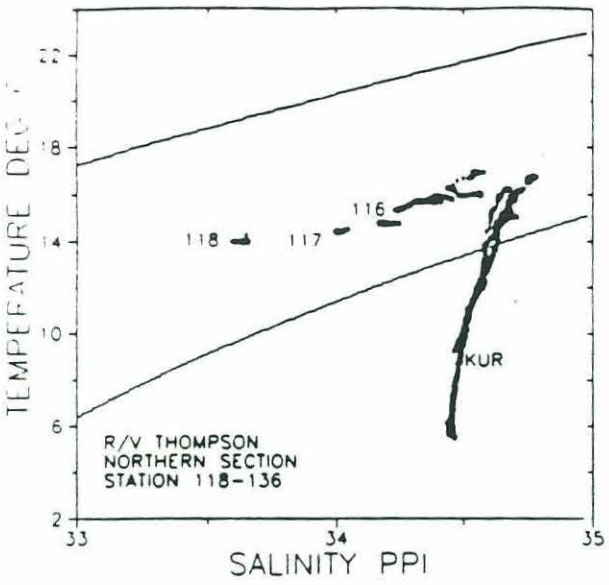

Figure 2.11:

The January 1986 T/S diagrams on the triangle section.

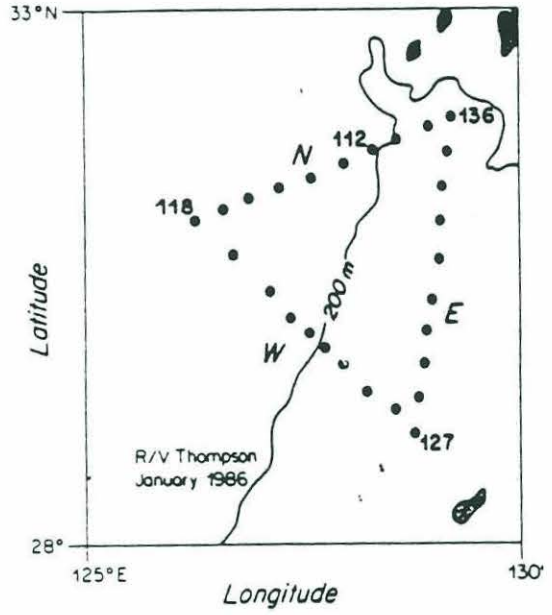

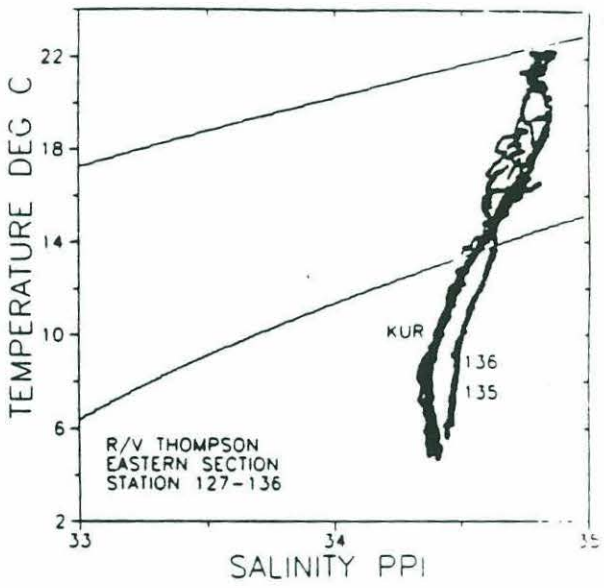

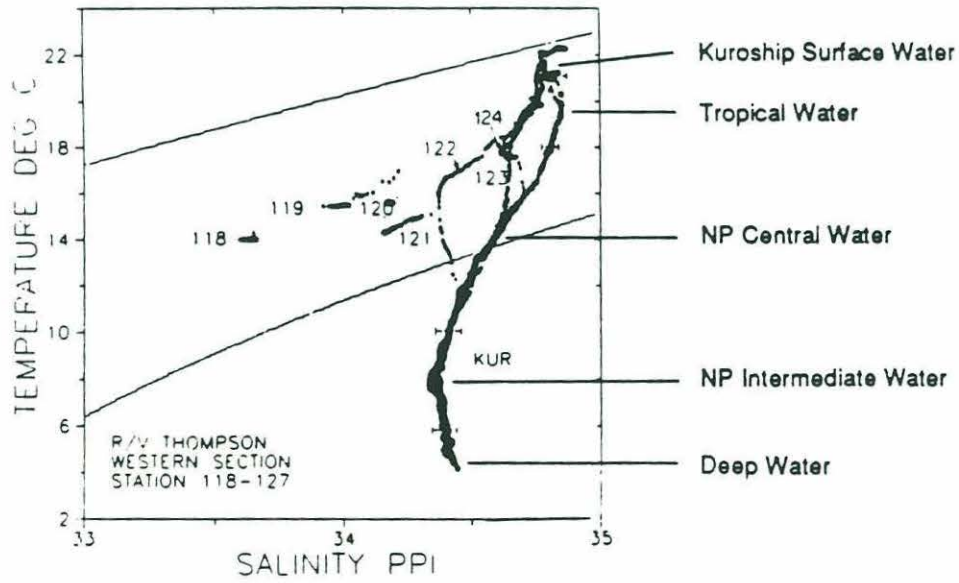

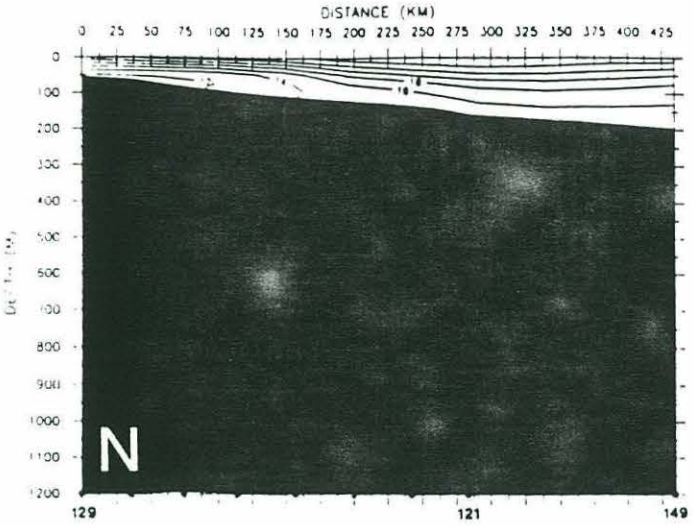

Figure 2.12:

The July 1986 vertical structure of temperature.
N: northern section.
E: eastern section.
W: western section.

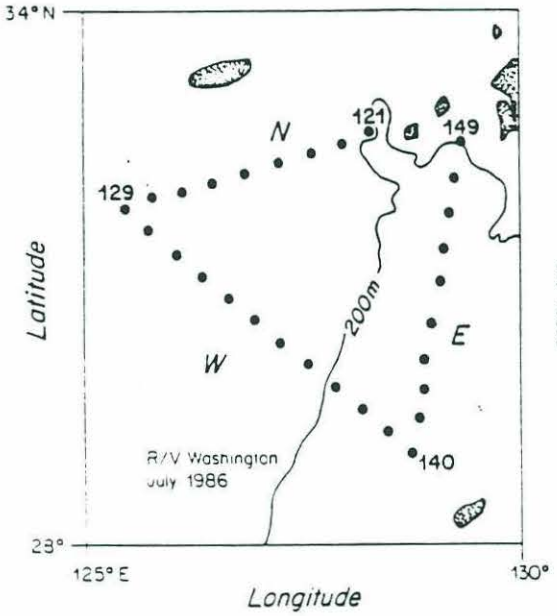

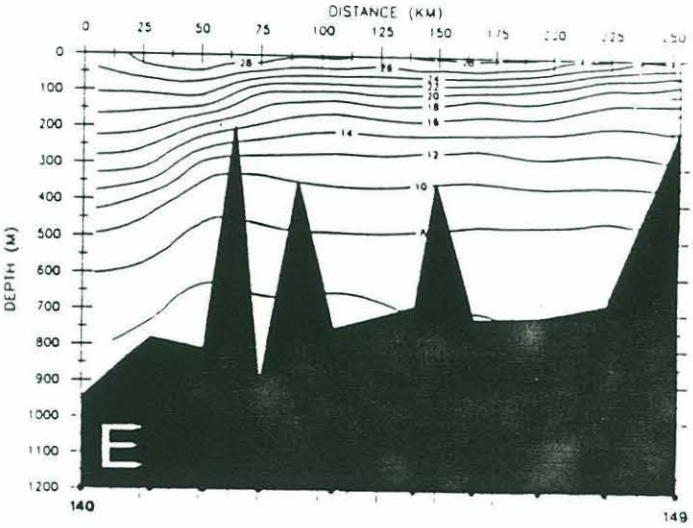

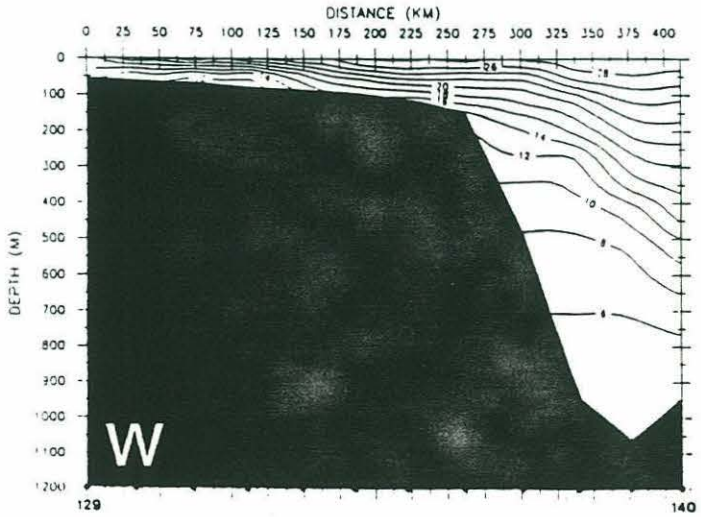

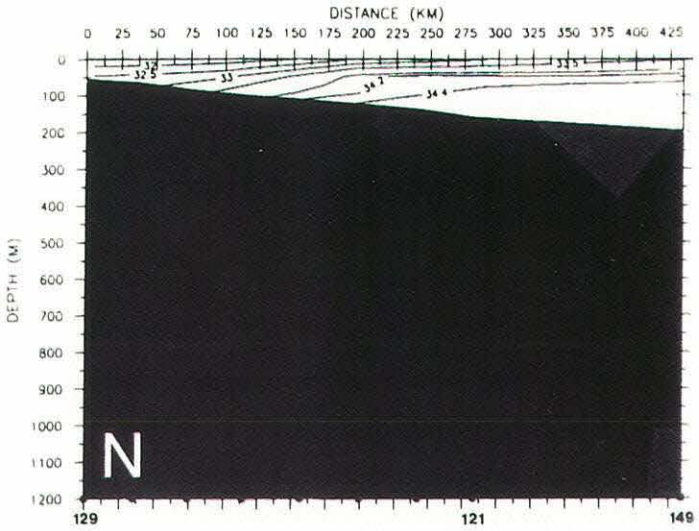

Figure 2.13:

The July 1986 vertical structure of salinity.
N:northern section.
E:eastern section.
W:western section.

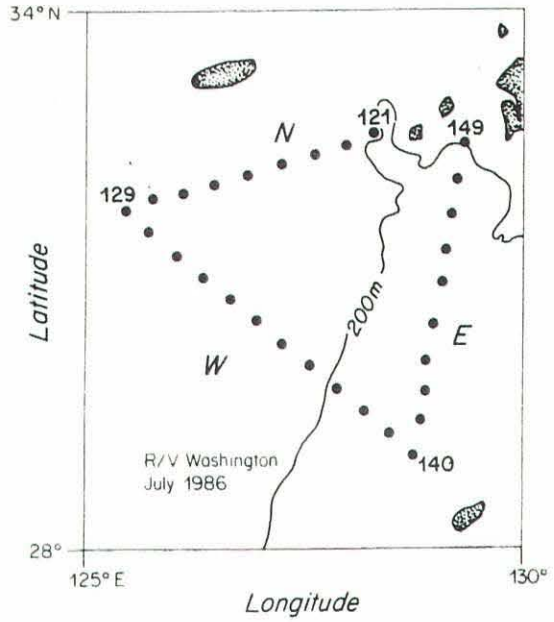

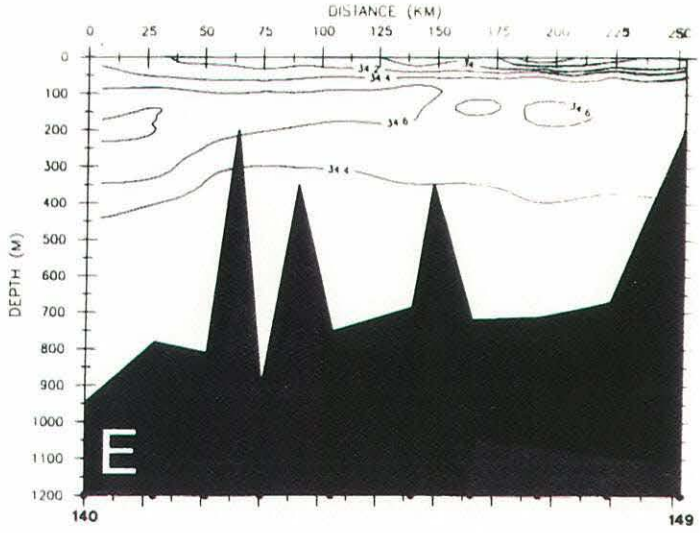

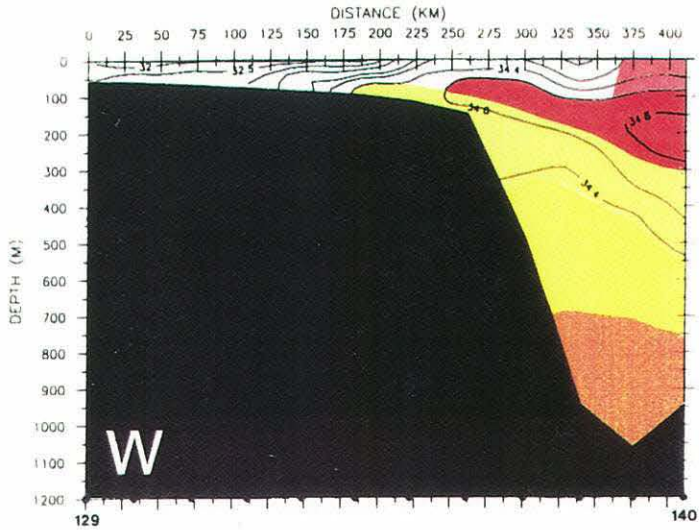

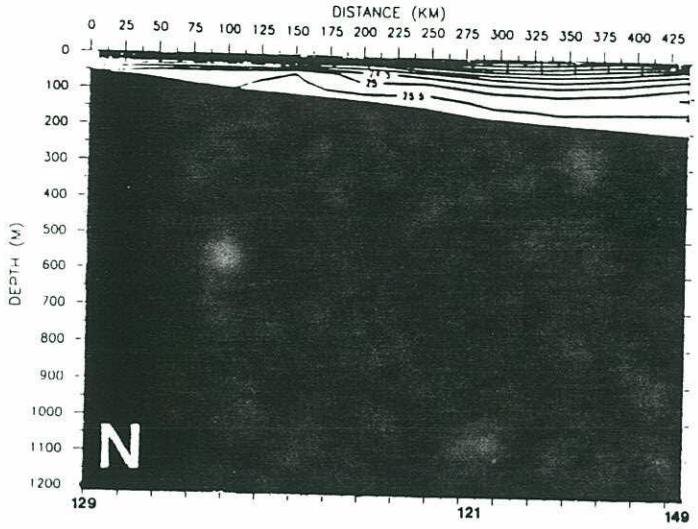

Figure 2.14:

The July 1986 vertical structure of sigma-t.
N:northern section.
E:eastern section.
W:western section.

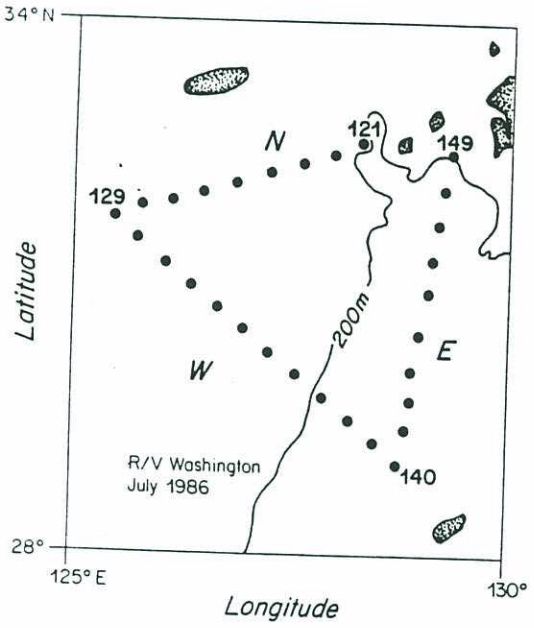

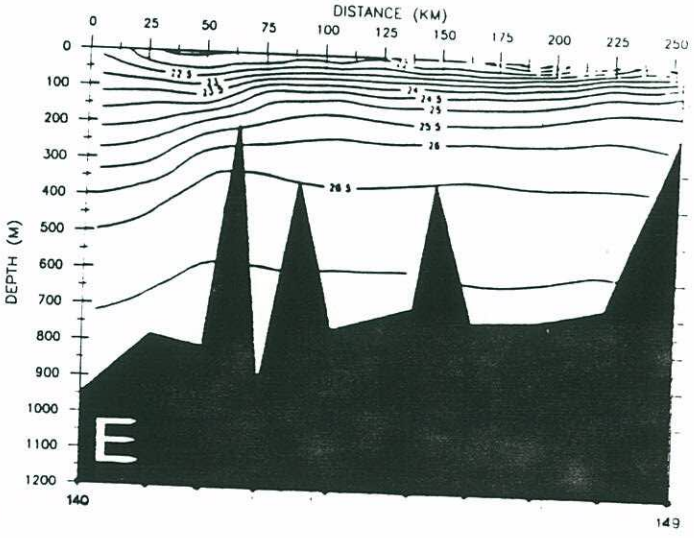

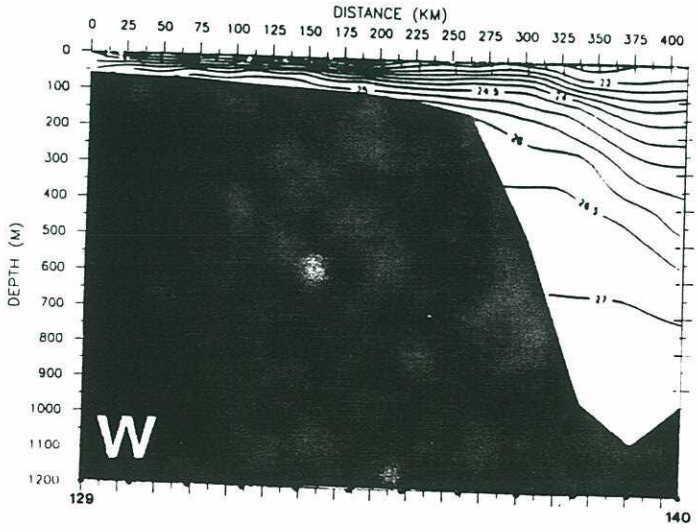

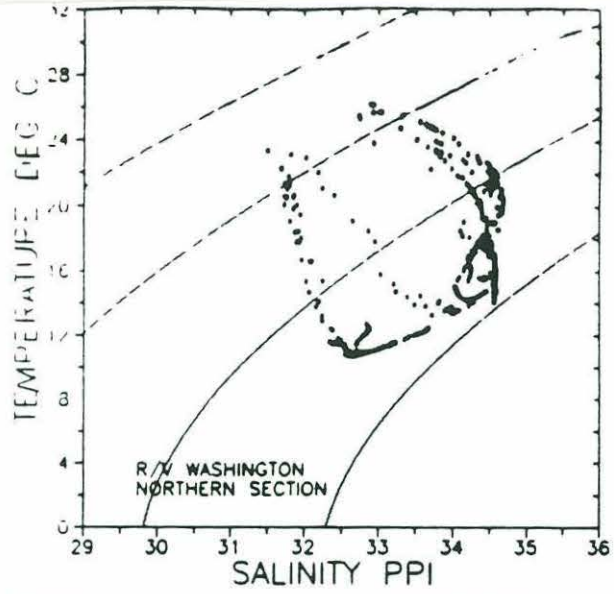

Figure 2.15:

The July 1986 T/S diagram on the triangle section.

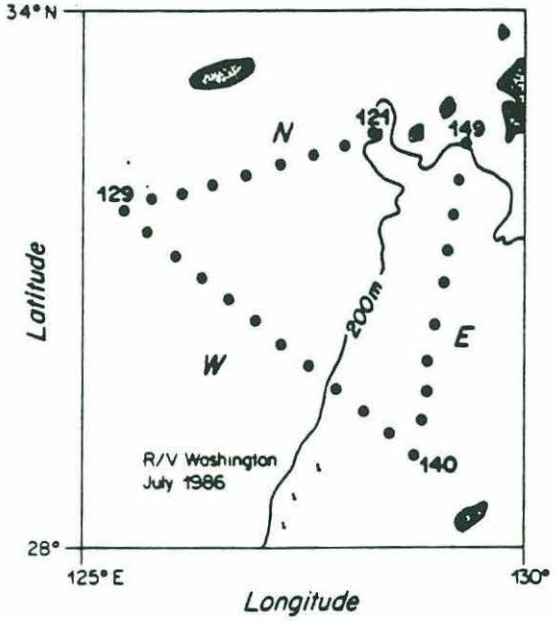

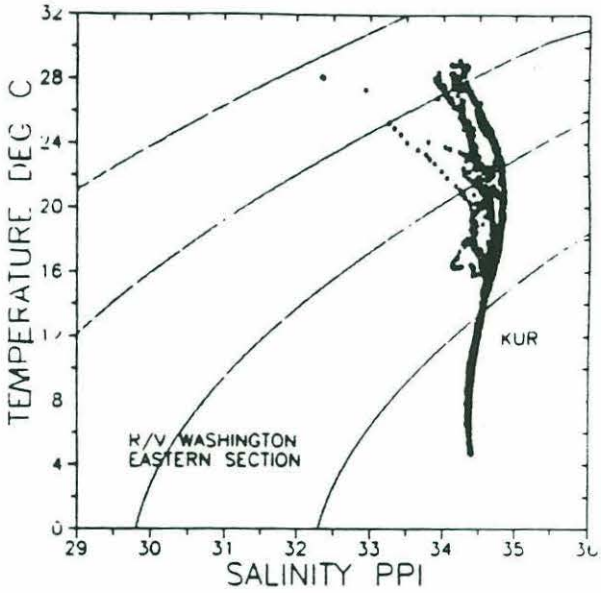

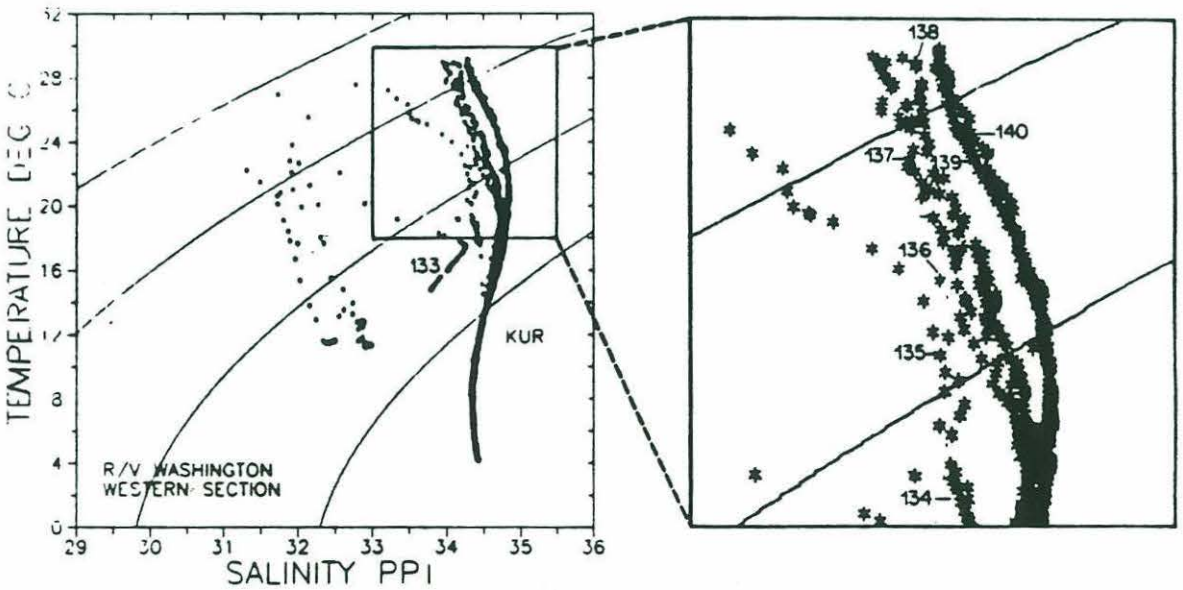

Chapter 3

The Geostrophic and Absolute Geostrophic Velocity Fields

3.1 Introduction

Ocean circulation is commonly inferred using hydrographic data by two main methods; water mass analysis and the dynamical method. Water mass analysis involves inferring the flow field from water properties such as temperature, salinity, dissolved oxgyen and sigma-t. An excellent example of this is the core method of Wüst (1935) who identified various core layers by their relative extremas of oxygen, salinity or temperature, and argued that general circulation must be consistent with the spatial pattern of these core layers. The dynamical method is based on the geostrophic balance for the large scale ocean circulation which permits the calculation of the vertical shear of the horizontal velocity from the horizontal density field determined by hydrographic data. The primary problem arising with determining the absolute geostrophic velocity is the choice of reference level velocity. At least five approaches have been used to infer the reference level velocity. First, the current is assumed to vanish at a great specified depth or the bottom. Second, the velocity is assumed to vanish in a finite thick layer of minimum shear (Defant, 1941), Third, the velocity is assumed to vanish at the level where dissolved oxygen reaches its minimum. Fourth is the β-spiral approach introduced by Stommel and Schott (1977), and the Fifth is Wunsch's inverse method

(Wunsch, 1977, 1978). However, all of these approaches are indirect, and only Wunsch's approach has direct applicability in a western boundary current.

The development of modern direct current measurement techniques has allowed direct determination of the reference level velocity and thus calculation of the absolute geostrophic velocity. Joyce et al. (1982) and Regier (1982) first applied the shipboard ADCP to make direct current measurements during hydrographic surveys. The methodology for using the ADCP as a survey tool has been developed and described by Joyce et al (1982, 1986, and 1988) and Kosro (1985), and so far, this approach has found increasing application in coastal circulation and Gulf Stream studies (Kosro, 1985, Joyce and Wunch et al., 1985, Barth and Brink, 1987). To my knowledge, Bryden et al. (1987) was the first to use ADCP data obtained in June 1985 aboard the R/V Thompson to estimate the absolute geostrophic velocity across the Kuroshio at 24°N. Bryden and co-workers also acquired ADCP data near the Tokara Strait. However, they found that the Loran C navigation errors near Tokara were too large to allow meaningful estimation of absolute geostrophic velocity. We experienced similar problems with Loran C during our January 1986 R/V Thompson cruise west of Kyushu. To overcome the uncertainty due to the Loran C navigation errors, a simple technique has been developed to estimate the average absolute velocity normal to the transect between adjacent hydrographic stations. This allows us to compute the absolute geostrophic velocity field for the R/V Thompson survey.

Since ADCP data were not obtained on the July 1986 R/V Washington survey, we will first describe in section 3.2 the geostrophic velocity field relative to the bottom to illustrate the seasonal variation of the current structure from January to July. Then the January 1986 ADCP data are analyzed and combined in section 3.3 with the hydrographic data to construct an absolute geostrophic velocity field. Finally, conclusions are given in section 3.4.

3.2 Geostrophic Velocity relative to the Bottom

One problem in computing geostrophic velocity relative to the bottom arises when the CTD section crosses the deep continental slope region since a large difference in depth occurs between two adjacant CTD stations. To overcome this difficulty, we choose the average depth of a CTD station pair as the reference bottom and linearly extrapolate the specfic volume anomaly from the deeper station to the shallower station along isobars (see Groem, 1948, and Reid et al, 1965). The geostrophic velocities for January and July, 1986 were then calculated relative to the reference bottom. To test the sensitivity of the approach, I have also calculated the geostrophic velocity using the shallower depth of the CTD station pair as the reference bottom. Little difference is found in the structure of the velocity field except for a total transport difference of about 2 Sv from one calculation to the other.

January 1986: The cross-stream structure and surface distribution of velocity in January 1986 are shown in Figures 3.1 and 3.2. The Kuroshio inflow was dominant on the western transect but limited to the Okinawa Trough with a width of about 150 km. The maximum velocity was about 103 cm/s, located respectively at the surface between stations 124-125 and at a depth of 100 m between stations 125-126, reflecting a tilt of maximum velocity axis from station 124 to 126. The shelf current on the western section between stations 119 and 122 was northeastward but weak, less than 5 cm/s in magnitude. On the eastern downstream section, the width of the main Kuroshio was about 120 km, stretching between stations 127 and 132, and the maximum velocity was about 125 cm/s at the surface between station 131 and 132. A strong westward flow or recirculation with the surface velocity of about 40 cm/s was found between stations 132 and 133. To its right, the current was dominated by outflow again. On the northern section, especially in the deeper region, the flow field was characterized by relative large outflow with a magnitude of 10 - 20 cm/s, even though there existed some weak inflow on the shelf.

In summary, the January 1986 structure of relative velocity implies that the Kuroshio flowed northeast from the western transect to the eastern transect, and then part of the Kuroshio recirculated to the west in the middle of the eastern transect. Where did this recirculation go ? Did the outflow near the northeastern corner of the triangle come from such a recirculation? The T/S analysis presented in section 2.4 suggests that the water near the northeastern corner consisted of a vertical mixture of Central and Intermediate Waters, originating in the Kuroshio. However, T/S analysis can not answer the above question since both the recirculation and main Kuroshio on the eastern or western transect had similar T/S properties. We will return to these questions in the next chapter after mass transport has been computed.

July 1986: As in January, the western transect was dominated by the strong Kuroshio inflow. The maximum velocity of the Kuroshio was 121 cm/s at about 45 m depth between stations 138 and 139, 18 cm/s larger than that in January. The Kuroshio axis, defined by its maximum velocity, moved south about 35 km from January to July. This was also evident on the eastern downstream section where the main Kuroshio was confined to the left of a sharp seamount between stations 142 and 143. The maximum velocity on this section was up to 146 cm/s at 145 m depth between stations 141 - 142, 33 cm/s larger than that in January. At the Kuroshio axis, the vertical shear of velocity was larger in July than in January (Figures 3.5 and 3.6), probably related to the surface stratification. The July pattern of flow on the eastern section was similar to that in January except that the recirculation was weaker and outflow area became larger on the eastern section.

The coastal current on the western section increased in strength from 5 cm/s in January to 25 cm/s in July, implying an intensification of the TWC in July. A wide northward flow of magnitude 10 cm/s was found on the northern section between stations 126 and 149. To its left, a southward inflow was found between stations 126-129, probably being the southward intrusion of the YSCC (see section 2.2).

The apparent downstream and seasonal increase in the maximum velocity on the eastern section is not surprising because of the large southward meander of the Kuroshio in July. The main Kuroshio was confined to a narrow region with a width of about 75 km in July, 45 km smaller than the January. Therefore, the velocity must increase to keep the same mass flux. In addition, the southward meander of the Kuroshio in July may be related to the seasonal variation of the circulation in the East China Sea. The increasing discharge of the Changjiang provides a strong horizontal buoyancy force to cause southward intrusion of Coastal Water. The Kuroshio may shift southward in response to this intrusion of Coastal Water.

A continuous horizontal pattern of flow on a isopycnal suface can not be drawn here using only three velocity sections because we do not know the relationship between the different patterns of flow on these sectons. However, the recirculation on the eastern section was too weak to support the outflow at the northeastern corner, suggesting that the outflow should chiefly come from the western section. The similarity of T/S characteristics between the mixed Coastal Water on the western section and the outflow on the northern section implies that the northward flow on the northern section can be traced to the western section.

3.3 Absolute Geostrophic Velocity Estimate

A Technique for ADCP Data Treatment

Joyce (1988) has derived expressions for the true water velocity in which the ADCP misalignment and sensitivity errors are defined and calculated. Let the (x, y) coordinate system be the true east, north coordinate frame in which the position and velocity of the ship are determined, and the (x', y') frame be that of the ADCP in which the velocity is decomposed into the east and north using the ship's gyro. Then, the absolute velocity (taken here as the water velocity) is equal to the vector sum of

the detected Doppler velocity $\vec{\mathbf{U}}_{\mathbf{d}}$ and the ship velocity $\vec{\mathbf{U}}_{\mathbf{s}}$. In the (x, y) frame this can be expressed by

$$U_w = U_s + (1 + \beta)(U_{d'}\cos\alpha - V_{d'}\sin\alpha), \tag{3.1}$$

$$V_w = V_s + (1 + \beta)(V_{d'}\sin\alpha - U_{d'}\cos\alpha), \tag{3.2}$$

where α is the counter-clockwise misalignment angle of the ADCP transducer or gyro error, and β is the correction factor due to sensitivity error.

In shallow regions less than 200 m, the ship's velocity can be measured directly with a 150 KHz ADCP, which is equal to the bottom velocity. In deeper regions, however, the ship's velocity must be determined by using Loran C or satellite navigation fixes. If α and β are known, the error of the estimate of absolute velocity is mainly dependent on that of the ship's velocity. In the Gulf Stream, high quality Loran C fixes are readily available almost every 3 minutes (R. Weller, personal communication), so that accurate estimates of the ship's velocity is possible provided some filtering is done to remove high frequency noise. However, on the January 1986 R/V Thompson cruise in the Kuroshio, Loran C fixes were obtained about every half hour, and only 3 to 4 Loran C fixes were recorded with each pair of CTD stations; thus the resulting calculation of the ship's velocity was relatively poor. A simple technique is developed in the following to calculate the averaged water velocity normal to the transect given by each pair of CTD stations.

Let A and B be the position of the ship at two successive CTD stations, and let $(\vec{p}, \vec{n})$ be directional unit vectors oriented either parallel or perpendicular to the station pair vector $\vec{AB}$, respectively. If the water velocity averaged in time over the distance from A to B is denoted by

$$\bar{U}_w = \bar{U}_s + \bar{U}_d, \tag{3.3}$$

$$\bar{V}_w = \bar{U}_s + \bar{V}_d, \tag{3.4}$$

where $U_d = (1 + \beta)(U_{d'}\cos\alpha - V_{d'}\sin\alpha)$ and $V_d = (1 + \beta)(V_{d'}\sin\alpha - U_{d'}\cos\alpha)$, then, the average water velocity normal to $\vec{AB}$ is given by

$$\bar{U}_{wn} = \bar{V}_w\cos\theta - \bar{U}_w\sin\theta = \bar{U}_{sn} + \bar{U}_{dn}, \tag{3.5}$$

where θ is the angle between $\vec{p}$ and $\vec{x}$, and $\bar{U}_{sn}$ and $\bar{U}_{dn}$ are the normal components of the ship's velocity and ADCP velocity, respectively.

If the ship starts at A and eventually reaches B, the average component of the ship's velocity normal to the section $\vec{AB}$ should vanish (i.e., $\vec{U}_{sn} = 0$), so the average water velocity $\bar{U}_{wn}$ reduces to

$$\bar{U}_{wn} = \bar{U}_{dn} = -\bar{U}_d\sin\theta + \bar{V}_d\cos\theta. \tag{3.6}$$

The error in this estimate associated with the positioning error of the ship will be discussed later. For the January 1986 R/V Thompson survey over the triangle sections, the bottom velocity was recorded on the shelf from station 112 to station 124, and high quality GPS data were recorded from station 126 to station 130 and station 136 to station 138. The positions of remaining stations were estimated using Loran C fixes. Therefore, estimation of absolute velocity should be better on the western section where the locations of only three stations were dependent on the Loran C fixes.

It should be pointed out that the averaging technique described above filters out any high resolution spatial and temporal variability in the absolute velocity structure, and does not allow determination of the two-dimensional current vector field. The averaged ADCP velocity still contains some ageostrophic components, such as tidal currents and inertial motions. These have been found to seriously contaminate ADCP data used for geostrophic reference in the open ocean (Toole, personal communication).

However, these ageostrophic motions may be small in the Kuroshio where the meridional flow is much stronger than the zonal flow. A simple scale analysis can help us to determine the relative sizes of these components.

Let H_1, H_2 and U_1^T, U_2^T be characteristic depths and tidal velocities in the Kuroshio and in the shelf region, respectively. Assuming the flow travels from the deep ocean onto the shelf, mass conservation gives

$$U_2^T \sim \frac{H_1}{H_2} U_1^T.$$

Based on the results of the numerical model of the M_2 tide in the East China Sea (Choi, 1980), $U_1^T \sim$ 100 cm/s at $H_1 \sim 10^3$ cm. Using the typical value $H_2 \sim 10^5$ cm in the Kuroshio, we find that

$$U_2^T \sim 1\ cm/s.$$

Since current velocities within the Kuroshio are of order 100 cm/s, it follows that tidal currents can be safely neglected.

The wind was very weak during the measurement time (Limeburner, personal communication). Therefore, the directly wind driven flows (Ekman flow and inertial motions in the surface water) were probably weak. In other words, the inertial term can be omitted if

$$O(\frac{\partial u}{\partial t})/O(fv) \ll 1$$

where f is the Coriolis parameter, u and v are zonal and meridional velocity components in the Kuroshio. Let T be the time scale over which the Kuroshio changes, and let U and V be characteristic values of u and v, respectively. It follows that the condition for inertial term to be neglected is

$$T \gg \frac{1}{f}(\frac{U}{V}).$$

In the Kuroshio west of Kyushu, with $f \sim 10^{-4}$ s, U $\sim$ 10 cm/s and V $\sim$ 100 cm/s, we find that

$$T \gg 0.3\ hr.$$

It follows that when the time scale of the motion is significantly longer than 0.3 hr, inertial term can be ignored. During our measurements, the time interval used for averaging the ADCP data between consecutive CTD casts was larger than 1 hr, one order of magnitude larger than 0.3 hr. Thus, the inertial term did not significantly contaminate our averaged ADCP data. We can still use the averaged ADCP data as the geostrophic reference to calculate the absolute geostrophic velocities.

Error Analysis

Two main errors must be taken into account when the technique introduced above is applied to find the absolute water velocity from the ADCP data: 1) the bias in the angle θ between the station pair orientation $\vec{AB}$ and the x-axis of the geographical coordinate frame, and 2) the misalignment α and sensitivity β (or ADCP calibration) errors. The error in θ results from uncertainty in the ship's position. A simple geometrical analysis reveals that this error is not only dependent on the absolute value of the circle error associated with each position fix but is also inversely proportional to the distance between two stations. The misalignment error α is caused by the small deviation of the orientation of the transducer head relative to the gyro reference orientation. The sensitivity error β can be caused by errors in the oscillator frequency or speed of sound and spreading of the acoustic beams, etc, which causes the ADCP velocity to be over or underestimated (See Kosro, 1985). Estimates of these errors are presented next.

Error in the angle θ

Two kinds of navigation data (Loran C and GPS) were used to determine the ship's position on the triangle sections during the January 1986 R/V Thompson cruise. The Loran C data were recorded almost every half hour, while GPS data were obtained only 3-4 hours each day. Since the typical distance between CTD station pairs was about 30 km, the contribution of about 3 to 10 m position uncertainty to the error in θ

in the GPS data was so small that it can be neglected. For this reason, the position error of the Loran C data has been calculated here based on the assumption that the GPS data were error free. The differences in latitude and longitude between simultaneous pairs of Loran C and GPS fixes are shown in Figure 3.7. The fact that the Loran C error was dominant in longitude means that the Loran C error would cause maximum errors in θ for station pairs oriented north-south. The distance errors between the simultaneous pairs of Loran C and GPS positions obtained during the interval from January 28 to January 30 are shown in Figure 3.8, in which the maximum values of the Loran C position error did reach 1 km and roughly satisfied the Gaussian distribution over the time interval. In order to estimate the error in θ, a simple statistical analysis is done in the following.

Let A_G and B_G be two GPS fixes and A_c and B_c be two Loran C fixes (see Figure 3a), Y_i is the distance error for each simultaneous pair of Loran C and GPS positions, and L is the distance from A_G to B_G (see Figure 3a).

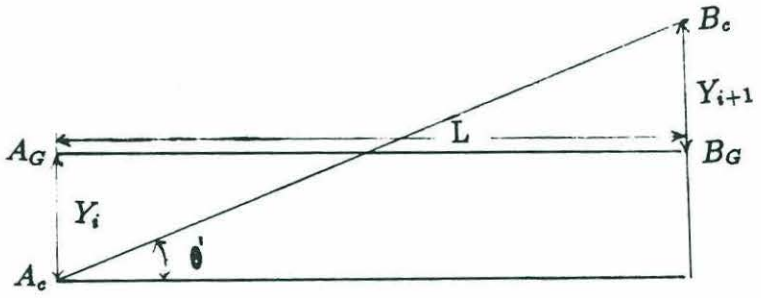

Figure 3a

Then, the largest angle error between the station pairs can be expressed as

$$\tan\theta' = \frac{Y_{i+1} + Y_i}{L}. \tag{3.7}$$

Suppose that θ' is small, so that the small angle approximation can be made,

$$\theta' \simeq \frac{Y_{i+1} + Y_i}{L}.$$

Take all the distance errors Y_i $(i = 1, N)$ as a set of independent random variables, with Y_i assumed to be Gaussian with mean $\bar{Y}$ and variance σ^2 about the mean. Then, the probability density function for each Y_i can be given by

$$P_{Y_i}(Y_i) = \frac{1}{\sigma\sqrt{2\pi}} e^{-\frac{(Y_i - \bar{Y})^2}{2\sigma^2}}. \tag{3.8}$$

Let $X_i = Y_i/L$, thus the probability density function of X_i is

$$P_{X_i}(X_i) = \frac{1}{\sigma\sqrt{2\pi}} e^{-\frac{(L\,X_i - \bar{Y})^2}{2\sigma^2}}. \tag{3.9}$$

Since θ' is a linear combination of X_i and X_{i+1}, the probability density function of θ' must satisfy the Gaussian distribution. Using some simple agebraic operations (see Appendix B), we can find the probability density function of θ' as

$$P_{\theta'}(\theta') = \frac{L}{2\sqrt{\pi}\sigma} e^{-\frac{L^2(\theta' - \frac{2\bar{Y}}{L})^2}{4\sigma^2}}. \tag{3.10}$$

Therefore, the expected value is equal to

$$\langle\theta'\rangle = \int_{-\infty}^{\infty} \theta' P_{\theta'}(\theta') d\theta' = \frac{2\bar{Y}}{L}, \tag{3.11}$$

and its variation relative to $\langle\theta'\rangle$ is found as

$$\sigma_{\theta'}^2 = \int_{-\infty}^{\infty}(\theta' - \langle\theta'\rangle)^2 P_{\theta'}(\theta')d\theta' = \frac{2\sigma^2}{L^2}, \tag{3.12}$$

so that the deviation of θ' is equal to

$$\sigma_{\theta'} = \frac{\sqrt{2}\sigma}{L}. \tag{3.13}$$

It follows that the mean of the angle error θ' and its deviation $\sigma_{\theta'}$ are inversely proportional to the distance L, therefore, the angle error can be reduced by increasing the averaging length.

The angle error θ' is then given by

$$\theta' = \frac{2\bar{Y}}{L} \pm \frac{\sqrt{2}\sigma}{L} \tag{3.14}$$

where $\bar{Y} = 702\ m,\ \sigma = 178\ m.$

The correction of angle error θ' for each CTD successive station pair has been done using the mean of θ'. Then the maximum error is estimated by $\sigma_{\theta'}$. This approach allows the maximum uncertainty error to be reduced to approximately 4-5 cm/s (see Table 3.1).

The misalignment and sensitivity errors

Starting with equations(3.1) and (3.2), Joyce (1988) derived formula for the calculation of misalignment and sensitivity errors for both bottom tracking and water

tracking modes. In water tracking mode, the assumption that the current $\vec{U}_w$ is equal before and after a single turn is used to eliminate $\vec{U}_w$ and then find α and β . The solutions for α and β require knowledge of the exact ship velocity, which we did not have for much of the cruise. In bottom tracking mode, $\vec{U}_w = 0$ at the bottom, so that α and β can be solved from equations (3.1) and (3.2) as follows

$$\tan\alpha = \frac{\langle U_{d'}U_s - V_{d'}V_s\rangle}{\langle U_{d'}U_s + V_{d'}V_s\rangle}, \tag{3.15}$$

$$1+\beta = \frac{\langle U_{d'}U_s + V_{d'}V_s\rangle}{\langle U_{d'}^2 + V_{d'}^2\rangle\cos\alpha}, \tag{3.16}$$

where the brackets $\langle\ \rangle$ refer to the average done over a chosen time interval.

Using these two formula, values of α and β were calculated during those time intervals in which GPS data were available for the entire January 1986 R/V Thompson cruise. The samples used in the calculation cover 8 days from January 21 to January 29, during which GPS fixes were recorded every 2 minutes for 3-5 hours each day. In our computation, $U_{d'}$ and $V_{d'}$ were given by the bottom track velocities, and U_s and V_s were calculated using GPS fixes, and then equations (3.15) and (3.16) were used to estimate α and β over a 30 minute averaging period. If the ship's course was relatively steady for a longer period, larger averaging time was used.

The resulting α and β values are shown in Figures 3.9 and 3.10. The mean value of α was 0.463°and its deviation was 0.146°. The mean value of $1+\beta$ was 0.993 and its deviation was 0.017. Therefore, we can use the mean value of α and $1+\beta$ to correct the water velocity, and the deviation to express the random errors. The computed misalignment and sensitivity errors for the January 1986 R/V Thompson survey were then

$$\alpha = 0.463^\circ \pm 0.146^\circ, \tag{3.17}$$

$$1+\beta = 0.993 \pm 0.017. \tag{3.18}$$

After correction, the error velocity due to misalignment and sensitivity was reduced to approximately 0.2 - 0.5 cm/sec in the Kuroshio region. The error velocity was smaller than 0.2 cm/s on the inner shelf where the current was weak and bottom tracking velocity was used for the ship's velocty.

The total error velocity due to navigation, misalignment and sensitivity errors are summarized in Table 3.1.

Table 3.1 : Maximum uncertainty in absolute ADCP velocity normal to CTD station pairs for January 1986 R/V Thompson survey

station pair	ship's navigation	ADCP bottom tracking	$\triangle V_{max}$ cm/s	comments
112-113	Loran C	yes	$< \pm 0.1$	errors small due to bottom tracking
113-114	GPS	yes	< 0.1	,, ,, ,,
114-115	GPS	yes	< 0.1	,, ,, ,,
115-116	GPS	yes	< 0.1	,, ,, ,,
116-117	Loran C	yes	< 0.1	,, ,, ,,
117-118	Loran C	yes	< 0.1	,, ,, ,,
118-119	Loran C	yes	< 0.1	,, ,, ,,
119-120	GPS	yes	< 0.1	,, ,, ,,
120-121	GPS	yes	< 0.1	,, ,, ,,
121-122	Loran C	yes	< 0.1	,, ,, ,,
122-123	Loran C	yes	< 0.1	,, ,, ,,
123-124	Loran C	yes	< 0.1	,, ,, ,,
124-125	Loran C	no	± 4.4	errors large due to Loran C
125-126	Loran C	no	± 3.9	,, ,, ,,
126-127	GPS	no	± 0.9	errors small due to GPS
127-128	GPS	no	± 0.7	,, ,, ,,
128-129	GPS	no	± 0.6	,, ,, ,,
129-130	Loran C	no	± 6.4	errors large due to Loran C
130-131	Loran C	no	± 5.3	,, ,, ,,
131-132	Loran C	no	± 5.4	,, ,, ,,
132-133	Loran C	no	± 5.6	,, ,, ,,
133-134	Loran C	no	± 5.6	,, ,, ,,
134-135	Loran C	no	± 5.5	,, ,, ,,
135-136	Loran C	no	± 6.2	,, ,, ,,
136-137	GPS	no	± 0.9	errors small due to GPS
137-138	GPS	no	± 1.1	,, ,, ,,
138-139	Loran C	yes	< 0.1	errors small due to bottom tracking

Absolute Geostrophic Velocity

In this section, we will use the averaged normal ADCP velocity at 60 m in the deeper water and 10 m in water shallower than 100 m as the reference level velocity for absolute geostrophic velocity calculations. The resulting sections of absolute geostrophic velocity and their corresponding reference velocities are shown in Figures 3.11 and 3.12. The Kuroshio flowed through the western section as a coherent current, and then split into two streams around a tall seamount as it left through the eastern section. Some countercurrents were found on the western section between the maximum velocity core of the Kuroshio and the slope, and on the eastern section to the north of the northern maximum velocity core of the Kuroshio around a seamount, as well as on the northern section over the slope. Compared with the geostrophic calculation relative to the bottom, we can see that some important features of the Kuroshio such as the flow splitting around the seamount on the downstream section and the recirculations (or eddies) of order 5 - 10 cm/s over the slope were missed in the geostrophic flow field relative to the bottom.

The actual bottom velocity was found to be about 10 cm/s at the center of the Okinawa Trough on the western section (Figure 3.13), and about 20 - 30 cm/s on the eastern section. A bottom velocity of order 10 cm/s was also found by Bryden et al (1988) in the upstream region of the Kuroshio near Ryuku Islands and by Brooks and Niiler (1977) in the Florida Strait for the Gulf Stream. It is because of the existence of such substantial bottom velocities that sections of relative geostrophic velocity must be modified by the barotropic part of the absolute velocity. As a result of the large bottom velocities, the maximum velocity of the Kuroshio increased about 10 cm/s on the western section and about 20 cm/s on the eastern section. The outflow through the northern section was also increased up to 20-30 cm/s, and the area of the recirculation on the eastern section became larger even though its speed remained almost the same.

The geostophic velocity estimate relative to the bottom underestimated the transport in the Kuroshio and missed some important features of the flow field.

Test of geostrophical approximation

When the Rossby number is the order of 0.1 or less, the large scale motion can be approximately described by the geostrophic balance. In the Kuroshio west of Kyushu, $f \sim 10^{-4}s$, $U \sim 1\ m/s$ and $L \sim 10^5 m$, so that $R_o = 10^{-1}$. Therefore, the cross-stream momemtun balance in the Kuroshio west of Kyushu should be almost geostrophic. Can this basic dynamic balance be demonstrated from our current measurements? Calculation of absolute geostrophic velocity, using the averaged ADCP velocity at 60 m as the reference level, in January, 1986 allows us to answer the question here by the comparison between the absolute geostrophic and averaged Doppler velocity profiles. These comparisons are shown in Figure 3.14 (a-i). The maximum difference, the mean difference and its deviation over the available depth interval are also shown in Table 3.2. For most station pairs except station pair 131-132, the vertical shear of absolute geostrophic velocity was in good agreement with the average ADCP velocity, implying that the thermal wind relation was a good approximation in the cross-stream direction in the Kuroshio. Although the maximum errors exceeded 10 cm/s for some station pairs, mean errors were less than 4.0 cm/s in magnitude, and their deviations relative to the mean errors were small except station pairs 125-126 and 131-132.

At station pair 131-132, the vertical shear of absolute geostrophic velocity was much different from the average ADCP velocity, and the deviation relative to the mean also exceeded 7 cm/s, an amount greater than 10 percent of total averaged velocity. This station pair was located at the margin of the Kuroshio outflow and its recirculation where the radius of curvaure R for the local flow was probably of order 20 km, yielding a curvature Rossby number $R_r = \frac{U}{fR} = 0.5$. The observed poor agreement between

the geostrophic and ADCP velocity shears is probably due to both curvature and time dependent effects.

The large deviation at station 125-126 and large maximum errors found at some other station pairs may also be due to measurement errors in the ADCP since these deviations were all located in the deeper depth bins of the ADCP where the ratio of signal to noise was small.

In hindsight, it is not surprising that the good coincidence between the ADCP and geostrophic velocities near the surface were observed because there were very weak winds at the surface in the time interval of the January 1986 survey (Limeburner, personal communication). Consequently the directly wind driven flows (Ekman flow and inertial motions in the surface water) were probably weak.

Table 3.2: Comparison between tha averaged ADCP velocity and absolute geostrophic velocity

station pair	maximum difference $\triangle u_{max}$ (cm/s)	mean difference $\overline{\triangle u}$ (cm/s)	standard deviation $\sigma_{\triangle u}(cm/s)$	depth interval (m)
124-125	-8.9	-1.7	4.0	1.5–118.5
125-126	-17.7	-3.2	7.1	4.5–127.5
126-127	2.8	-0.4	1.4	4.5–124.5
127-128	-4.4	-0.3	1.3	4.5–139.5
128-129	16.0	3.6	3.7	4.5–139.5
129-130	-7.3	-3.5	2.6	4.5–142.5
130-131	-5.2	-0.5	3.1	4.5–148.5
131-132	-14.1	0.5	7.1	4.5–100.5
132-133	-5.1	1.2	2.5	4.5–127.5
133-134	9.1	1.9	3.9	4.5–127.5
134-135	9.5	1.1	4.5	1.5–139.5
135-136	-5.2	-0.1	2.7	1.5–133.5
136-137	2.2	-0.3	1.1	1.5–139.5
137-138	3.5	0.7	1.4	1.5–139.5

3.4 Conclusion

A large southward displacement of the Kuroshio was found between January and July, 1986 in the study area. The axis of maximum velocity of the Kuroshio on the upstream western section was located at the center of the Okinawa Trough in January, 60 km away from the shelf break. It had shifted southward about 35 km in July. The width of the Kuroshio was about 120 km when it left through the eastern section in January, but was reduced to a narrower region of about 75 km south of a tall seamount in July.

A simple averaging technique has been used to convert the ADCP data in January, 1986 into an absolute velocity. A detailed error analysis shows that the total error in the average ADCP absolute velocity was within $\pm 5\ cm/s$. The absolute geostrophic velocity using the average Doppler velocity at 60 m (or 10 m over the shelf) as the reference velocity was then calculated for the sides of the triangle. The results show that the ADCP velocity shear was in reasonably good agreement with the geostrophic shear in the Kuroshio. The Kuroshio flowed through the western section as a coherent current, and then split into two streams around a tall seamount as it left through the eastern section. Some countercurrents were found on the western section between the maximum velocity core of the Kuroshio and the slope, and on the eastern section north of the northern maximum velocity core of the Kuroshio as well as on the northern section over the slope. The bottom velocity in the Kuroshio was about 10 cm/s on the western section and about 20-30 cm/sec on the eastern section. These flow features illustrate the importance of using direct current measurement ADCP data to calculate the absolute geostrophic velocity.

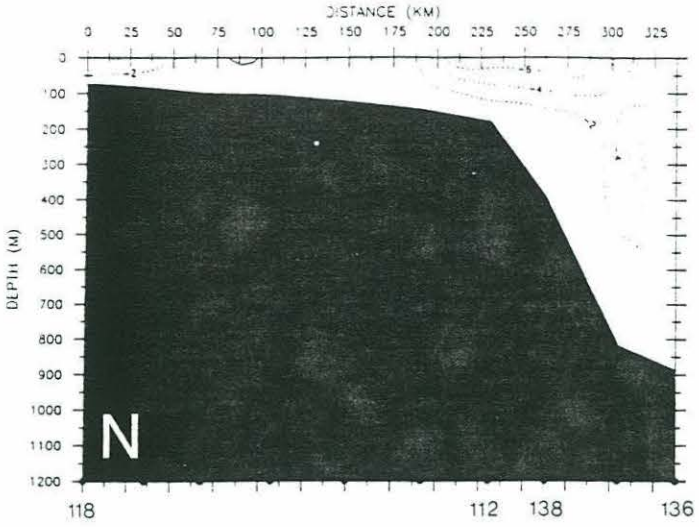

Figure 3.1:

The January 1986 cross-stream structure of geostrophic velocity relative to the bottom.
Positive: inflow.
Negative: outflow.

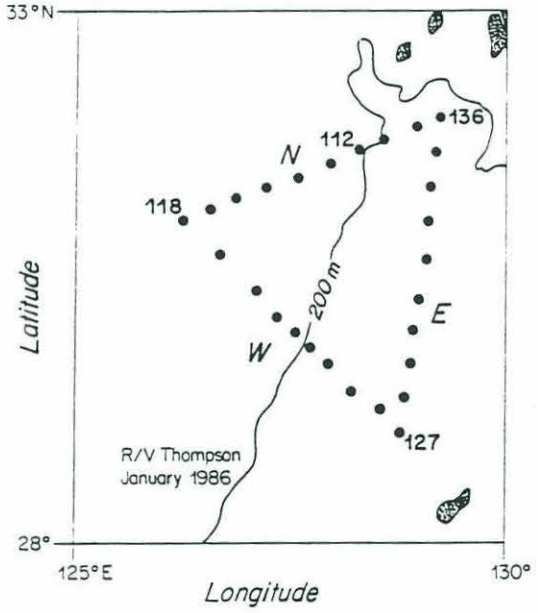

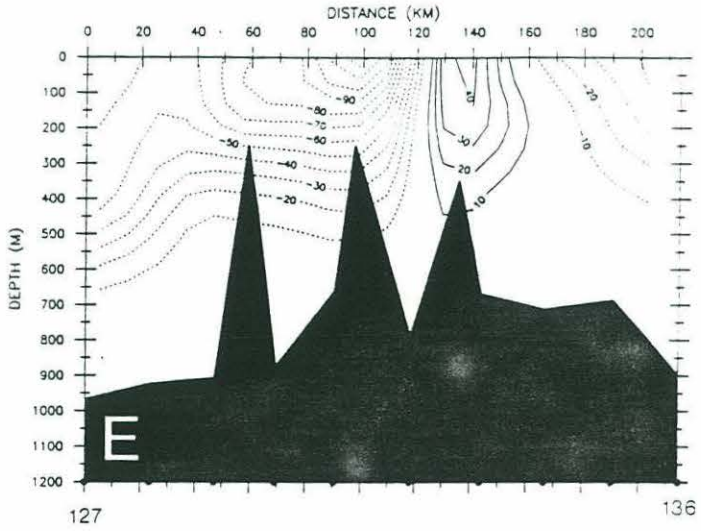

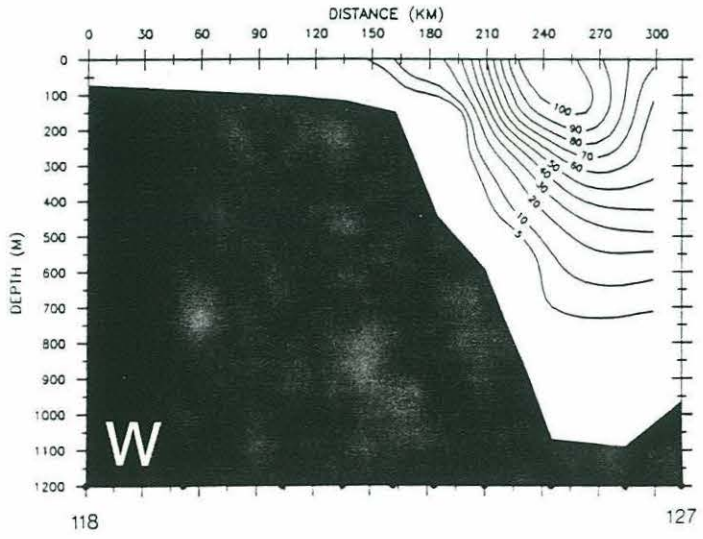

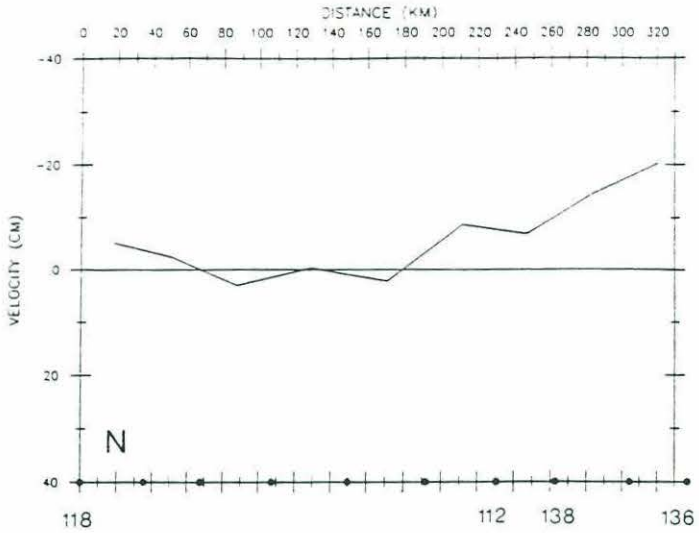

Figure 3.2:

The January 1986 surface geostrophic velocity.
Positive: inflow.
Negative: outflow.

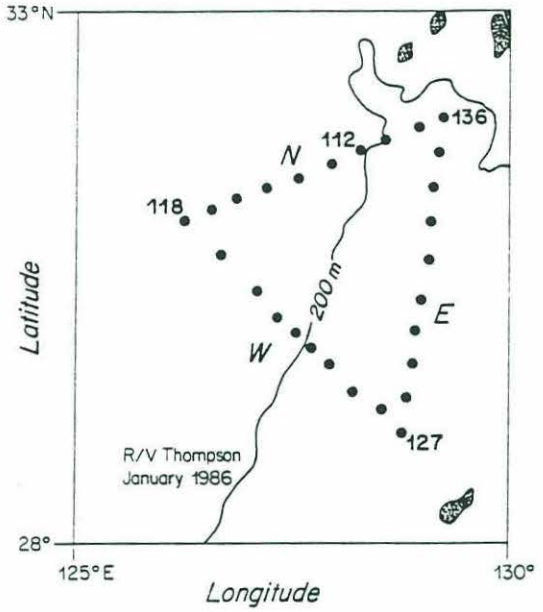

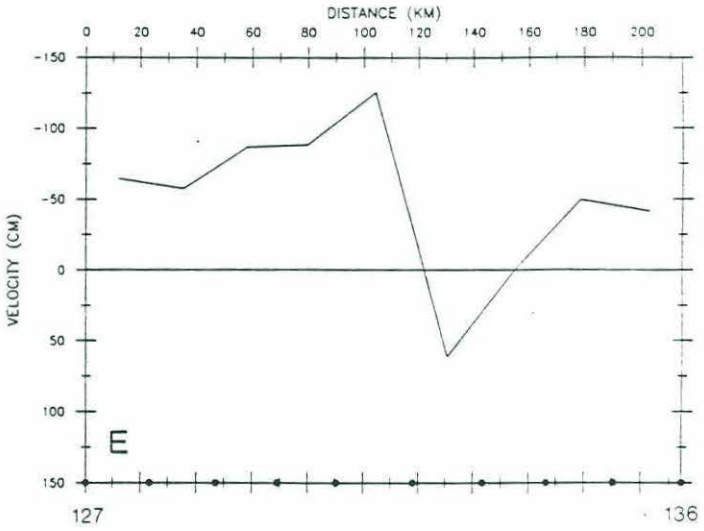

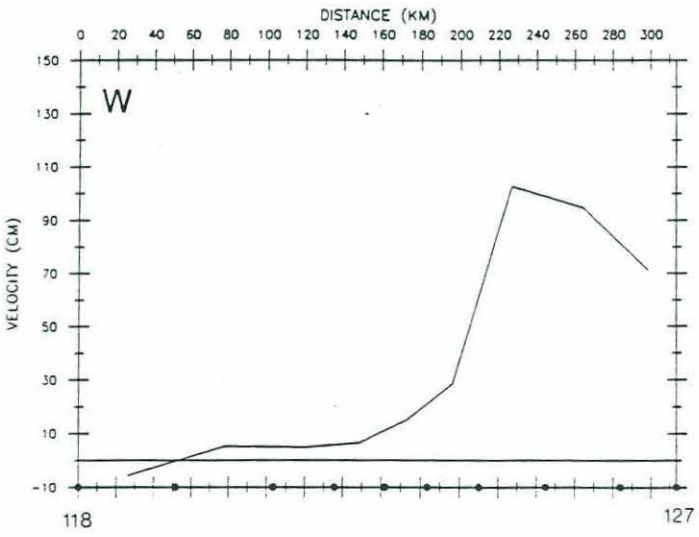

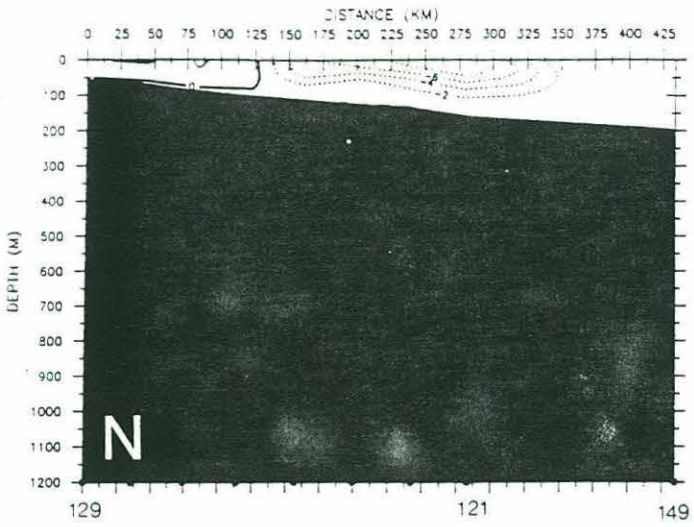

Figure 3.3:

The July 1986 cross-stream structure of geostrophic velocity relative to the bottom.
Positive: inflow.
Negative: outflow.

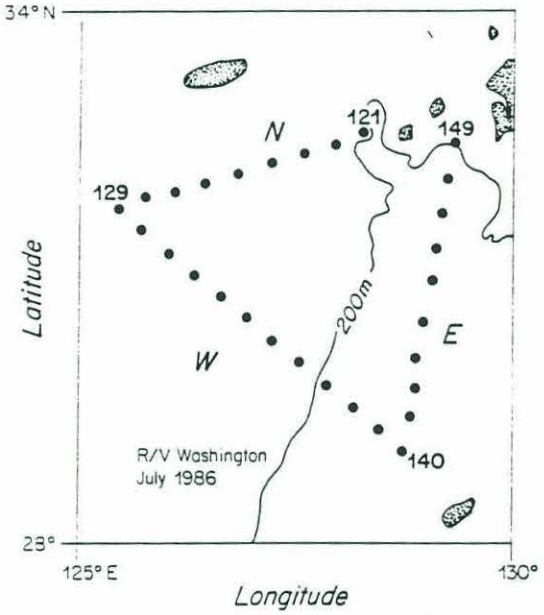

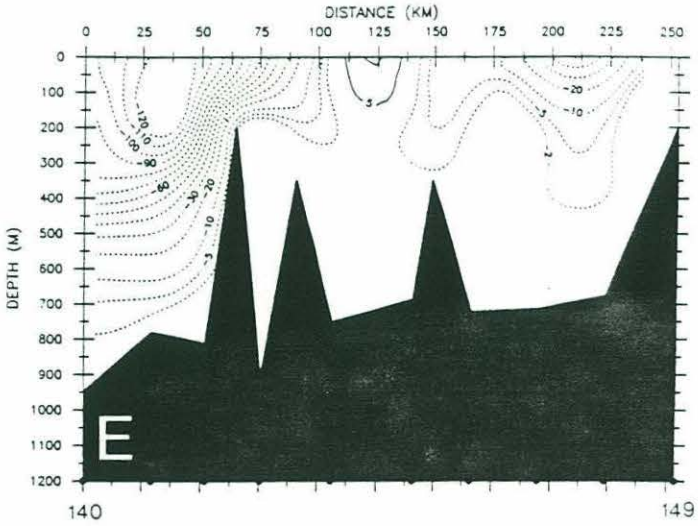

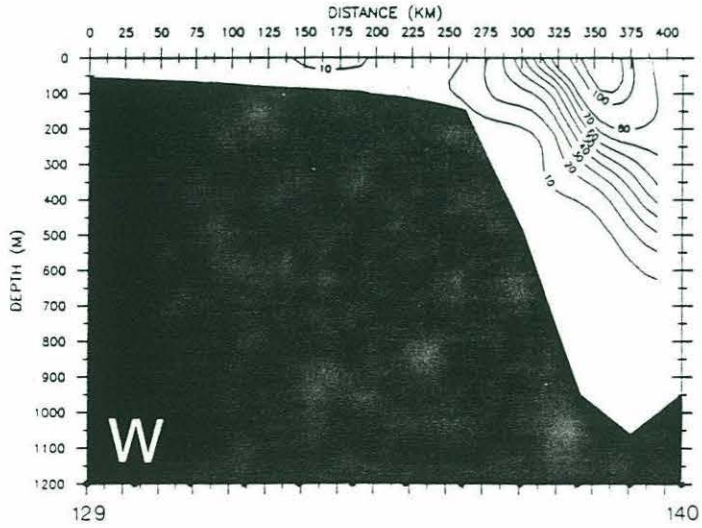

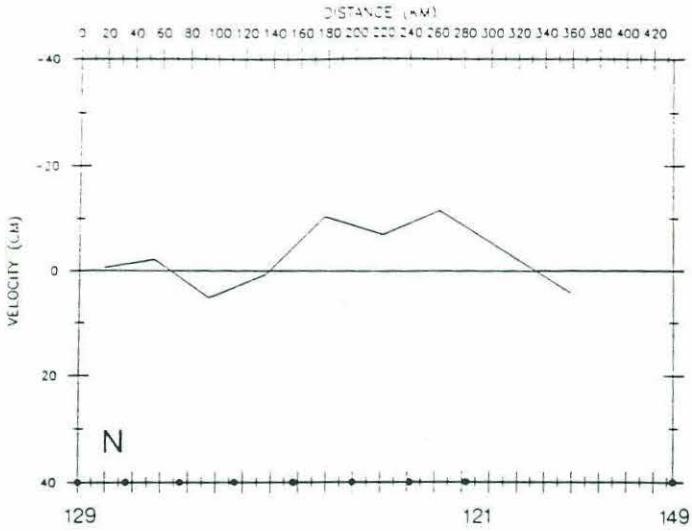

Figure 3.4:

The July 1986 surface geostrophic velocity. Positive: inflow. Negative: outflow.

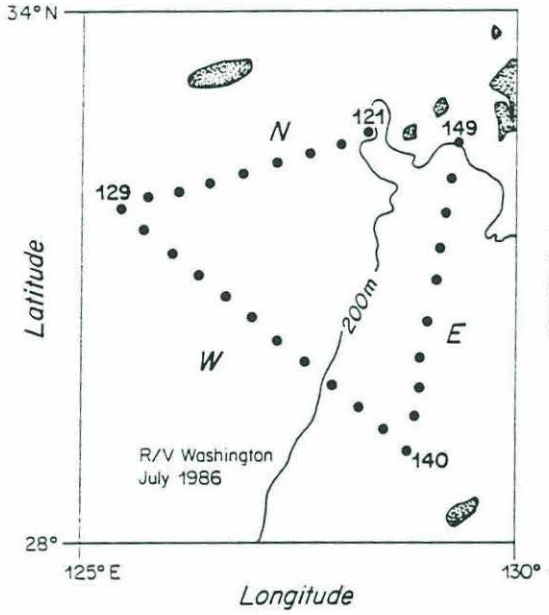

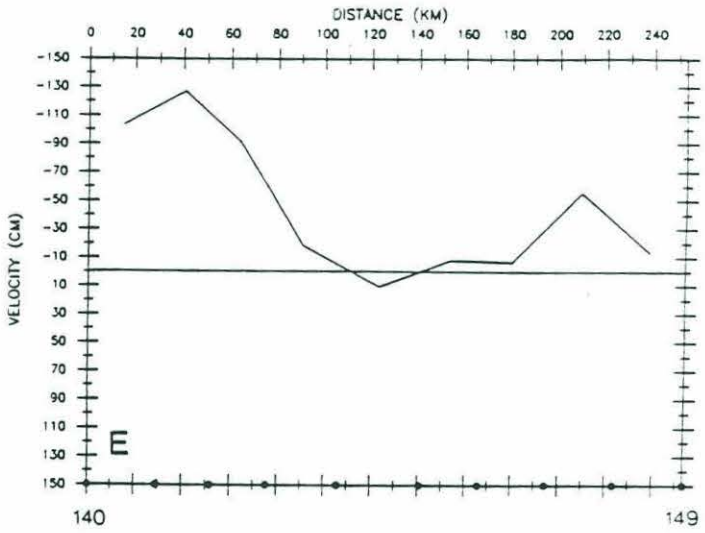

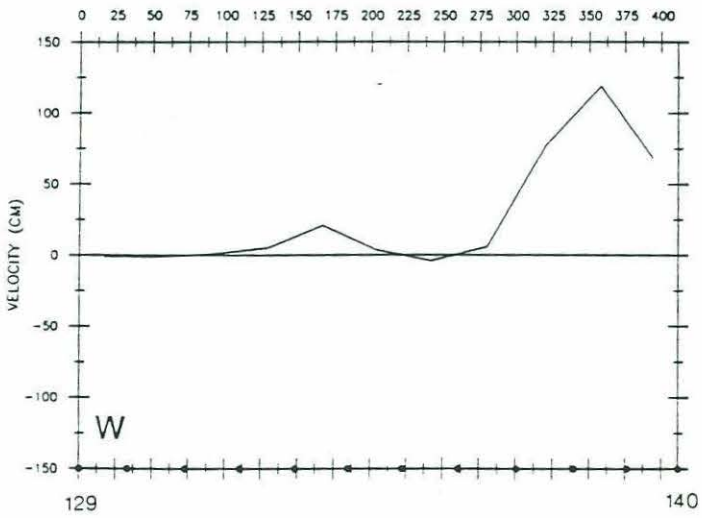

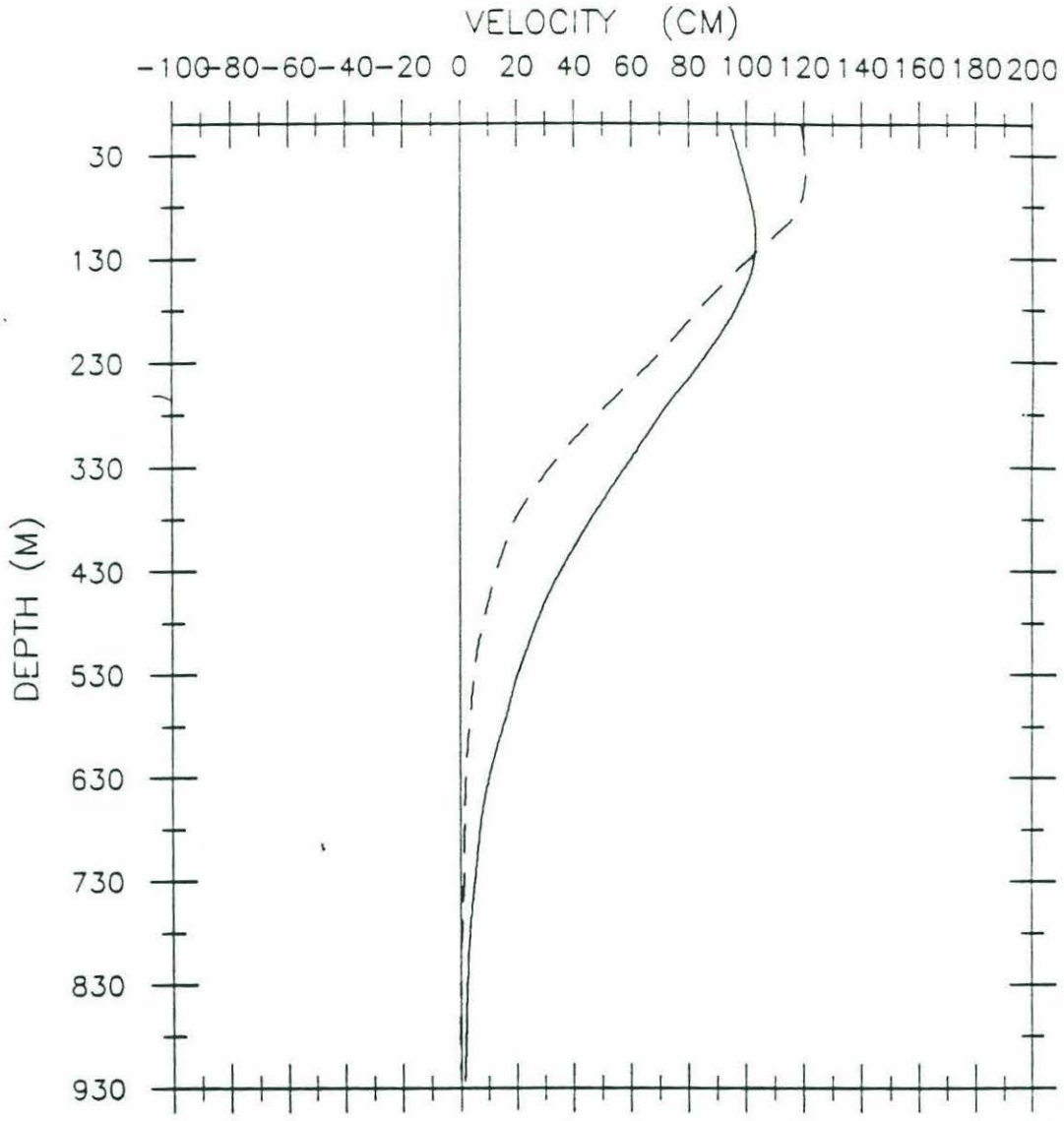

Figure 3.5: The comparison between the January and July geostrophic velocities relative to the bottom on the western section (station pairs 125-126 and 138-139).
Solid line: January
Dash line: July

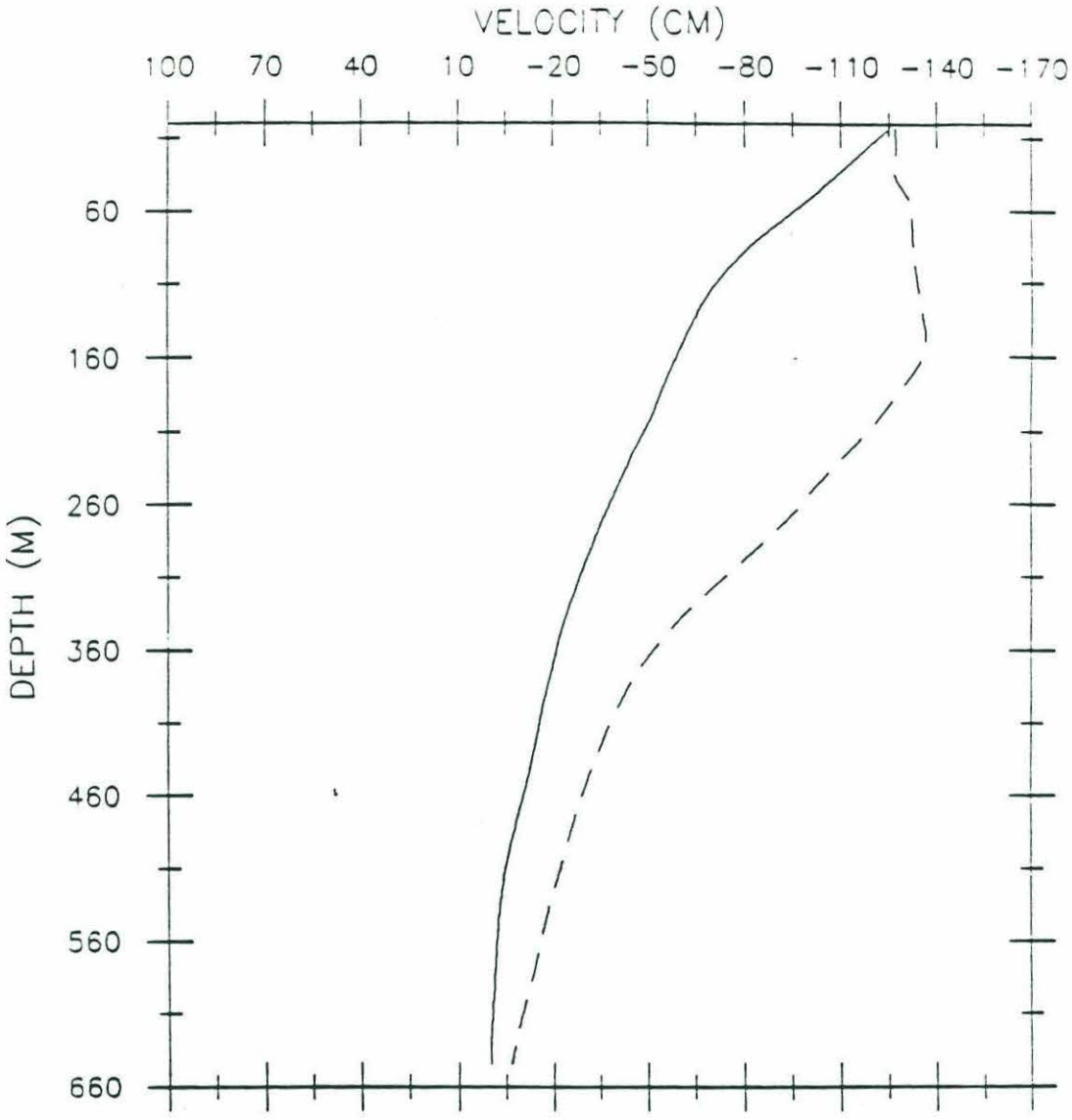

Figure 3.6: The comparison between the January and July geostrophic velocities relative to the bottom on the eastern section (station pairs 131-132 and 141-142).

Solid line: January.

Dash line: July.

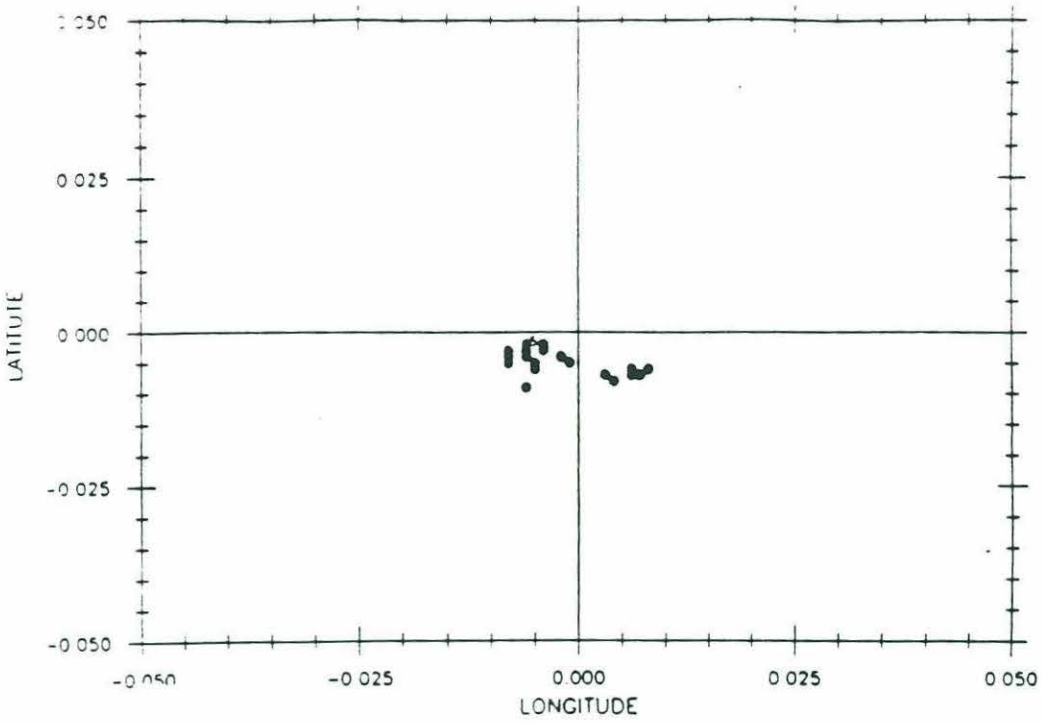

Figure 3.7: The difference between Loran.C and GPS data.

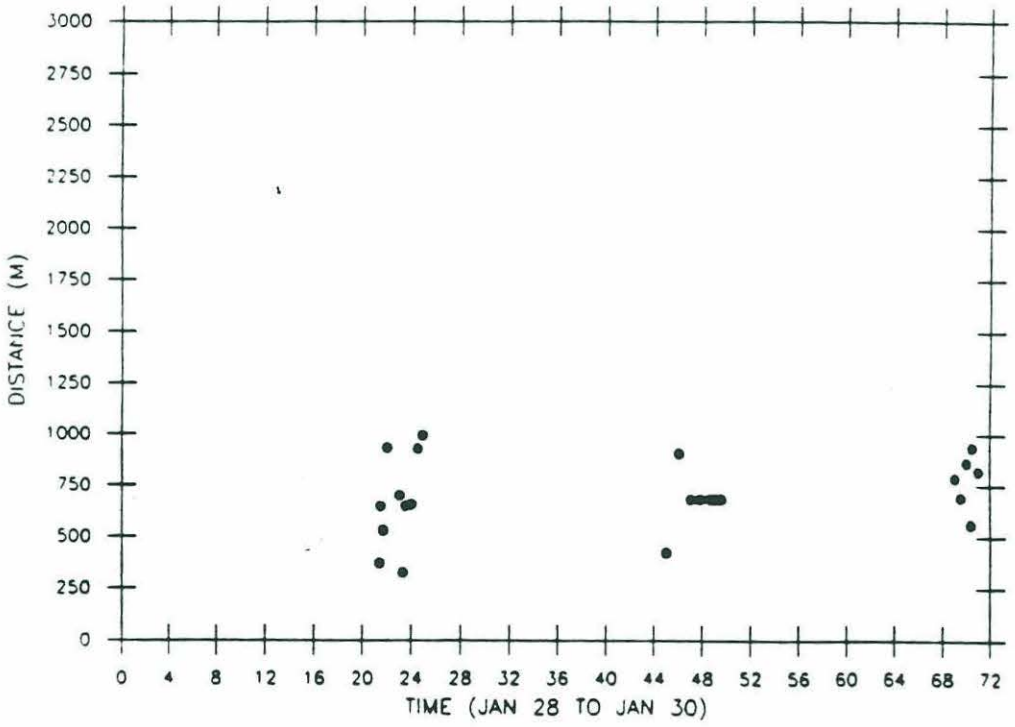

Figure 3.8: The distance from Loran.C fix to the GPS fix.

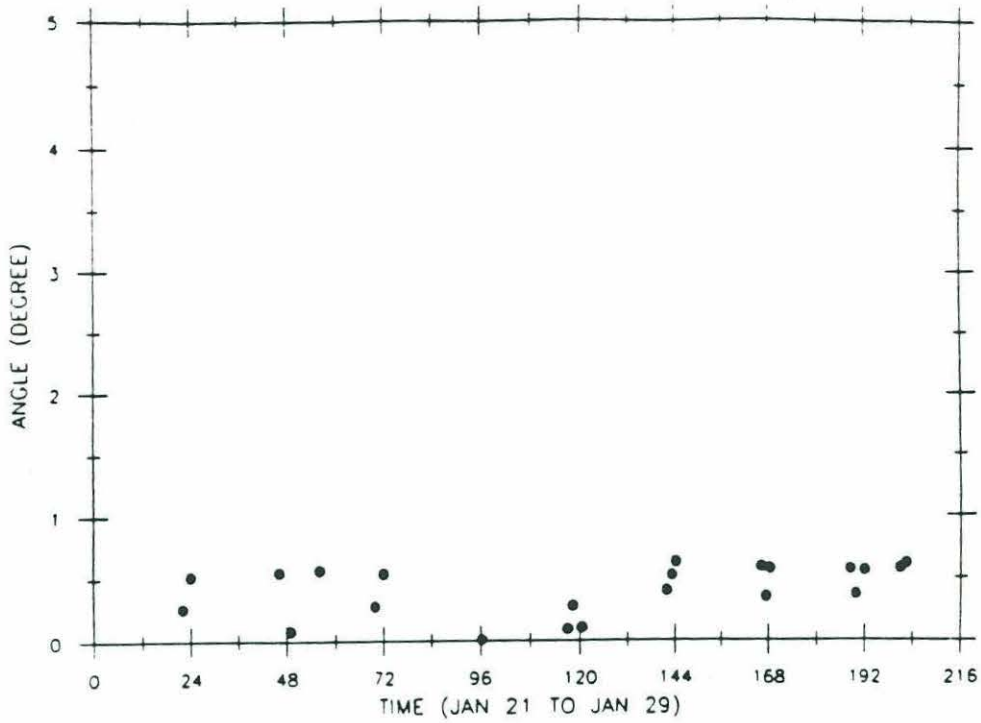

Figure 3.9: Misalignment error.

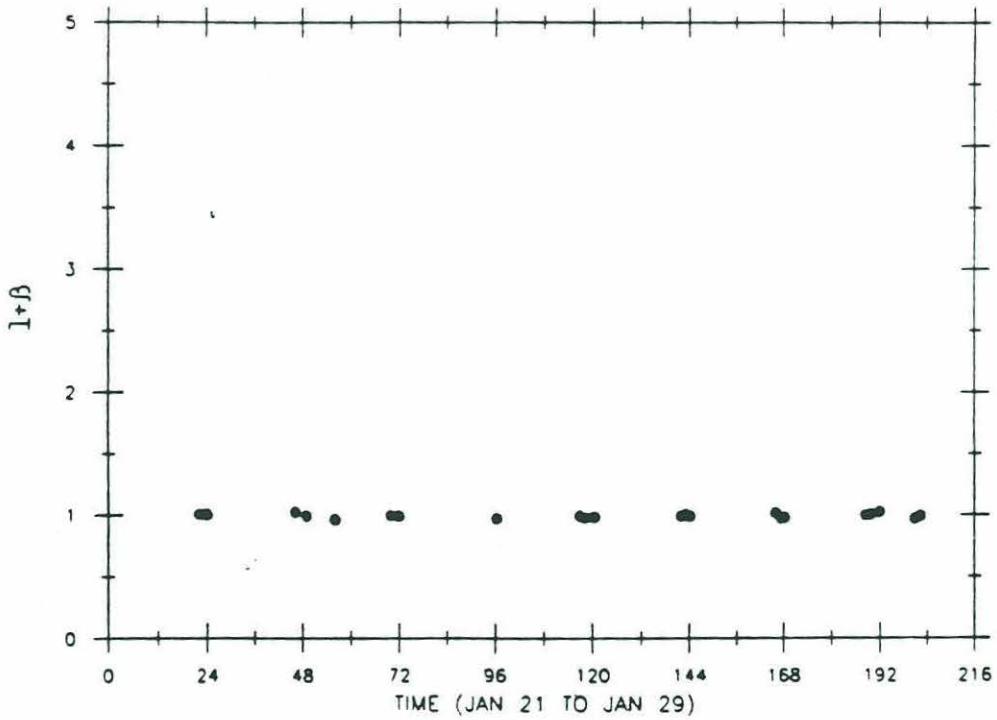

Figure 3.10: Sensitivity error.

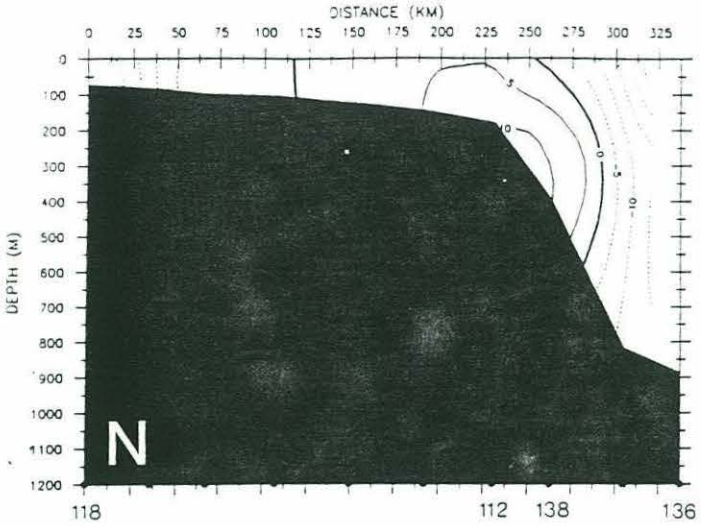

Figure 3.11:

The January 1986 cross-stream structure of the absolute velocity.
Positive: inflow.
Negative: outflow.

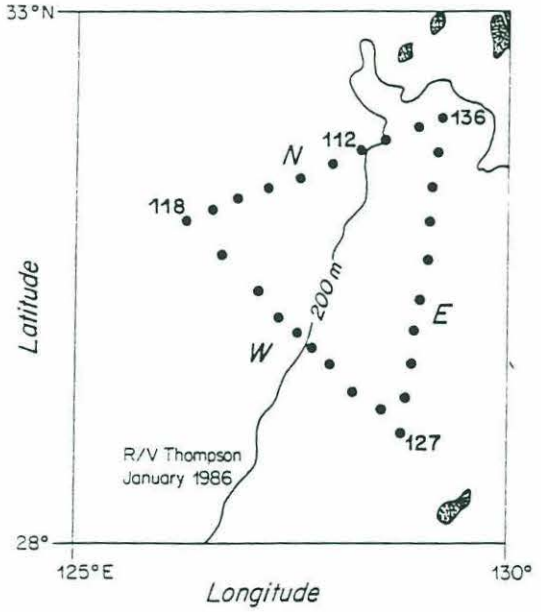

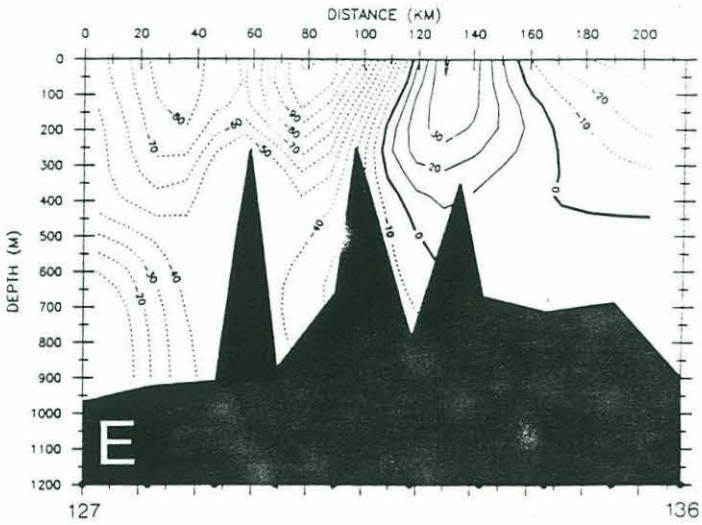

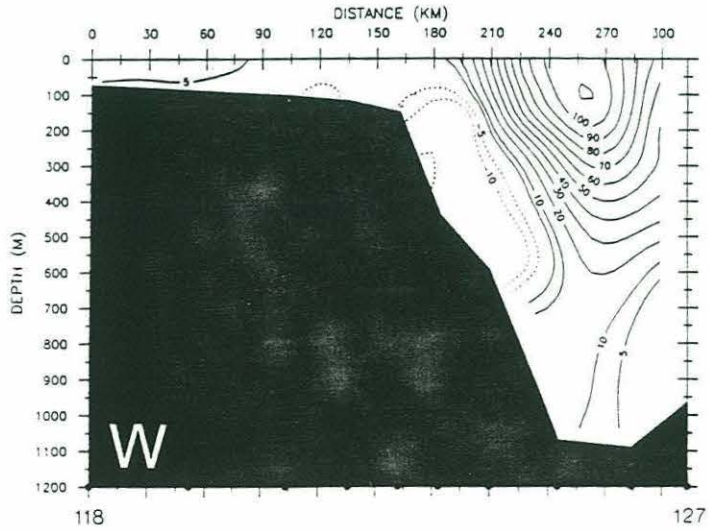

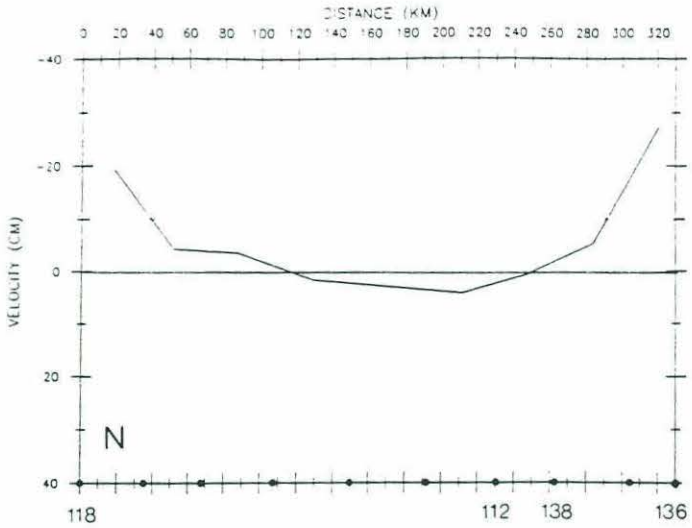

Figure 3.12:

The reference level velocity at 60 m on the triangle section except over the shelf where 10 m is chosen (N: northern E: eastern; W: western). Positive: inflow. Negative: outflow.

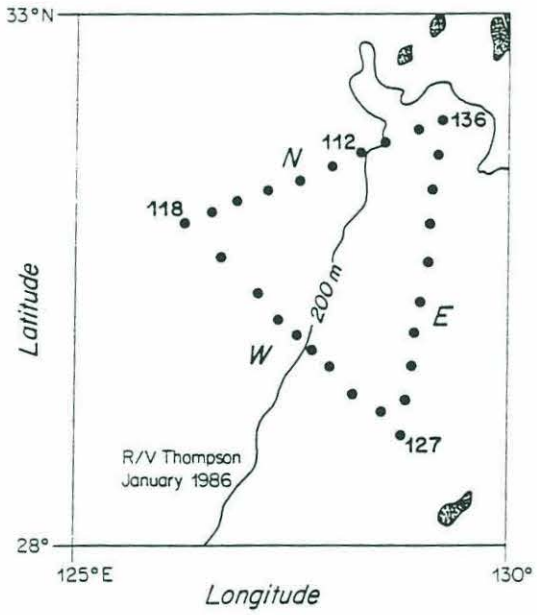

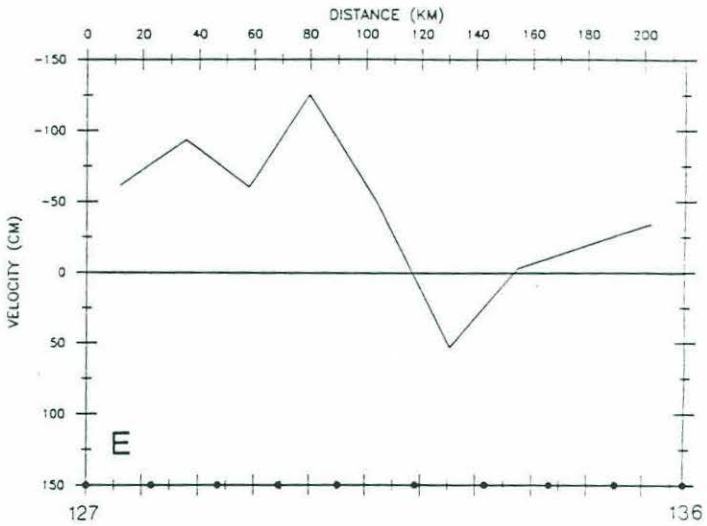

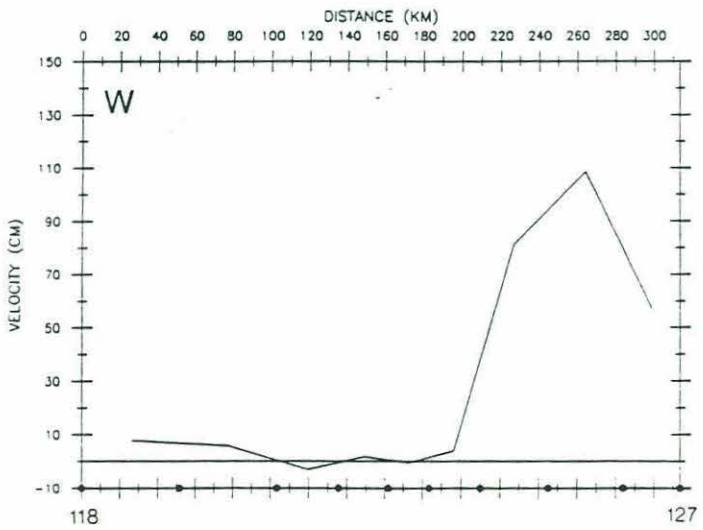

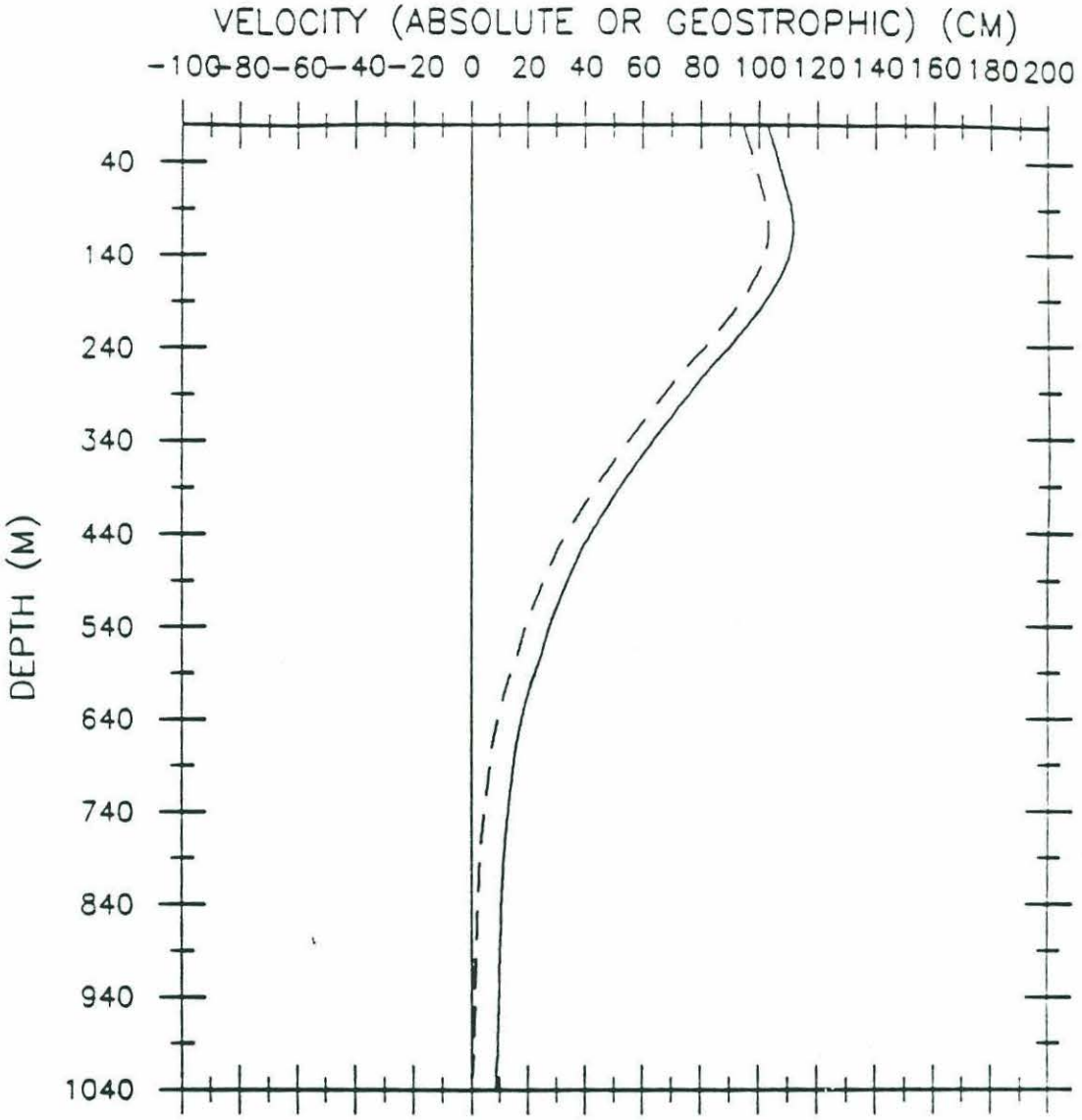

Figure 3.13: The comparison between the absolute and relative velocities at station pair 125-126 on the western section.
Solid line: absolute velocity.
Dash line: relative velocity.

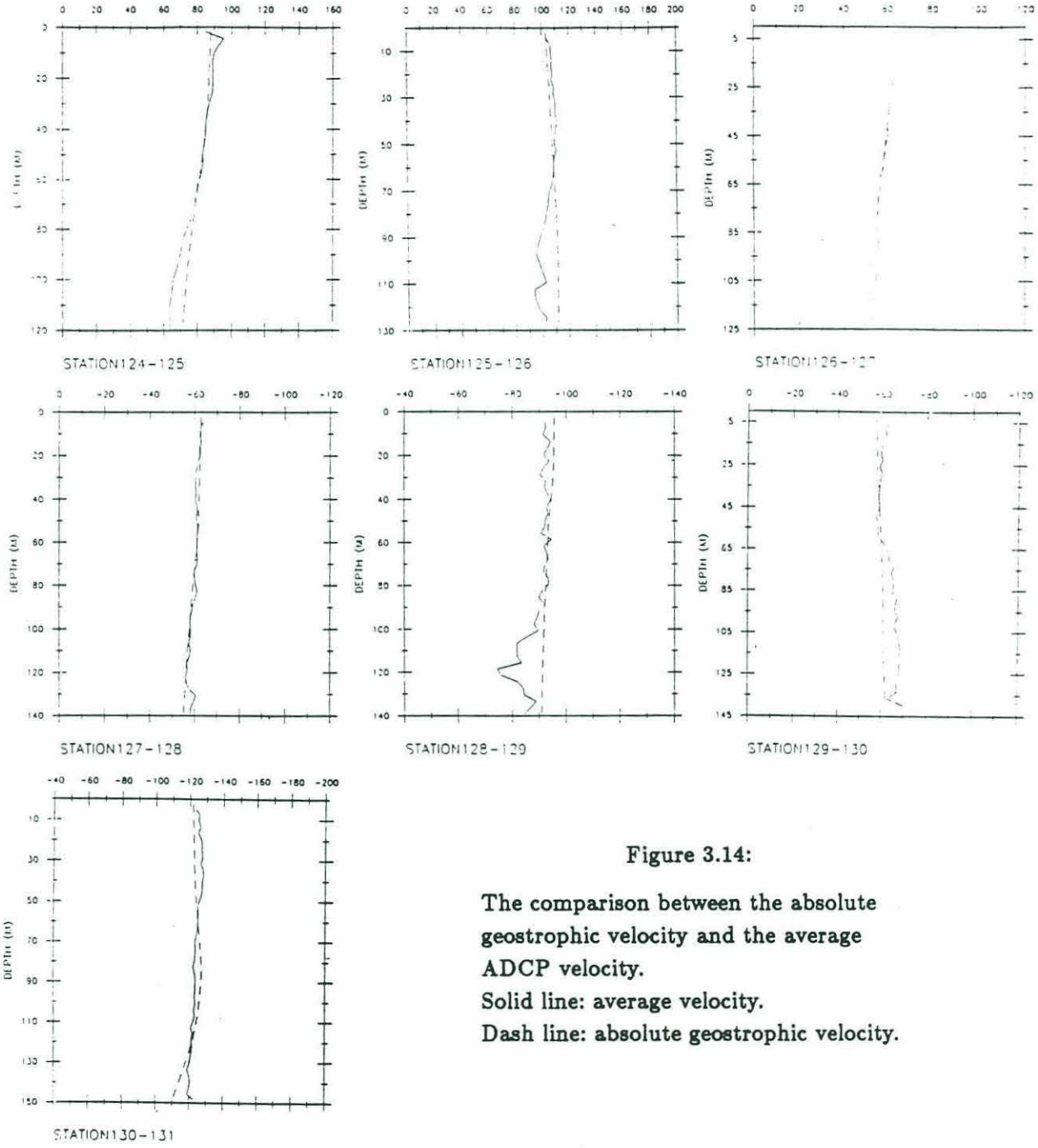

Figure 3.14:

The comparison between the absolute geostrophic velocity and the average ADCP velocity.
Solid line: average velocity.
Dash line: absolute geostrophic velocity.

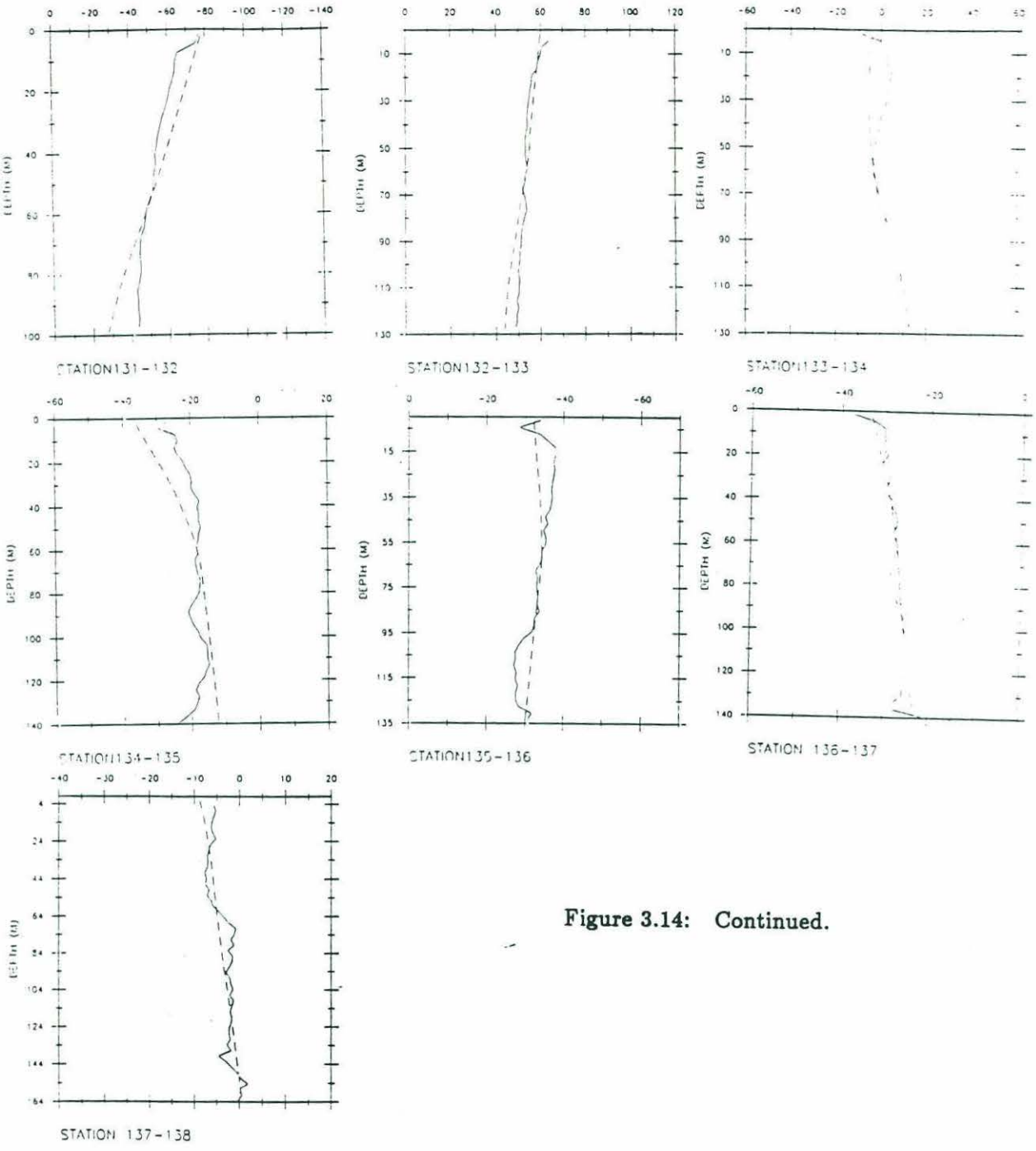

Figure 3.14: Continued.

Chapter 4

The Geostrophic and Absolute Geostrophic Transports

4.1 Introduction

To understand the role of the Kuroshio in maintaining the global oceanic and atmospheric climate, it is fundamentally important to know its volume, heat and salt transports. Study of transports of the Kuroshio can be traced back to World War II during which most of the observations were made south of Japan by Japanese fishermen and navigators. Since then, many studies have been made on the Kuroshio from its beginning near Luzon Island to the Kuroshio extension at 40°N. A summary of previous transport estimates of the Kuroshio is given in Figure 4.1 and Table 4.1. The Kuroshio changes a lot in its transport when it flows from south to northeast through the East China Sea. The large transports east of Luzon and Taiwan are believed due to the existence of large warm eddies. The smooth downstream increase in total transport south of Japan due to recirculation and eddies is similar to the Gulf Stream north of Florida Strait (see Figure 4.2 and Table 4.2 taken from Knauss, 1969), implying a dynamical similarity of the western boundary current in these two regions. However, unlike the Gulf Stream system where absolute volume transports are relatively well known from combined CTD and direct current measurements, very few good estimates of the absolute transports of the Kuroshio have yet been made. Most previous transport calculations are based on the assumption of a deep level of no motion.

The interannual variability of the Kuroshio was described first by Saiki (1982) who calculated annual volume transports of the Kuroshio in the East China Sea near 27°N and 126°E from 1955 to 1978 based on the geostrophic velocities relative to 700 db, and found 5.5 and 8 year period variations of volume transport in the Kuroshio. On the same survey section, Pu et al(1987) discussed the seasonal variation of volume transport in the Kuroshio by calculating the monthly baroclinic volume transport of the Kuroshio relative to 800 db over the 48 cruises from 1972 to 1982 (Figure 4.3). They found that there were two maximum peaks of the transport in the Kuroshio around a year; one was in later spring between March and May, another was in summer between July and August. A similar result was obtained by Blaha and Reed (1982), who calculated the seasonal amplitude of the sea level difference across the Kuroshio in the Tokara Strait. Based on Pu's transport data shown in Figure 4.3, we calculated the deviation of monthly volume transport to the annual mean value. The results show that the mean deviation to the annual transport over ten years was about 2 Sv but the extrema can reach 5.3 Sv difference from mean for some years. A similar seasonal variability structure was also found in the Gulf Stream in the Florida Strait near 27°N by Leaman (1987) who calculated monthly absolute volume transport averaged over two years from April 1982 through July 1984 using PEGASUS data. He found that both the baroclinic and barotropic volume transports had two maximum peaks in May and July or August. The variability was much larger in the barotropic component than in the baroclinic (Figure 4.4). The maximum deviation of the monthly mean transport to its annual mean value exceeded 4 Sv in the barotropic part but it was just 1-2 Sv in the baroclinic part. Although there is at yet no corresponding time series of absolute volume transport measurement in the Kuroshio, we can still see some similarity in the seasonal variation between the Kuroshio and Gulf Stream in the baroclinic transport. On the other hand, the large contribution of the barotropic component to the seasonal variation of volume transport in the Gulf Stream implies an

importance of absolute velocity measurement in determining the seasonal structure of western boundary currents.

A direct measurement was recently made in the Kuroshio off Tanegashima Island, south of Kyushu by Takematsu *et al.* (1986), who used moored current meters to measure the absolute velocities in the upper 1000 m from 1972 to 1982. The total volume transport was estimated to be 25 Sv south of Tanegashima Island, at 30°N, 131°E, downstream of our study area. Bryden *et al.*(1987) used the average Doppler velocity at 100 m as the reference velocity for their geostrophic calculations and found that the total volume transport was equal to 26 Sv near Ryuku Islands, at 26°N, 125°E, about 350 km upstream of our triangle area. If the seasonal and interannual variabilities were small, the volume transport through our study triangle section should be very similar to their results.

The January CTD data and computed absolute geostrophic velocity field allow the direct calculation of volume, heat, and salt transports in the Kuroshio during January, 1986. In addition, the calculations of geostrophic volume transports relative to the bottom for January and July provide a possible view of its seasonal variation. All of these will be discussed in detail in sections 4.2-4.4, respectively. Since the results show that the volume transports through the triangle domain were conserved within the measurement uncertainty, a streamfunction can be defined by the transport. The streamfunction will be used in section 4.5 to determine the horizontal structure of the flow field in the study triangle. Conclusions will be made in section 4.6.

4.2 Volume Transports

The two triangle surveys made on the R/V Thompson and R/V Washington cruises provide across-stream profiles of geostrophic velocity so that the geostrophic volume transports of the Kuroshio can be estimated. The island located near the

southern corner of the triangle confines the Kuroshio on its southern side, and it is generally believed that the Kuroshio countercurrent is dominant to the south of the island (Nitani, 1972). Thus, calculation of transport through the triangle section should include almost all of the transport through the Okinawa Trough but not the net transport through the East China Sea. In addition, the smooth topography on the western section makes the calculation of transport more accurate than the other two sections. Therefore, the transport estimates for the western section should be representative of the Kuroshio transport.

Geostrophic Volume Transports relative to bottom

Figure 4.5 shows the results of the volume transport calculations based on the geostrophic velocities relative to the bottom for the January 1986 R/V Thompson cruise. The total eastward transport was found to be 33.8 Sv on the western section, and -31.0 Sv on the eastern section as well as -2.5 Sv on the northern section. The net inflow into the triangle was equal to 0.3 Sv, implying a good conservation of the transport in this closed triangle domain. However, such a conservative result of transports may be obtained by accident because the sharp seamounts were not taken into account in the calculations of transport on the eastern section. On the other hand, the seamounts on the eastern section were related to the outflow of the Kuroshio and the countercurrent, respectively, and then the contributions of these seamounts on the flow may cancel each other so that the conservative transport system was obtained in our results. The similar calculations done for the July 1986 R/V Washington cruise are shown in Figure 4.6. The total eastward volume transport was estimated to be 31.7 Sv on the western section and -29.0 Sv on the eastern section as well as -0.3 Sv on the northern section. The net inflow transport was equal to 2.4 Sv, still implying a conservative transport field within the uncertainty of these measurements.

A comparison between the July and January volume transports of the Kuroshio may be made using the T/S analysis presented in section 2.4 to indicate that the inner

edge of the Kuroshio is at station 122 in January and at station 133 in July. The corresponding transports of the Kuroshio, according to this definition, were 33.7 Sv in January and 31.7 Sv in July, a difference of 2.0 Sv. Since the core of the Kuroshio moved southward during July, 1986, some transport near the southeast corner of the triangle section was probably missed due to the incomplete coverage across the East China Sea. The distance from the southeast corner of the triangle to the island is about 10 km, the average depth between them is 800 m. If the velocity decreases linearly from a value of 0.7 m/s at the surface to zero at the bottom, then the missed transport in the July survey would be 2.8 Sv. Therefore, the calculated difference of 2 Sv may not be representative of seasonal variation of the volume transports of the Kuroshio. On the other hand, the large transport, as mentioned before, usually occurs in later spring between March and May or in summer between July and August. A small difference in transport between January and July 1986 may imply a weak seasonal variability in that year.

It should be noted that the geostrophic transports relative to the bottom missed the contribution of the barotropic part of the current field. As we know, the bottom velocity in the Kuroshio west of Kyushu was not equal to zero in the study triangle. Therefore, the transports obtained from relative velocities are not necessarily representative of the true transports of the Kuroshio, especially if the barotropic velocity component changes with time, as is likely as in the Gulf Stream in the Florida Stream.

Absolute Geostrophic Volume Transport

One problem in calculating geostrophic transport is our poor knowledge of the bottom bathymetry along the eastern transect, especially near the seamounts. In order to overcome this difficulty, we consider two limiting cases. First, we ignore the seamounts completely and assume a smooth deep bottom. Second, we treat the seamounts as rectangular shapes. Therefore, the true transport should be between these two limits. The absolute volume transports in January, 1986 calculated with the

smooth deep bottom on eastern section are shown in Tables 4.3 - 4.5. The total inflow transport of the Kuroshio was equal to 30.3±2.0 Sv on the western section, while the outflow transports were -26.3±2.7 Sv on the eastern section and -4.6±0.4 Sv on the northern section. The net transport into the triangle was - 0.6 ±3.3 Sv. When rectangular seamounts are assumed for the eastern section, the outflow transport on the eastern section increased to -30.1±2.6 Sv (see Table 4.6). The real outflow transport on the eastern section was likely between -26.3±3.0 Sv and -30.1±2.6 Sv. Considering the size of the experimental uncertainties of these transport estimates, we conclude that the total volume transport field was conserved in the closed domain.

The missed transport due to the incomplete coverage of the passage can be roughly estimated using the same method as before. The distance from the southeast corner of the triangle to the island is 10 km. The depth is 800 m at the southeast corner of the triangle and zero at the coast of the island. If the velocity was assumed as 60 cm/s at the surface and 10 cm/s at the bottom (based on the velocity profile at station pair 125-126), then, the missed transport is estimated to be 1.4 Sv, only 4.7 percent of the total absolute transport. The total transport over the shelf region was almost equal to zero. Therefore, the best estimate of Kuroshio volume transport in January, 1986 should be expressed by the transport on the western section plus the missed transport at the southeast corner of the triangle, which is 31.7 ± 2.0 Sv.

The small difference between the absolute and relative volume transports is within measurement uncertainty. Relative volume transport calculations overestimated the transport by missing of the recirculations on the flanks of the Kuroshio while underestimating the velocities in the center of the Kuroshio where the bottom velocity was about 10 cm/sec.

The westward outflow transport over the slope region in the western section was about 0.5 Sv. This outflow is probably recirculated from the main Kuroshio near the western section since there was no evidence of similar T/S curves on the downstream

sections. A large countercurrent transport of order 4.1 Sv to 6.9 Sv was found on the eastern section. At the same time, the same order outflow transport of 6.8 Sv was also found around the northeastern corner of the triangle from stations 134 to 137, suggesting the outflow near the northeastern corner may come from the recirculation on the eastern section. In addition, on the northern section, an inflow transport of 1.0 Sv was computed for the band of station 112-115 and 137-138 as well as 138-112 . Based on the results of the T/S analysis presented in section 2.4, this inflow may come partly from the recirculation on the northeast corner of the triangle and partly from the southward flow prevailing around the year over the shelf (Nagata, 1981). A clear path of the Kuroshio and its adjacent currents will be given in section 4.5 when the streamlines are defined by the transports.

4.3 Heat Transport

It is well known that the net absorption of solar heating over the globe is unequally distributed from the equator (net gain) to the pole (net loss). The atmosphere and ocean must transfer this heat poleward in order to maintain a quasi-steady global climate. The fact that there is the net poleward heat transport in the North Atlantic and North Pacific Oceans has been demonstrated in many previous papers (Oort and Vonder Haar, 1976; Wunsch, 1978; Hastenrath, 1980; Roemmich 1984; Hall and Bryden, 1982; Bryden et al., 1987 etc.,). In the North Atlantic and North Pacific, the basic pattern of circulation consists of a two gyre system, with subtropical and subpolar gyres. Most of the subtropical gyre is dominated by slow southward flow except near the western boundary where there exists a strong northward boundary current such as the Kuroshio and Gulf Stream. Therefore, the Gulf Stream and Kuroshio play an important role in providing poleward heat transport.

The direct method to calculate heat transport is given by

$$Q_T = \int\int C_p \theta V \, \rho dz dx, \tag{4.1}$$

where ρ is the fluid density , C_p the specific heat capacity, θ potential temperature and V the north-south component of absolute velocity. Since the choice of temperature scale is arbitrary, the heat transport obtained directly above is meaningful only when the mass of the system is conserved (Montgomery, 1974). For this reason, oceanic heat transport is usually computed on a section across the whole ocean basin based on the assumption that a southward interior mass transport equals the sum of the wind driven Ekman and northward western boundary current transports. The calculation of heat transport of the Kuroshio or Gulf Stream (strictly speaking, it should be called the temperature transport, see Hall and Bryden, 1982)[1], as a part of the total heat transport, is useful to understand the contribution of the Kuroshio (or Gulf Stream) to the net poleward heat transport. An example is given by Hall and Bryden (1982) who divided the velocity and the potential temperature into a sum of a barotropic and baroclinic components, i.e,

$$Q_T = \int\int \bar{V}\bar{\theta} C_p \rho dz dx + \int\int V'\theta' C_p \rho dz dx, \tag{4.2}$$

and calculated the heat transport of the Gulf Stream in the Florida Strait. Using the Niiler and Richardson (1973) volume transport measurements where the volume transport equaled 32.9 Sv in summer with an annual average of 29.5 Sv, Hall and Bryden found that the baroclinic heat transport equaled 5.0 $\times 10^{14}$ W, while the barotropic part was about 21 $\times 10^{14}$ and 18.8 $\times 10^{14}$ W, respectively corresponding to the summer and annual volume transports. Thus, the total heat transport of the Gulf Stream in the

[1] We will use " heat transport " but mean " temperature transport ".

Florida Strait was approximately equal to 23.8×10^{14} W for a volume transport of 29.5 Sv and 26.0 $\times 10^{14}$ W for a volume transport of 32.9 Sv. Bryden et al (1987) also used the same method to estimate the heat transport of the Kuroshio, and found that the baroclinic heat transport at 24°N in June, 1985 equaled 8.9 $\times 10^{14}$ W. The volume transport across the Kuroshio was estimated to be 26.2 Sv and the mean potential temperature was 11.6°C. If $C_p = 4.0\ J/g°c$ and $\rho = 1.026 \times 10^6\ g/m^3$, then the total barotropic heat transport was 12.0 $\times 10^{14}$ W. Thus, the total heat transport at 24°N was 20.9 $\times 10^{14}$ W in June ,1985. Since a typical Kuroshio current is 100 cm/s and Doppler velocity error is about 5 cm/s or 5 percent, we expect that the total heat flux estimated by Bryden et al (1987) will have the same percent error. Therefore, the heat transport of the Kuroshio was $20.9 \pm 1.1 \times 10^{14}$ W for a volume transport of 26.2 ± 1.3 Sv in June, 1985.

In this present work, I will consider the triangle study area as a closed system. The January 1986 volume transport calculations discussed before exhibit mass conservation which allows the estimate of heat transport in such a system. Heat transports for each section in the triangle are shown in Tables 4.3-4.6. The total eastward inflow heat transport on the western section was $27.6 \pm 1.8 \times 10^{14}$ W, while the outflow heat transports were $-26.0 \pm 3.1 \times 10^{14}$ W (without seamounts) or $-27.2 \pm 2.3 \times 10^{14}$ W (with rectangular seamounts), and $-2.4 \pm 0.2 \times 10^{14}$ W on the northern section. The net loss of heat in the triangle was -0.8±3.2 (without seamounts) or -2.0 ±2.9 (with seamounts) $\times 10^{14}$ W. The results indicate that the net heat loss in January at that latitude is not significantly different from zero since the order of the net heat loss was smaller than that of the errors due to the uncertainty of the absolute velocity estimates.

The missed heat transport due to the incomplete coverage of the passage can be roughly estimated using the missed volume transport near the southeast corner of the triangle. Suppose that the average potential temperature and density are 13°C and $1.028 \times 10^6\ g/m^3$, respectively. If $C_p = 4.0\ J/g°\ C$, then missed heat transport

can be estimated to be 0.7×10^{14} W for a volume transport of 1.4 Sv. Therefore, the best estimate of the heat transport across the Kuroshio can be expressed as the sum of the heat transport through the western section plus its missed part near the southeast corner of the triangle which equals 28.2 ± 1.8 $\times$ 10^{14} W for a volume transport of 31.7 ± 2.0 Sv in January, 1986.

Using the mass transport to weigh the heat transport, we can find the " mean temperature ", which is useful to isolate transport change from water temperature change. Interestingly, the mean temperature was colder in the 1985 Bryden's summer data than our 1986 winter data even though the shelf temperatures were colder. In hindsight, the mean temperature in our 1986 summer data was warmer than our winter data, suggesting that some special cooling processes might occur in the 1985 summer near Ryuku Islands.

The heat transports for the Kuroshio and Gulf Stream taken from Bryden et al (1987), Niiler and Richardson (1973) and Leaman (1987), together with our present result, are plotted with respect to volume transport in Figure 4.7. A good correlation between the heat and volume transports found in Figure 4.7 implies a small variability in potential temperature for the calculation of heat transport. A linear regression equation can be determined for these heat and volume transports using a least square fit. The root-mean square deviation is about $1.1\times10^{14}W$, which is much smaller than the general uncertainties of heat transport measurements (see Leaman, 1987), implying a linear correlation between heat and volume transports in the Gulf Stream and Kuroshio. What does this mean physically? If mean potential temperature across a section is constant, then all the variabilities of the Kuroshio or the Gulf Stream are barotropic and uniform across the passages.

4.4 Salt Transport

Since the salt does not cross the air-sea interface, there should be no local change of salt. That is, the salt flux divergence through the triangle must be equal to zero. Therefore, the mass conservation in the triangle mentioned before should be demonstrated with the salt transports. A example of salt transport for the January R/V Thompson survey is given in Tables 4.3 - 4.6 based on the estimate of the absolute geostrophic velocity. The total entering salt transport was found to be 108.0 $\pm 7.3 \times 10^{10}$ kg/s on the western section, while the total leaving salt transport equaled a sum of -93.8$\pm$9.6$\times 10^{10}$ kg/s without seamounts to -107.1$\pm$9.3$\times 10^{10}$ kg/s with seamounts on the eastern section and -16.2$\pm$1.4$\times 10^{10}$ kg/s on the northern section. The net salt transport was -2.3$\pm$12.1 to -15.3$\pm$11.9 $\times 10^{10}$ kg/sec. Therefore, in so far as the acceptable errors the salt was conserved in the triangle during January, 1986.

The outflow salt transport on the slope region of the western section was about 5.3×10^{10} kg/s, 4.9 percent of the total salt transport. A large salt transport of about 21.9×10^{10} kg/s due to recirculation of the Kuroshio was found on the eastern section. At the same time, it was also found that about 24.0×10^{10} kg/s salt transport flowed out near the northeastern corner of the triangle from station 133 to station 137, suggesting again that the countercurrent on the eastern section was directly responsible for the outflow near the northeastern corner. A detail discussion for the path of the Kuroshio and its adjacent current is given next.

4.5 Path of the Kuroshio and Its Adjacent Currents

The approximate conservation of volume transport through the triangle discussed before allows us to define a transport streamfunction Ψ by the continuity equa-

tion,

$$\frac{\partial U}{\partial x} + \frac{\partial V}{\partial y} = 0, \tag{4.3}$$

where $U = \int_0^h u dz$, $V = \int_0^h v dz$ are the volume transports in the water column per horizontal unit. Since

$$V = \frac{\partial \Psi}{\partial x}, \tag{4.4}$$

the streamfunction Ψ can be found by integrating the above equation with respect to x,

$$\Psi(x) = \int_{x_\circ}^{x} V dx + \Psi(x_\circ). \tag{4.5}$$

If $x_\circ$ is fixed at the southeast corner point of the triangle, we can set $\Psi(x_\circ) = 0$, and use (4.5) to compute Ψ as a function of x taken here as the distance along the station sections.

The contours of the streamfunction so defined by the absolute geostrophic transport are drawn in Figure 4.8 for the January 1986 R/V Thompson survey. At this time, the Kuroshio flowed through the western section as a coherent current and then split into two branches around the seamount when it left through the eastern section. To the north of the Kuroshio, a countercurrent flowed into the triangle between stations 131 and 133 on the eastern section. This current went up to the slope first and then turned anticyclonically to leave the study region again near the northeastern corner of the triangle. At the same time, on the western section, a small part of the Kuroshio was recirculated on the slope. Combined with the T/S analysis presented in section 2.4, we find that part of outflow near the northeastern corner of the triangle was recirculated cyclonically on the northern section between stations 113 and 138 and then

joined the outflow again between stations 136 and 138. Based on the above pattern of the Kuroshio, we conclude here that the outflow near the northeastern corner of the triangle was mainly from the countercurrent through the eastern section.

Finally, let's discuss where the outflow near the northeastern corner of the triangle section can go. Can it partly flow into the Korea Strait as a portion of the Tsushima Current? Nagata (1981) discussed surface current data in the East China Sea and west of Kyushu during summer and argued that since a southward current prevails over most of the region west of Kyushu, no Kuroshio water should flow directly into the Korea Strait. However, Nagata's conclusion may be incomplete since some Kuroshio Water may flow northward near the bottom. Without CTD data further north, we can not say much about the path of the outflow near the northeastern corner west of Kyushu. Based on the shape of the 200 m isobath near the northeastern corner of the triangle, it seems quite possible that at least part of the outflow near the northeastern corner could flow along the upper slope, and then flow southwestward again to exit the East China Sea through the Tokara Strait.

4.6 Conclusion

The volume, heat and salt transports of the Kuroshio have been calculated using the January 1986 R/V Thompson ADCP and CTD data. The volume transport of the Kuroshio west of Kuroshio in January 1986 was 31.7±2.0 Sv, the salt transport was about 108.0±7.3 $\times 10^{10}$ kg/s, and the advective heat transport was 28.2±1.8 $\times 10^{14}$ W. The volume transport of the Kuroshio west of Kuroshio is similar to that of the Gulf Stream in the Florida Strait and the heat transports in these two region are roughly linearly correlated with the volume transport.

Conservation of mass transport in the study triangle allows us to define a streamfunction by the transport. The resulting streamlines clearly explain the horizontal

structure of the flow field in the Kuroshio and the adjacent region in January 1986. The recirculated waters at the middle of the eastern section and over the slope of the northern section were responsible for the relatively large outflow near the northeastern corner of the triangle, and there is no evidence to show the direct relation between the countercurrent on the eastern section and the recirculation on the slope.

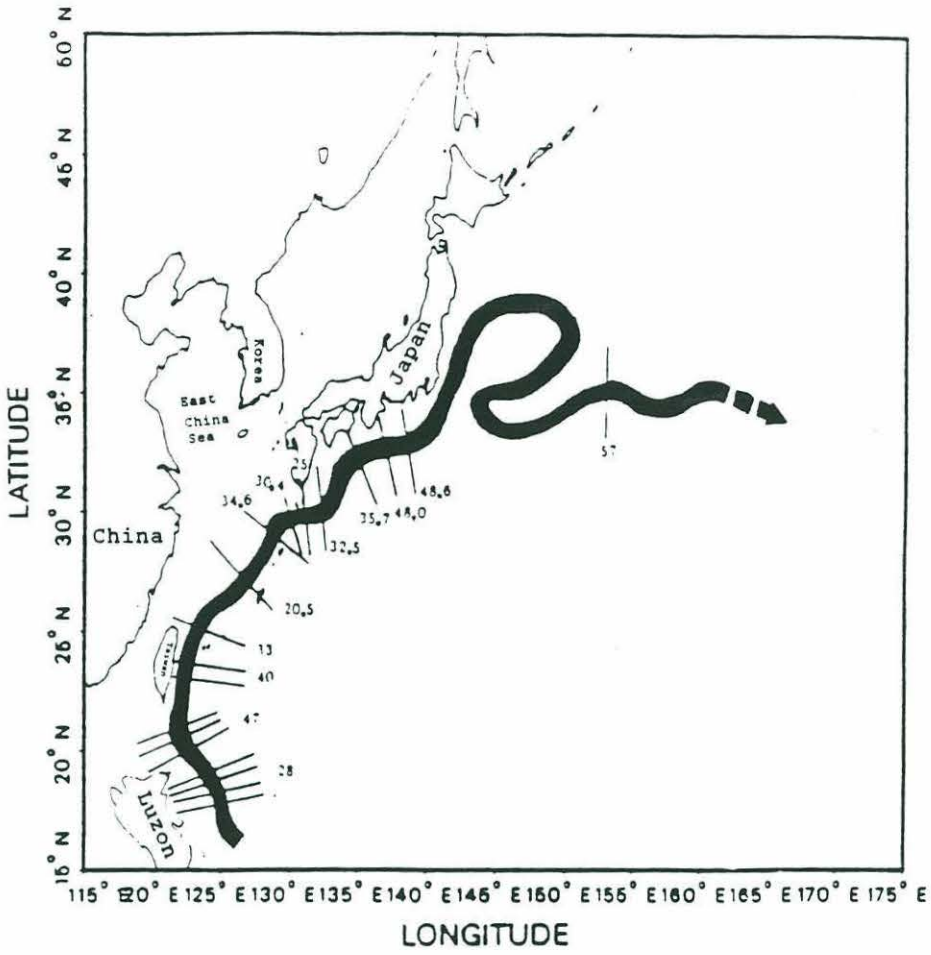

Figure 4.1: The summary of Hydrographical sections across the Kuroshio from east of Luzon to Kuroshio extension.

TABLE 4.1 : VOLUME TRANSPORT OF THE KUROSHIO

section	reported by	method	date	lat or long	transport (sv)	average transport (sv)
East of Luson	Nitani (1972)	G1	May,1959	18° 20′N	27	28
		,,	Aug,1965	17° 45′N	36	
		,,	Aug,1966	17° 00′N	20	
		,,	Feb,1967	18° 00′N	28	
Luson Strait	Nitani (1972)	G1	May,1959	20° 00′N	55	47
		,,	Aug,1965	19° 30′N	48	
		,,	Jul,1966	20° 15′N	42	
		,,	Feb,1967	20° 10′N	45	
East of Taiwan	Wyrtki (1961)	G1	Feb,1967	23° 00′N	29	40
	Nitani (1972)	,,				
		,,	Jul,1965	23° 00′N	(47)	
		,,	Jan,1966	23° 00′N	45	
		,,	Jul,1966	23° 00′N	46	
		,,	Jul,1966	23° 45′N	34	
Entrance of East China Sea	Nitani (1972)	G1	Oct,1942	25° 00′N	29	33
		,,	Oct,1961	25° 00′N	33	
		,,	Aug,1965	25° 00′N	30	
		,,	Jan,1966	25° 00′N	33	
		,,	Jul,1966	25° 00′N	32	
East China Sea	Bryden et al (1987)	DG	Jun,1985	24°-28°N	26.2	20.5
		G1				
	Nitani (1972)	,,	Summer, 1965-1966	26°-30°N	35	
		,,		26°-30°N		
	Saiki (1982)	G2	1955-1980 (71 cruises)	26°-30°N	21.3	
	Nishisawa et al(1982)	G2	1955-1980	26°-30°N	19.7	
	Pu Yongxin (1987)	G3	1972-1983 (48 cruises)	26°-30°N	19.6	
	Chen et al (1989) (present work)	DG	Jan,1986	27°-30°n	31.7	
		,,				
South of Japan	Takematsu et al(1986)	T	1972-1982	130°-131°E	25	
	Taft (1972)	G3	1956-1964	131°E	30.4	
		,,	,, ,,	133°E	32.5	
	,, ,,	,,	,, ,,	135°E	35.7	
	,, ,,	,,	,, ,,	137°E	48.0	
	,, ,,	,,	,, ,,	139°E	48.6	
Kuroshio Extension	Niiler et al (1985)	G4	1980-1981	152°E	57.0	

G1: Estimates based on the geostrophic velocity relative to 1200db.
G2: Estimates based on the geostrophic velocity relative to 700db.
G3: Estimates based on the geostrophic velocity relative to 800db.
G4: Estimates based on the geostrophic velocity relative to bottom.
DG: Estimates based on the combiniation of the ADCP and CTD.
T : Estimates based on the Mooring and CTD.

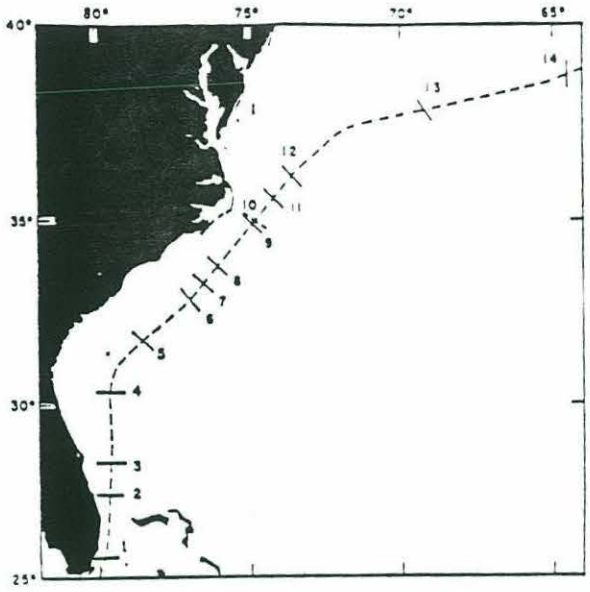

Figure 4.2: The location of the fourteen set of volume transport measurements given in Table 4.2 (from Knauss, 1969)

TABLE 4.2 : VOLUME TRANSPORT OF THE GULF STREAM

Measured by	*Date*	*Location* (km)	*Transport* (10^6 m^3/sec)
(1) RICHARDSON and SCHMITZ (*T*)	Aug., Oct., Dec. 1964 Apr. 1965 (7) May, June 1965 (23)	0	33
(2) RICHARDSON, SCHMITZ and NIILER (*T*)	June, Aug. 1966 May, June 1967	210	33
(3) RICHARDSON, SCHMITZ, and NIILER (*T*)	May, June 1967	300	35
(4) RICHARDSON, SCHMITZ, and NIILER (*T*)	May, June 1967	530	37
(5) KNAUSS (*T*)	Sept. 1966	725	52
(6) RICHARDSON, SCHMITZ, and NIILER (*T*)	June, July 1968	910	55
(7) SWALLOW and WORTHINGTON (*G*)	March, 1957	980	64
(8) KNAUSS (*T*)	July, Aug. 1965	1050	57
(9) KNAUSS (*T*)	July 1967	1215	63
(10) BARRETT (*G*)	Oct. 1962	1225	60
(11) WORTHINGTON and WRIGHT (*G*)	Nov. 1966	1315	74
(12) KNAUSS (*T*)	July, Aug. 1965	1400	76
(13) WARREN and VOLKMANN (*G*)	June 1966	1840	101
(14) FUGLISTER (*G*)	May, June 1960	2270	147

Volume transport estimates of the Gulf stream using geostrophic measurements and neutrally buoyant floats (G) and measurements of the vertically integrated horizontal velocity using transport floats(T) (taken from Knauss, 1969)

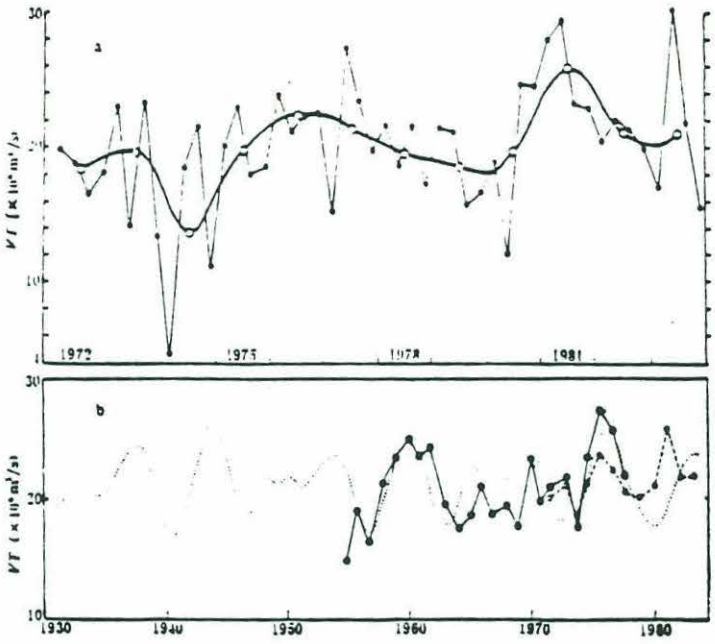

Figure 4.3:

Volume transport of the Kuroshio at 27°N and 135°E.
a: the seasonal variability of volume transport."○" and "●" are the annual and monthly mean transports relative to 800 db from 1972 to 1982 (from Pu, 1987)
b:" ●" is the annual mean transport relative to 700 db from 1955 to 1978 and dash line is the predicting curve based on 8 and 5.5 year periods (from Saiki, 1982) and "○" is the annual mean transport relative to 800 db (from Pu, 1987).

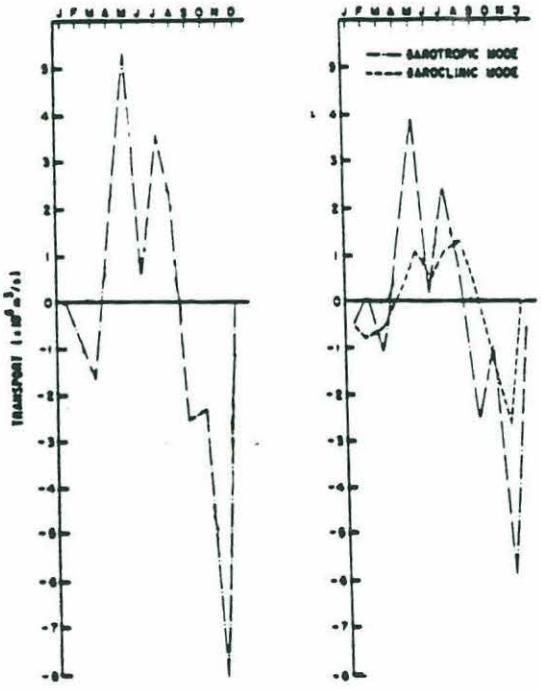

Figure 4.4:

a: Monthly absolute transports measured by STACS PEGASUS at 27°N in the Florida Strait from April 1982 to July 1984. (from Leaman, 1987)
b: Decomposition of total transport into baroclinic and barotropic components.

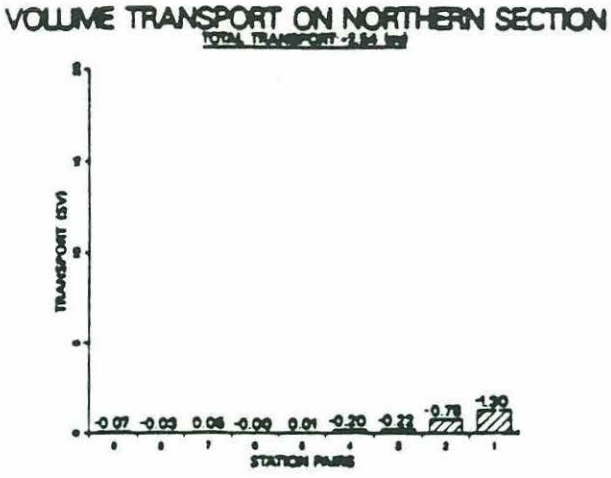

Figure 4.5:

The January 1986 geostrophic volume transport relative to the bottom.
Positive: inflow.
Negative: outflow.

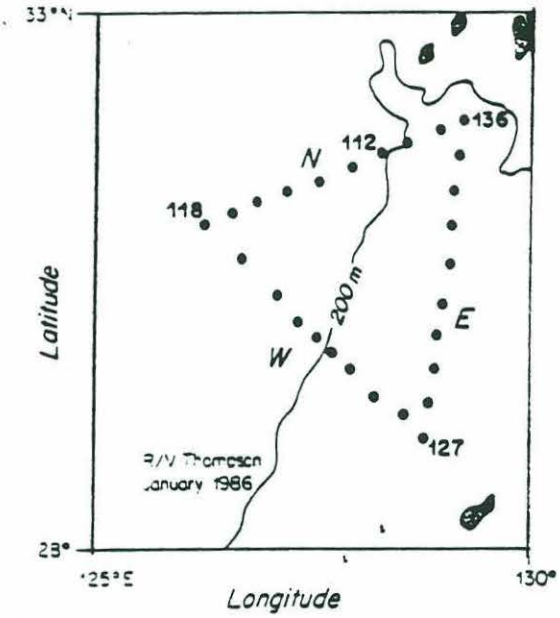

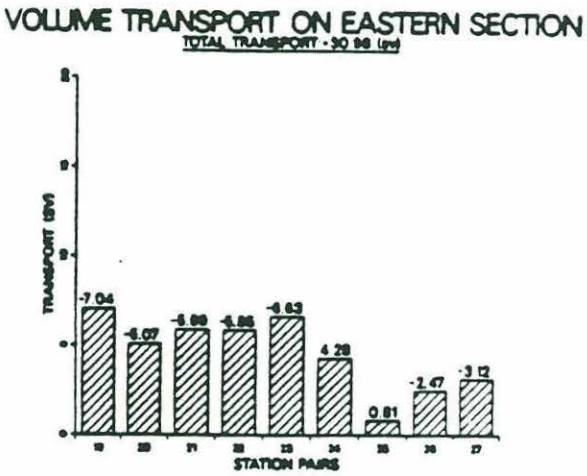

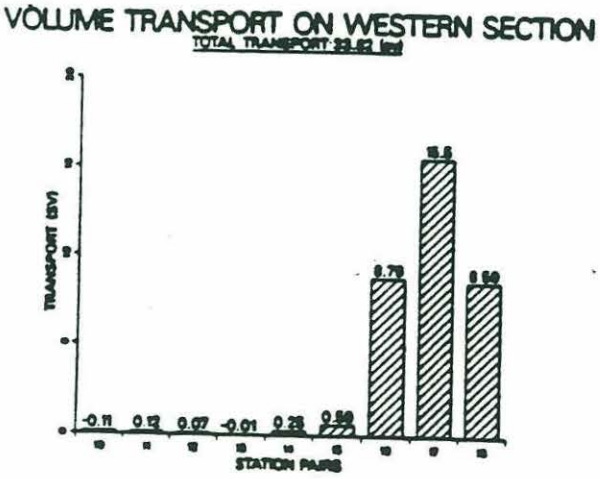

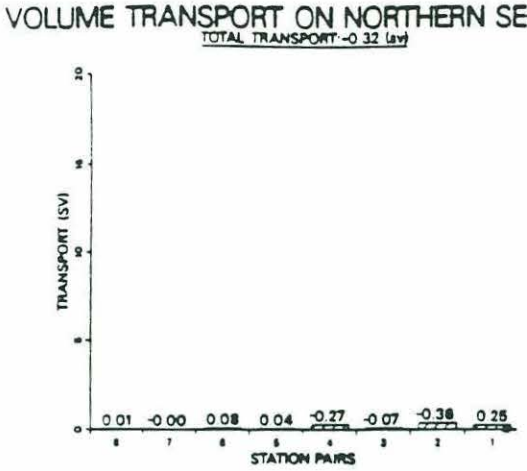

Figure 4.6:

The July 1986 geostrophic volume transport relative to the bottom.
Positive: inflow.
Negative: outflow.

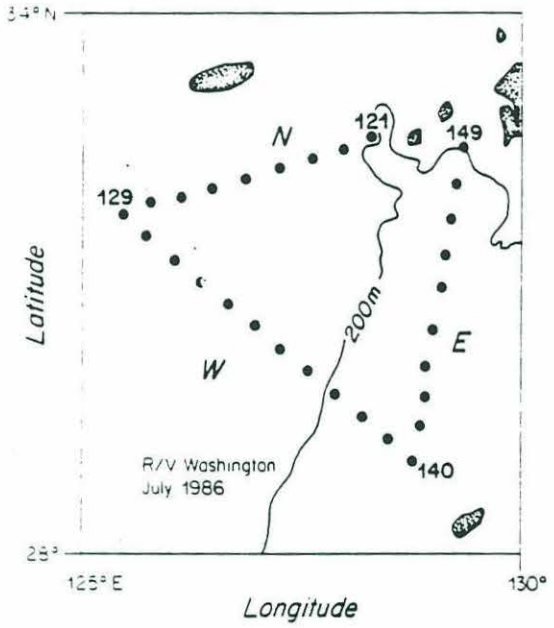

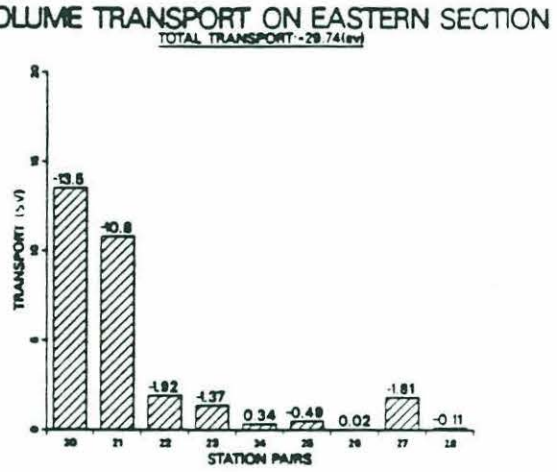

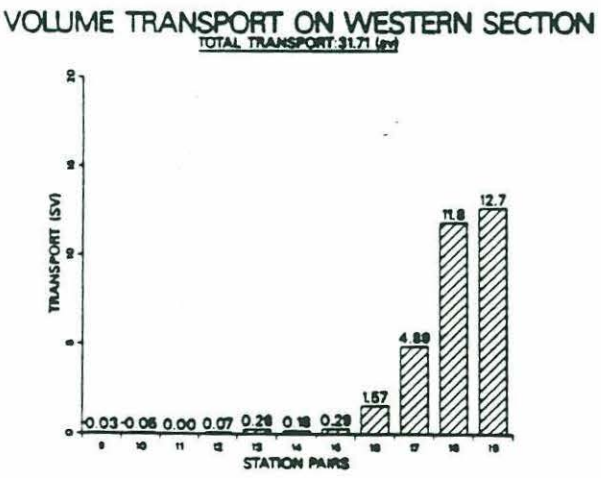

TABLE 4.3 : TRANSPORTS ON NORTHERN SECTION

station pair	volume transport (sv)	error	mass transport (10^9 kg/s)	error	salt transport (10^{10} kg/s)	error	heat transport (10^{14} J/s)	error
1	-4.8	±0.2	-4.9	±0.2	-16.9	±0.8	-2.5	±0.1
2	0.1	±0.3	0.1	±0.3	0.4	±1.1	-0.0	±0.2
3	0.3	< 0.1	0.3	< 0.1	0.9	< 0.1	0.2	< 0.1
4	0.4	,,	0.4	,,	1.4	,,	0.3	,,
5	0.1	,,	0.1	,,	0.4	,,	0.1	,,
6	0.1	,,	0.1	,,	0.3	,,	0.1	,,
7	-0.2	,,	-0.2	,,	-0.6	,,	-0.1	,,
8	-0.1	,,	-0.1	,,	-0.3	,,	-0.1	,,
9	-0.5	,,	-0.5	,,	-1.8	,,	-0.4	,,
total	-4.6	±0.4	-4.7	±0.4	-16.2	±1.4	-2.4	±0.2

Table 4.3- 4.6
The January 1986 absolute transports.
Positive: inflow.
Negative: outflow.

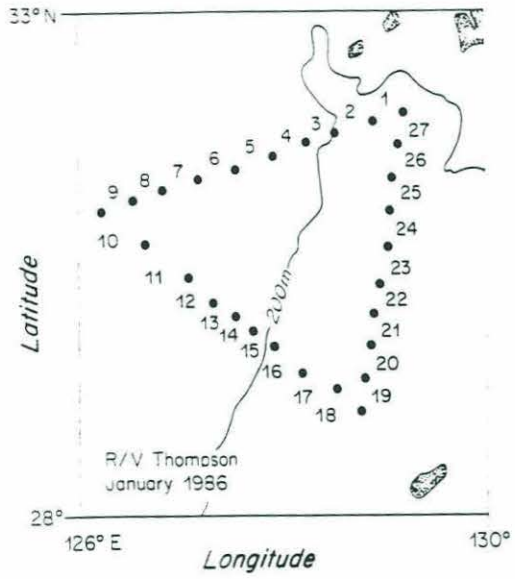

TABLE 4.6 : TRANSPORTS ON EASTERN SECTION

station pair	volume transport (sv)	error	mass transport (10^9 kg/s)	error	salt transport (10^{10} kg/s)	error	heat transport (10^{14} J/s)	error
19	-6.7	±0.2	-6.8	±0.2	-23.8	±0.5	-6.2	±0.1
20	-13.2	±0.1	-13.5	±0.1	-46.8	±0.4	-10.1	±0.1
21	-1.5	±0.8	-1.6	±0.8	-5.5	±2.9	-2.6	±1.4
22	-10.4	±0.8	-10.7	±0.8	-37.0	±2.9	-8.7	±0.7
23	-0.5	±0.8	-0.6	±0.9	-2.0	±3.0	-1.2	±1.9
24	4.0	±0.9	4.1	±0.8	14.2	±3.0	3.0	±0.7
25	0.3	±1.1	0.3	±1.1	0.9	±3.7	0.3	±1.1
26	-0.3	±1.1	-0.4	±1.1	-1.2	±3.9	-0.3	±1.1
27	-1.7	±1.3	-1.7	±1.4	-5.9	±4.7	-1.4	±1.1
total	-30.1	±2.6	-30.8	±2.7	-107.1	±9.3	-27.2	±2.3

Note: With the sharp seamount bottom.

TABLE 4.5 : TRANSPORTS ON EASTERN SECTION

station pair	volume transport (sv)	error	mass transport (10^9 kg/s)	error	salt transport (10^{10} kg/s)	error	heat transport (10^{14} J/s)	error
19	-6.7	±0.2	-6.8	±0.2	-23.8	±0.7	-6.2	±0.2
20	-13.2	±0.1	-13.5	±0.1	-46.8	±0.4	-10.1	±0.1
21	-0.3	±0.2	-0.3	±0.2	-1.0	±0.7	-2.3	±1.5
22	-10.4	±0.8	-10.7	±0.8	-37.0	±2.9	-8.4	±0.6
23	1.9	±1.1	1.9	±1.2	6.5	±3.8	-0.4	±0.2
24	4.1	±1.0	4.2	±1.1	14.5	±3.5	3.0	±0.7
25	0.3	±1.1	0.3	±1.1	0.9	±3.3	0.3	±1.1
26	-0.3	±1.1	-0.4	±1.1	-1.2	±4.4	-0.6	±2.1
27	-1.8	±1.3	-1.7	±1.4	-5.9	±4.3	-1.4	±1.0
total	-26.3	±2.7	-27.0	±2.7	-93.8	±9.6	-26.0	±3.1

Note: No sharp seamount bottom.

TABLE 4.4 : TRANSPORTS ON WESTERN SECTION

station pair	volume transport (sv)	error	mass transport (10^9 kg/s)	error	salt transport (10^{10} kg/s)	error	heat transport (10^{14} J/s)	error
10	0.2	< 0.1	0.2	< 0.1	0.8	< 0.1	0.2	< 0.1
11	0.2	,,	0.2	,,	0.7	,,	0.2	,,
12	-0.1	,,	-0.1	,,	-0.5	,,	-0.1	,,
13	-0.1	,,	-0.1	,,	-0.2	,,	-0.0	,,
14	-0.1	,,	-0.1	,,	-0.3	,,	-0.1	,,
15	-1.2	,,	-1.3	,,	-4.3	,,	-0.6	,,
16	5.7	±1.1	5.8	±1.1	20.2	±3.7	5.8	±1.1
17	18.9	±1.7	19.4	±1.8	67.3	±6.2	15.6	±1.4
18	6.8	±0.3	7.0	±0.3	24.3	±1.0	6.6	±0.2
total	30.3	±2.0	31.1	±2.1	108.00	±7.3	27.6	±1.8

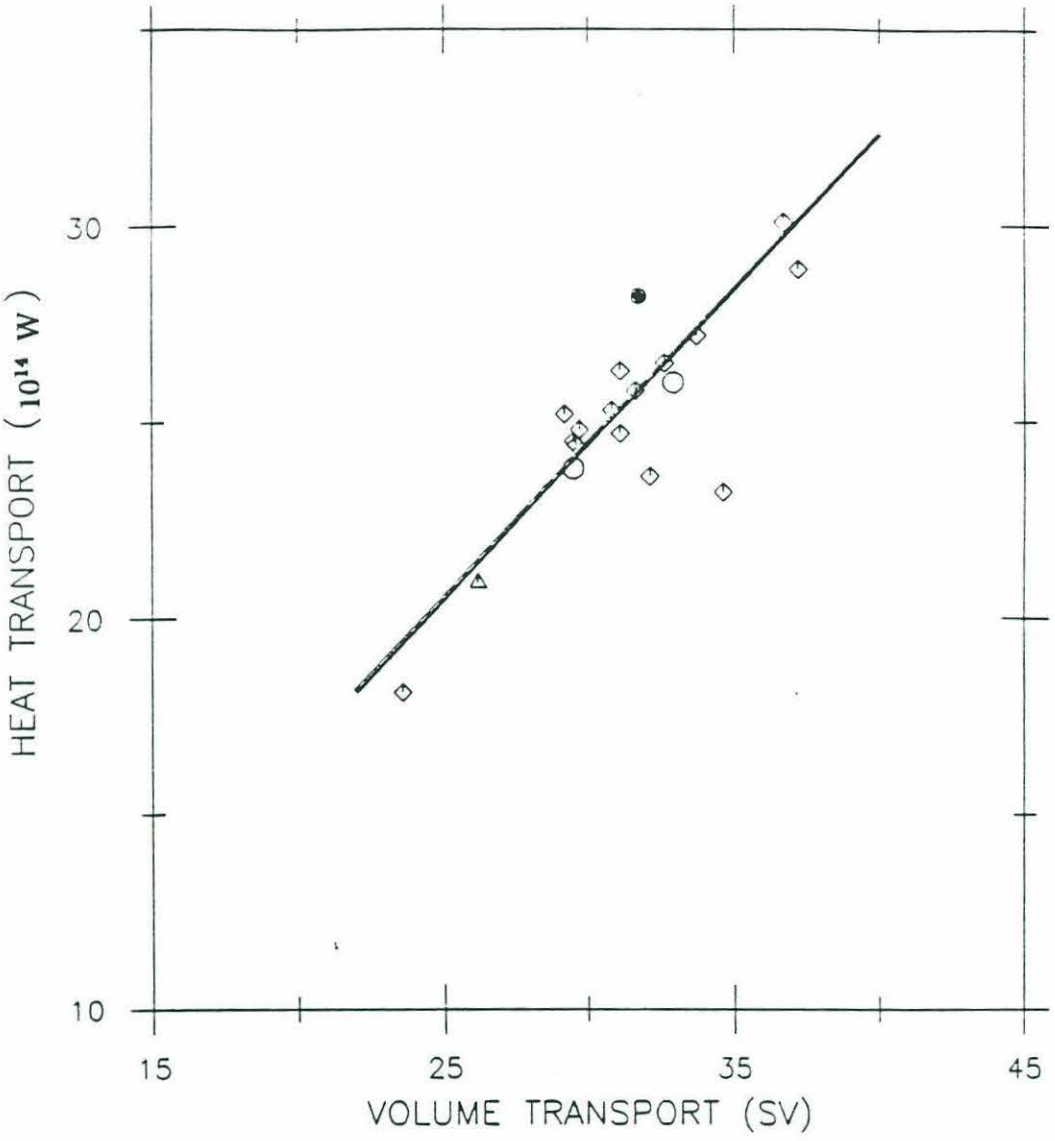

Figure 4.7: Summary of heat transports obtained from the Kuroshio in the East China Sea(▷, Bryden, 1988: •, present work) and the Florida current at 27°N (taken from Niiler and Richardson, 1973,○; Leaman, 1987, ◇)

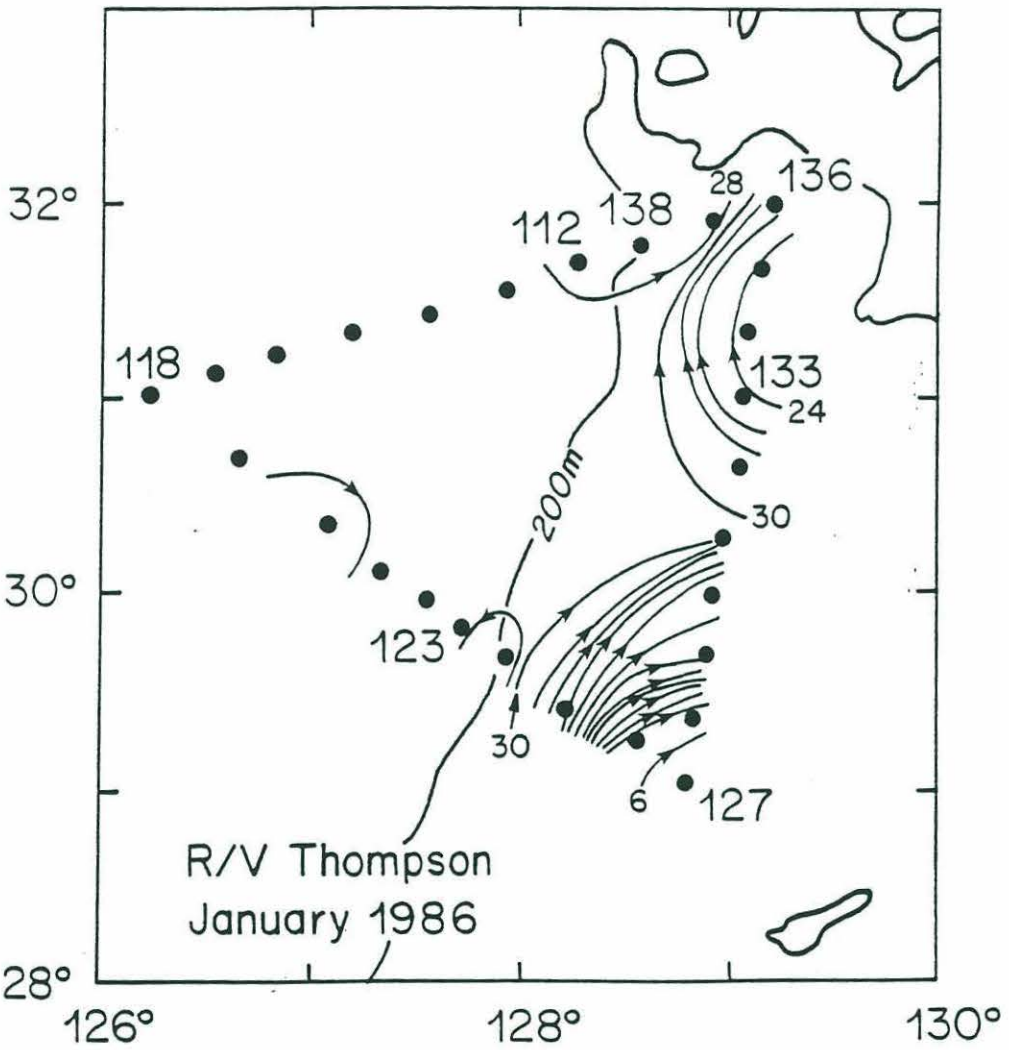

Figure 4.8: The January 1986 streamfunction defined by the transport (unit: $10^6\ m^2/s$)

Chapter 5

Potential Vorticity Across the Kuroshio

5.1 Introduction

Potential vorticity conservation plays an important role in the field of geophysical fluid dynamics and has been widely used to study the horizontal and vertical structures of oceanic circulation. Excellent examples can be found in the thermocline theories done by Rhines and Young (1982) and Luyten, Pedlosky and Stommel (1983), who explained the vertical structure of general oceanic circulation from the viewpoint of potential vorticity conservation. Stommel (1958) used an uniform potential vorticity assumption to calculate the velocity field across the Gulf Stream and found that the resulting velocities were in a good agreement with the geostrophically computed velocities. That result then encouraged him to suggest modeling the Gulf Stream as a flow with an inviscid uniform potential vorticity. Gill(1977) presented several sections of potential vorticity across the Agulhas current and found a good coincidence between the potential vorticity contours and streamlines. He also suggested the use of potential vorticity as a tracer to study the western boundary currents. McCartney (1982) pointed out that the Thermocline Water characterized by minimum hydrostatic stability is usually associated with relative uniform minimum potential vorticity which can be traced on potential density surfaces. Since the wind-driven gyre provides the source water of the Gulf Stream, it might be expected that one could trace such uniform potential vorticity

layer across the Gulf Stream. This was tested by Watts (1983) who presented sections of potential vorticity across the Gulf Stream at 73°W and indeed found a relatively large region of Thermocline Water with uniform potential vorticity in that region. Similar results have been found by Johns (1984) and Hall (1985) in their analysis of the potential vorticity for the Gulf Stream.

Unlike the Gulf Stream, a detailed analysis of potential vorticity in the Kuroshio has not yet been done (to my knowledge). One reason has been the lack of absolute velocity data. The calculation of relative vorticity using just the geostrophic velocity field will miss the contribution from the barotropic velocity component which may be comparable to that from the baroclinic part. The accurate estimation of the absolute geostrophic velocity given in the previous chapters permits calculation and analysis of the potential vorticity in the Kuroshio in this chapter. Since the alongstream velocity can exceed 100 cm/s in the Kuroshio and both horizontal and vertical gradients of potential density are comparable in the main thermocline, the potential vorticity in the Kuroshio may not be simply expressed by the product of planetary vorticity and vertical gradient of potential density. A detailed scale analysis of the potential vorticity will be given in section 5.2 to determine a proper, approximate form for total potential vorticity in the Kuroshio. Then sections of potential vorticity will be presented in section 5.3, by which, the path of the Kuroshio will be described using potential vorticity as a tracer. In section 5.4, we will calculate the gradient of potential vorticity across each section to examine the stability of the Kuroshio. Finally, conclusions will be given in section 5.5.

5.2 Contribution of the component terms of potential vorticity

Ertel (1942) showed that a parcel of water conserves its potential vorticity in the absence of dissipation and adiabatic processes. The total potential vorticity can be

expressed by

$$q = -\frac{(2\Omega + \nabla \times \mathbf{u})}{\rho} \bullet \nabla\lambda, \tag{5.1}$$

where 2Ω is planetary vorticity, $\nabla \times \mathbf{u}$ is relative vorticity, ρ is density and λ is any conservative scalar property of the flow (for a comprehensive discussion, see Pedlosky, 1979). Taking λ to be potential density σ_θ, (5.1) yields

$$q = -\frac{1}{\rho}[(f + v_x - u_y)\sigma_{\theta z} + (h + u_z - w_x)\sigma_{\theta y} + (w_y - v_z)\sigma_{\theta x}], \tag{5.2}$$

where x and y are oriented east and northward respectively, and f and h are the vertical ($2\Omega\sin\theta$) and horizontal ($2\Omega\cos\theta$) components of planetary vorticity.

Since the Kuroshio flows as a narrow, intense boundary current in this region, the potential vorticity can be rewritten in approximate form in natural coordinates (Johns, 1984) as

$$q = -\frac{1}{\rho}[(f + kv + \frac{\partial v}{\partial n})\frac{\partial \sigma_\theta}{\partial z} - \frac{\partial v}{\partial z}\frac{\partial \sigma_\theta}{\partial n}], \tag{5.3}$$

where n is the cross-stream coordinate, v is the alongstream velocity, k is the streamline curvature, and kv is the curvature vorticity. It is well known that in the interior ocean the water column is vertically stratified and has relatively weak horizontal gradients in velocity and potential density, hence, the potential vorticity is dominated by the product of the planetary vorticity and the vertical density gradient. However, in the Kuroshio where the alongstream velocity is approximately ten times larger than that in the interior ocean, the horizontal and vertical shears of the alongstream velocity may become large enough to be important. In the main thermocline, the horizontal gradient of the potential density in the Kuroshio may be so large that the product term

of the vertical shear of the alongstream velocity and horizontal gradient of potential density may also become important in comparison with planetary vorticity. A detailed discussion of the contribution of each term in the potential vorticity and its distribution across the Kuroshio is given in the following.

The kv Contribution

In the main Kuroshio where v is positive, the contribution of curvature vorticity $kv = v/R$ (R the radius of curvature) only depends on the sign of k which is positive for a cyclonic meander and negative for an anticyclonic meander. As an example, for the cyclonic meander, the curvature vorticity may tend to reinforce (cancel) the shear vorticity $\frac{\partial v}{\partial n}$ to the left (right) of the axis of maximum velocity. When R is rather small the kv contribution may be comparable with the other terms in q.

Since v is given from the absolute geostrophic velocity, the calculation of kv is simplified to estimation of the radius of curvature R. Two possible ways can be used for this purpose. The first is to estimate the mean radius of curvature using horizontal current maps. An example of this approach can be found in Watts' (1983) or Johns (1984)'s work for the Gulf Stream. In the present work, the Kuroshio split into two branches when it flowed around a seamount, thus, two possible choices of R exist on the upstream western section. In the recirculation zone in the studing triangle, it is difficult to define an average R. The second approach uses the gradient wind equation and inversely determines R by combining average ADCP velocity with absolute geostrophic velocities. However, this method may lead to a wrong result because of the errors in the average ADCP velocity measurements. Good agreement between absolute geostrophic and averaged ADCP velocities in January 1986 implies that the curvature radius should be large enough to ignore curvature vorticity in most of study region. This can be also demonstrated by the following simple scale analysis.

The ratio of the curvature vorticity to the planetary vorticity can be expressed by the curvature Rossby number R_r which is defined as

$$R_r = \frac{U}{Rf}, \tag{5.4}$$

where U is the magnitude of the alongstream velocity. According to the streamline distribution in Figure 4.8, R is roughly equal to 100 km. Choosing $U \sim 1.0$ m/s and $f \sim 10^{-4}$ s^{-1}, then

$$R_r \sim \frac{1}{10^{-4} \times 10^5} \sim 0.1.$$

It follows that in general the curvature vorticity was small enough compared with the planetary vorticity that it can be neglected for the mean path of the Kuroshio during the January 1986 Thompson survey.

Rossby Number

The Rossby number R_o, defined by the ratio of relative vorticity $\partial v/\partial n$ to planetary vorticity f, shows the relative importance of the relative vorticity in the total potential vorticity. The Rossby number distribution in the Kuroshio has been calculated using the January 1986 absolute geostrophic velocity data. The cross-stream sections of R_o shown in Figure 5.1 illustrate the relatively large value of about 0.2-0.4 near the axis of maximum velocity and at the margin between the Kuroshio and recirculated water on both western and eastern sections. Watts (1983), Johns (1984) and Hall (1985) reported similar values of $R_o \sim 0.2$ for the Gulf Stream.

Since the axis of maximum absolute velocity in the Kuroshio on the western section was located at the center of the Okinawa Trough, the contributions of relative vorticity tend to decrease the total potential vorticity on its right where $\partial v/\partial n < 0$

and increase it on its left where $\partial v/\partial n > 0$. As a result, the total potential vorticity is not uniform across the Kuroshio on a potential density surface where the relative vorticity is important. The same results can be found on the eastern section where the Kuroshio splits into two branches. Similar analyses were done by Watts (1983), Johns (1984) and Hall (1985) who found that a strong potential vorticity jump occurs in the slope region where the potential vorticity is several times larger in the slope water than in the Sargasso Sea. Since the sign change of relative vorticity across the section is associated with a relatively large Rossby number, it is important to include the contribution of relative vorticity in estimating the total potential vorticity in the Kuroshio.

The $-\sigma_{\theta z}$ distribution

Three sections of vertical gradient of the potential density $-\sigma_{\theta z}$ west of Kyushu in January 1986 are shown in Figure 5.2. On the western section , a minimum value of -$\sigma_{\theta z}$ less than $0.2 \times 10^{-2} kg/m^4$ was found near the surface of the Kuroshio and over the shelf region, implying a minimum hydrostatic stability in the Surface Water of the Kuroshio and Coastal Water. The maximum value of $-\sigma_{\theta z}$ of about $1.2 \times 10^{-2} kg/m^4$ occurred near the shelf break at the depth of 100 m . In the main thermocline between the 16°C and 20°C isotherms , -$\sigma_{\theta z}$ gradually decreased seaward, and near the center of the Okinawa Trough where the axis of the Kuroshio was located, a relatively uniform and intermediate value of $-\sigma_{\theta z}$ of about $0.8 \times 10^{-2} kg/m^4$ was found at the depth of 200 m to 350 m. Below the main thermocline, $-\sigma_{\theta z}$ decreased with depth, and a minimum uniform value of $-\sigma_{\theta z}$ of less than $0.2 \times 10^{-2} kg/m^4$ was found beneath 600 m, implying that the Intermediate and Deep Waters in the Kuroshio west of Kyushu were associated with minimum hydrostatic stability. A similar structure of $-\sigma_{\theta z}$ can also be found on the eastern section where an uniform value of $-\sigma_{\theta z}$ of about $0.8 \times 10^{-2} kg/m^4$ occupied a large area from 200 m to 300 m, implying that the main Thermocline Water spread out when the Kuroshio flowed from the upstream western section to the eastern section.

Since the total width of the eastern or western section was less than 3° in latitude, the planetary vorticity f does not change much across each section. Then the distribution of $-\sigma_{\theta z}$ must be proportional to $-f\sigma_{\theta z}$ which is generally used to describe the general circulation pattern in subtropic and subpolar gyres. The fact that the distribution of $-\sigma_{\theta z}$ can not detect the feature of splitting of the Kuroshio path implies that the relative vorticity plays an important role in determining the structure of the total potential vorticity.

The $-v_z\sigma_{\theta n}$ distribution

Since the thermal wind relation holds to a high degree of accuracy in the Kuroshio, the vertical shear of the velocity can be replaced by the horizontal shear of the potential density, so that

$$\frac{\partial v}{\partial z}(\frac{\partial \sigma_\theta}{\partial n}) \simeq \frac{g}{f\rho}(\frac{\partial \sigma_\theta}{\partial n})^2. \tag{5.5}$$

The term -$v_z\sigma_{\theta n}$ will always make a positive contribution to the total potential vorticity in the triangle study area where the Kuroshio flowed from south to northeast.

Three sections of the distribution of $-v_z\sigma_{\theta n}$ are shown in Figure 5.3. On the western section, a small value $-v_z\sigma_{\theta n}$ was found near the surface and over the coastal region, indicating that the Surface and Coastal Waters were horizontally relatively uniform. A large value of $-v_z\sigma_{\theta n}$ was observed in the main thermocline , a consequence of a large horizontal gradient of potential density. Unlike the distribution of $\sigma_{\theta n}$, the maximum value of $\frac{g}{f\rho}\sigma_{\theta n}^2$ was located close to the center of the Okinawa Trough rather than at the shelf break, and the slope of its maximum axis was much larger than that of the main thermocline. Below the thermocline, the value of $-\frac{g}{f\rho}\sigma_{\theta n}^2$ decreased with depth and then become relatively uniform beneath 700 m, reflecting the uniform properties of the Deep Water. A similar structure can be also found on the eastern

section where the maximum core of $-\frac{g}{f\rho}\sigma_{\theta n}^2$ was located at 250 m between stations 128 and 130.

The ratio of $\frac{g}{f\rho}\sigma_{\theta n}^2$ to $f\sigma_{\theta z}$ is shown in Figure 5.4 to estimate the relative contribution of $-\frac{g}{f\rho}\sigma_{\theta n}^2$ to the total potential vorticity. The relative magnitude of $-\frac{g}{f\rho}\sigma_{\theta n}^2$ was much less than 0.1 over most of the triangle section except in the region close to the axis of the Kuroshio where it did reach a value of 10^{-1}. Since the term $\frac{g}{f\rho}\sigma_{\theta n}^2$ tends to increase the potential vorticity everywhere and is almost one order smaller than the term $f\sigma_{\theta z}$, we will neglect it here.

Summary of the scale analysis of potential vorticity

From the above discussions, we conclude that the total potential vorticity can be approximated to within 10 percent roughly by

$$q = -(f + \frac{\partial v}{\partial n})\frac{1}{\rho}\frac{\partial \sigma_\theta}{\partial z} \tag{5.6}$$

Sections of potential vorticity through the Kuroshio calculated with (5.6) will be discussed next.

5.3 The Potential Vorticity Sections

The distribution of the approximate total potential vorticity on each section is shown in Figure 5.5. First of all, the most significant feature, which can be easily found in comparison with the vertical gradient of the potential density,was that the structure of the total potential vorticity in the main thermocline strongly depended on the distribution of relative vorticity. On the western section, the anticyclonic relative vorticity near the shelf break reduced the total potential vorticity and so there was no longer an abrupt jump of the potential vorticity at the shelf break which was found

by Watts (1983), Johns (1984) and Hall (1985) for the Gulf Stream. Between the recirculation and axis of the Kuroshio, the cyclonic relative vorticity led to an increase of the potential vorticity. To the right of the Kuroshio axis, the potential vorticity decreased again due to the anticyclonic relative vorticity. Therefore, a core of the maximum potential vorticity with values of larger than $0.7 \times 10^{-9}/sm$ was found in the main thermocline between stations 123 and 126. This core deepened seaward in the Kuroshio corresponding to the main thermocline structure. In the Surface Water above the main thermocline, the potential vorticity decreased sharply upward, with values reducing to $0.1 \times 10^{-9} m^{-1} s^{-1}$ or smaller at the surface. In the region deeper than 400 m, the potential vorticity tended toward an uniformly low value with depth, corresponding to the Intermediate and Deep Water.

A similar structure of total potential vorticity was also found on the eastern section near the surface and in the deep regions. Since the Kuroshio split into two branches when it flowed from the western section to the eastern section, the relative vorticity was anticyclonic to the right of each core of maximum velocity (looking downstream), but cyclonic to the left of each core, causing the total potential vorticity to decrease on the right side of the maximum velocity core and increase on the left side. Therefore, two cores of maximum potential vorticity were found to the left sides of two maximum velocity cores. Since part of the Kuroshio was recirculated on the eastern section between stations 131 and 134, the northern core of potential vorticity covered a relative larger area than the southern one due to the positive contribution of relative velocity from part of the recirculation.

Two significant similarities can be found in comparing the eastern section with the upstream western section. First, the three cores of maximum potential vorticity had the same maximum value of larger than $0.7 \times 10^{-9} s^{-1} m^{-1}$ and all of them were relatively uniform in their interior. Second, if one faces the direction of the current and goes along the axis of the Kuroshio, he will find that the maximum core of potential

vorticity was always located to his left. Therefore, instead of the velocity distribution, the path of the Kuroshio can be traced by the core of the maximum potential vorticity. On the other hand, since no evidence in the distribution of $f\sigma_z$ showed the splitting of the Kuroshio path, the distribution of relative vorticity played an important role in determining the real structure of the Kuroshio west of Kyushu.

Interestingly, there was no evidence of the 18°Water in our sections of the potential vorticity, which is characterized by a minimum potential vorticity. A similar result was also shown in the Florida Current by Brooks and Niiler (1977), who found that the potential vorticity distribution horizontally decreased from the shelf and had a distinct maximum at mid-depth. It suggests that the 18°Water must have been modified when it left its source region and joined the Kuroshio or it has not yet joined the Kuroshio. Watts (1983) and Johns (1984) indeed showed the trace of 18°Water in the center of the Gulf Stream below the Surface Water at 73°W and 70°W, where the Gulf Stream had already left the shelf and entered the North Atlantic Ocean. The very strong recirculation observed in that region implies the intrusion of the 18°Water from the interior ocean.

The potential vorticity contours and streamlines on the potential density surface $\sigma_\theta = 25.7$ are also plotted in Figure 5.6 to investigate the conservation of the potential vorticity in the Kuroshio west of Kyushu. Since the maximum core of the potential vorticity was divided into two cores when the Kuroshio flowed from the upstream western section to the eastern section, a semi-enclosed and relatively low potential vorticity contour occurred between these two maximum cores on the eastern section. To the southern side of the southern maximum potential vorticity core, the contours of the potential vorticity were almost parallel to the streamlines, implying that the potential vorticity was conserved along those streamlines. However, between the two cores of maximum potential vorticity, the Kuroshio water crossed potential vorticity contours as it flowed northeastward from the western section and split around the seamount on

the eastern section. Potential vorticity (as we have estimated it) was not conserved along the streamlines in that region. In the countercurrent area on the eastern section, the water almost flowed along the streamlines from the middle of that section and finally outflowed near the northeastern corner of the triangle, indicating again the conservation of potential vorticity on streamlines. Therefore, potential vorticity was almost conserved in most of the triangle study area except between two maximum cores of potential vorticity where part of the Kuroshio split to the northeast and outflowed through the eastern section on the northern side of the southern seamount.

In the absence of strong forcing, dissipation and mixing, fluid parcels tend to conserve their potential density and potential vorticity. If the motion is also steady, then parcels will maintain their potential vorticity along streamlines on the potential density surfaces. A rough calculation shows that it took about one and a half days for a parcel to flow from the western section to the eastern section. Since the period of variation of the Kuroshio near Kyushu is thought to be about 20-40 days (Ichikawa, 1987), the Kuroshio can be treated as a steady current during the time we measured. Moreover, the potential density surface for analysis did not outcrop to the sea surfaces; thus, the water on that potential density surface had been not directly affected by the surface wind stress curl(at least not recently). In any event, there was no strong local wind forcing during the measurement time (Limeburner, personal communication). Therefore, the effect of the surface wind and its variation can be ignored in this case. The potential density surface crossed the maximum potential vorticity region with large $\sigma_{\theta z}$. As a result, it is unlikely that convective mixing occurred in such a strongly stratified area. The rough bottom topography on the downstream eastern section may produce a relatively large bottom friction which dissipated the potential vorticity, so that the potential vorticity was no longer conserved following a parcel. If this is true, however, why was the potential vorticity conserved on streamlines in the other regions where seamounts also exist.

What caused the variation of potential vorticity on streamlines around the seamount between two cores of maximum potential vorticity? As we know, the Kuroshio split into two branches around a seamount with a width of about 30 km in that region as it left through the eastern section. The curvature vorticity v/R may be large where the fluid flowed around the seamount, so that the deviation of the total potential vorticity estimeted on streamlines around the seamount might be due to the missing contribution of curvature vorticity to the total potential vorticity.

Choosing a streamline on the potential density surface $\sigma_\theta = 25.7$, which started at the core of maximum potential vorticity on the western section and went around the seamount on the eastern section, we can simply calculate the necessary value of R for the total potential vorticity to be conserved on that streamline. The conservation of potential vorticity on the streamline requires that

$$q_1 = -\frac{1}{\rho_2}(f_2 + \frac{v_2}{R} + \frac{\partial v_2}{\partial n})\frac{\partial \sigma_{\theta 2}}{\partial z}, \tag{5.7}$$

where the subscripts 1 and 2 refer to the values along the streamline on the western and eastern sections, respectively. Therefore, the necessary value of R for the potential vorticity to be conserved on the streamline can be given by

$$R = \frac{v_2}{q_1/\frac{1}{\rho_2}\frac{\partial \sigma_{\theta 2}}{\partial z} - f_2 - \frac{\partial v_2}{\partial n}}. \tag{5.8}$$

Based on Figures 3.11, 5.2 and 5.5, $q_1 = 0.6 \times 10^{-9}\ m^{-1}s^{-1}$, $\frac{1}{\rho_2}\frac{\partial \sigma_{\theta 2}}{\partial z} = -0.1 \times 10^{-4}\ m^{-1}$, $v_2 = 50\ cm/s$, $\partial v_2/\partial n = -0.27 \times 10^{-4} s^{-1}$, and $f_2 = 0.6 \times 10^{-4} s^{-1}$, we find that

$$R = 18.5\ km.$$

The radius of the seamount between the two cores of maximum potential vorticity on the eastern section is about 15 km, as the same order as R. It follows that the lack of conservation of total potential vorticity on streamlines around the seamount may be due to the missing the curvature vorticity component.

5.4 Instability of the Kuroshio

A comprehensive discussion for the linear instability problem was given by Pedlosky (1979). The instability of the flow in a bounded channel requires that the potential vorticity gradient q_x changes its sign at least one time across the stream or in the vertical direction. In addition, the necessary condition for instability is also related to vertical shear of the basic flow at the surface and the bottom slope. For simple applications, the tendency for instability of the Kuroshio can be directly observed on the section of potential vorticity using the gradient of potential vorticity.

In a linear system, the advective effects of potential vorticity are ignored. Therefore, the barotropic and baroclinic instability problems can be separated in such a system. As far as q_x is concerned, the barotropic instability requires that q_x changes its sign at least one time along a horizontal surface across the stream. The baroclinic instability needs vertical-banded positive and negative q_x regions. However, if we transfer our coordinate onto potential density surfaces, the requirement for barotropic instability mentioned above is also the condition for baroclinic instability. Therefore, the best way to discuss the instability of the Kuroshio is to use potential density coordinates.

On the western section, in the upper 500 m, the region of maximum potential vorticity was located offshore at station 124, 45km away from the shelf break. There were two regions of maximum potential vorticity gradient q_x on both sides of the core of maximum q_x between the shelf break and the center of Okinawa Trough. That

is, q_x changed its sign twice across the Kuroshio on a potential density surface on the western section. This was also true in the vertical direction where the potential vorticity gradient changed its sign across the core of maximum potential vorticity. Therefore, the Kuroshio was potentially unstable on the western section in the upper region. In the deep region below 600 m, the gradient of potential vorticity was almost constant across the stream, implying that the Deep Water was much more stable than the main Thermocline Water in the Kuroshio.

Similar results were also found on the downstream eastern section where the gradient of the potential vorticity changed its sign across the stream on a potential density surface and also in the vertical direction. Moreover, since the Kuroshio split into two branches around the seamount on this section, it may be more relevant to discuss the effects of bottom topography on the instability of the Kuroshio. However, since the geostrophic theory is not applicable to the eastern section where the sharp seamounts exist, a model of such a problem must involve strong non-linear effects, which is beyond the scope of the present work.

5.5 Conclusion

The combination of CTD and ADCP data obtained on the January 1986 R/V Thompson survey allows the calculation and analysis of total potential vorticity in the Kuroshio. First, it has been found that the total potential vorticity in the Kuroshio may be approximately given by the product of the vertical gradient of potential density and the sum of the planetary and relative vorticities, while the product of the vertical shear of velocity and the horizontal shear of potential density was negligible even though it seems to be relatively important in the Gulf Stream. Second, the distribution of relative vorticity played a significant role in determining the structure of potential vorticity in the Kuroshio. The path of the Kuroshio can be traced by the core of maximum potential

vorticity. Facing the direction of the current, the axis of maximum velocity is located to the right of the core of maximum potential vorticity. Third, the potential vorticity was conserved along streamlines on the potential density surface. Local deviation of the contours of potential vorticity from streamlines around a seamount was due to missing the curvature contribution to the total potential vorticity. Finally, the Kuroshio was potentially unstable as it flowed along the continental margin in the Okinawa Trough because the gradient of potential vorticity changed sign across the Kuroshio on potential density surfaces.

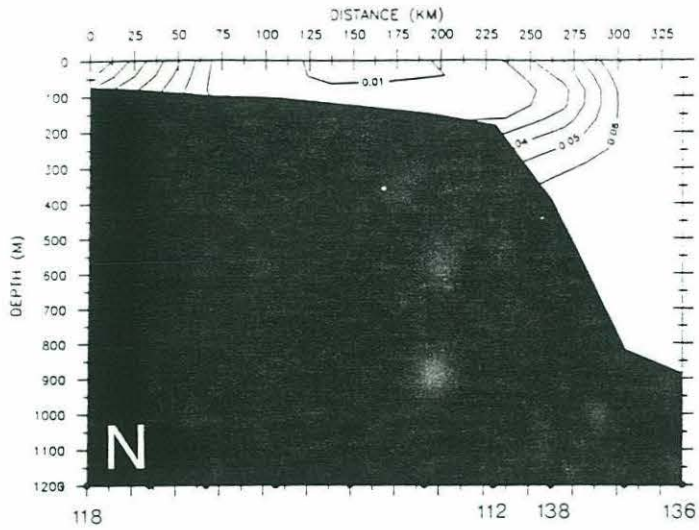

Figure 5.1:

Rossby number defined by the ratio of relative vorticity to planetary vorticity.

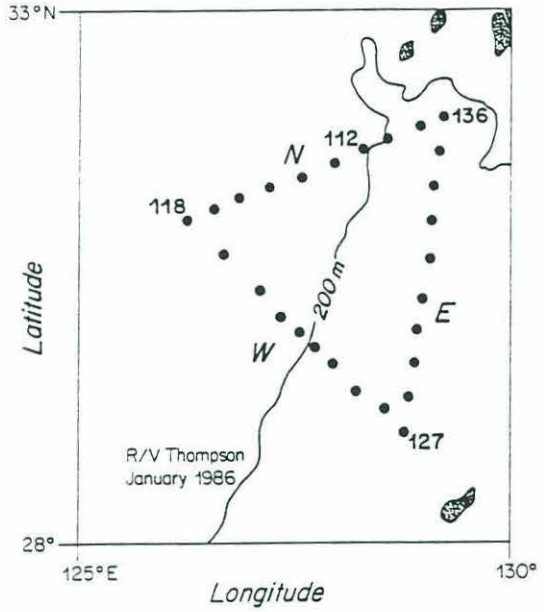

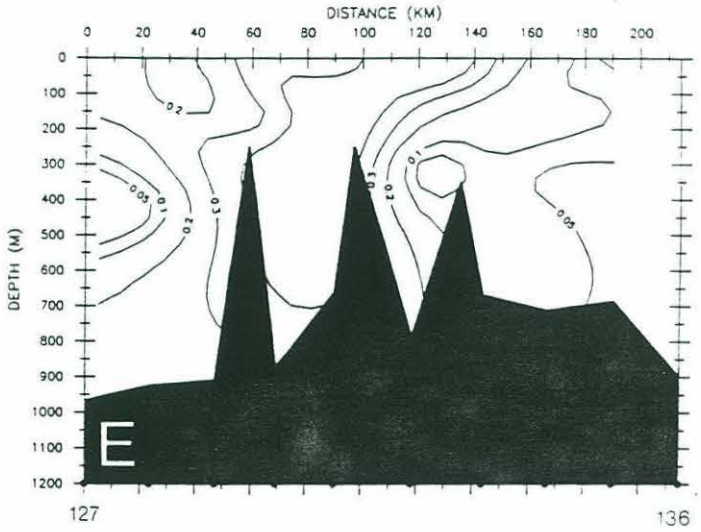

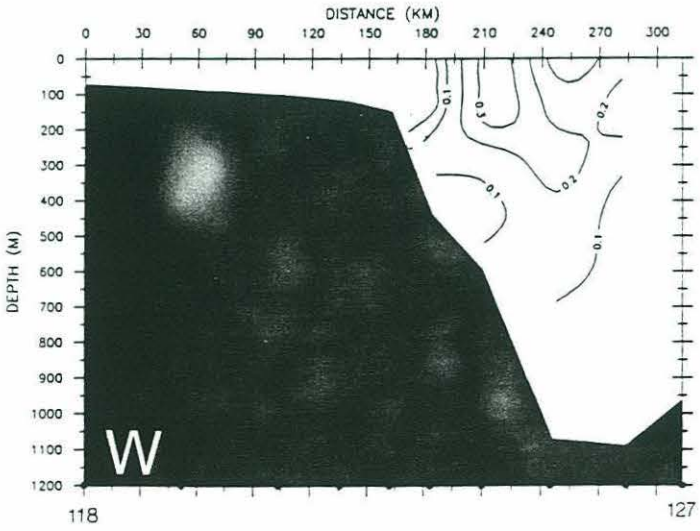

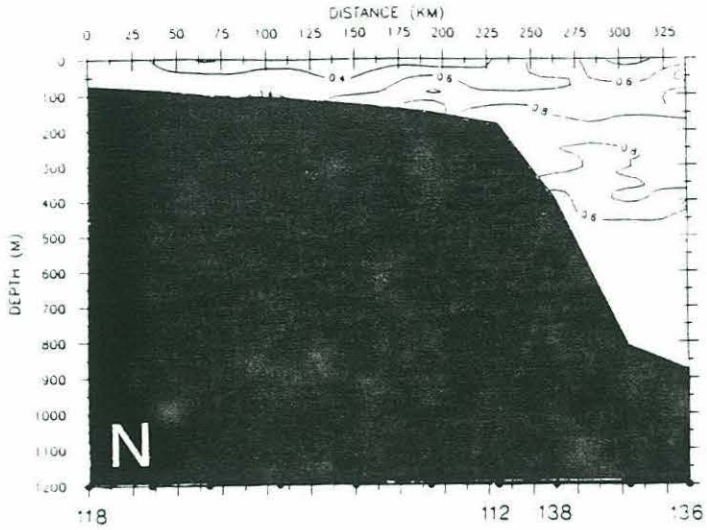

Figures 5.2:

The distribution of the vertical gradient of potential density $-\sigma_{\theta z}$ $(10^{-2} kg/m^4)$.

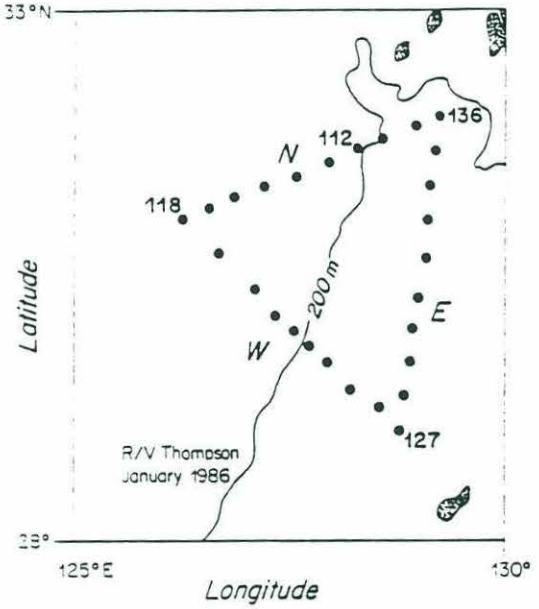

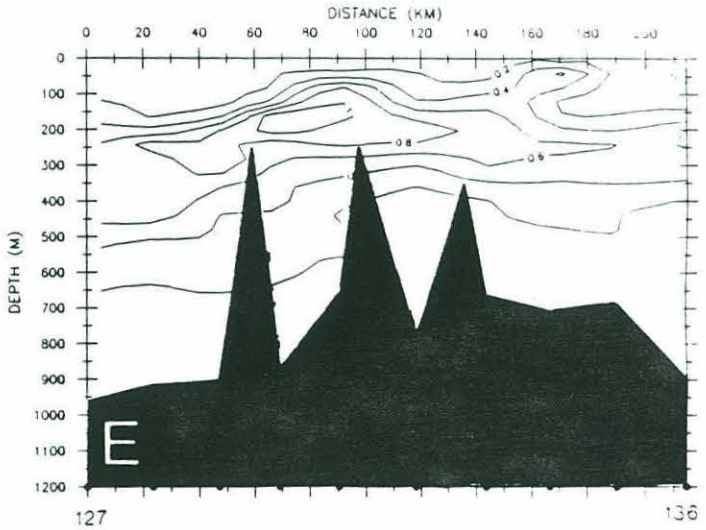

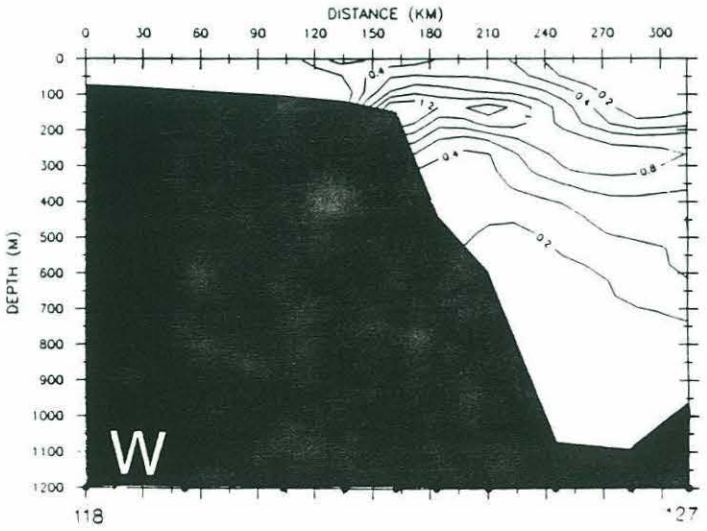

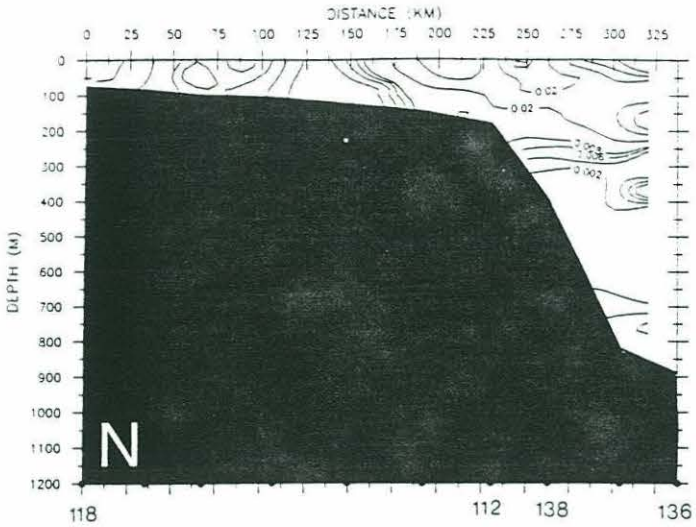

Figure 5.3:

The vertical distribution of $\frac{g}{\rho f}(\frac{\partial \sigma_\theta}{\partial x})^2$ on the triangle section $(10^{-7} kg/sm^4)$.

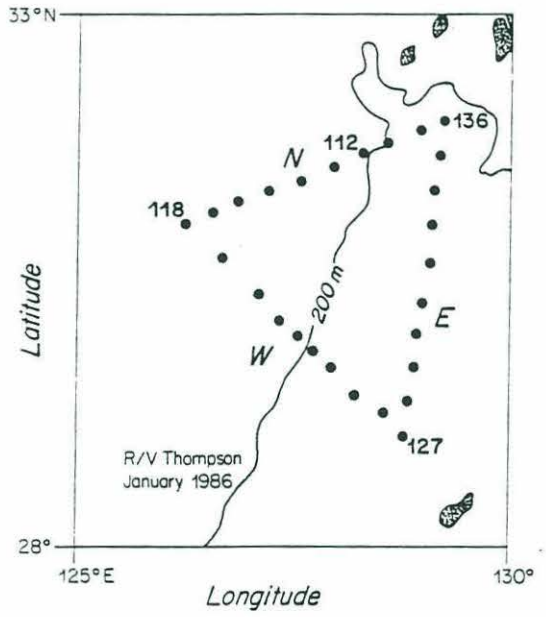

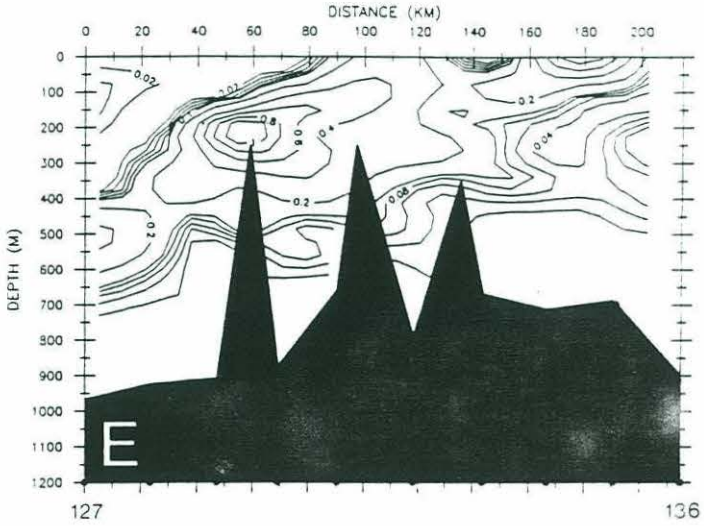

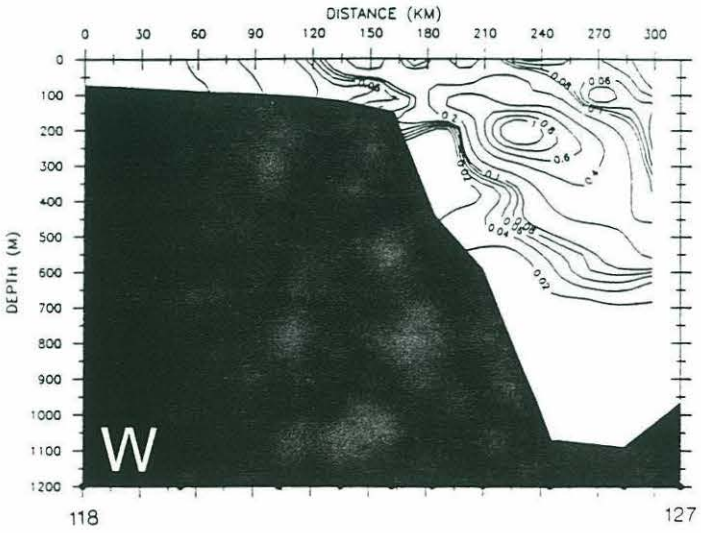

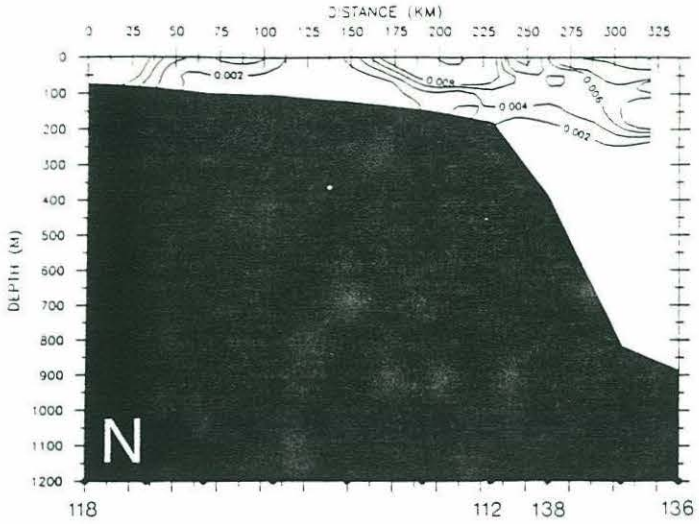

Figure 5.4:

The ratio of the $-v_z\sigma_{\theta n}$ to $f\sigma_{\theta n}$ on the triangle section.

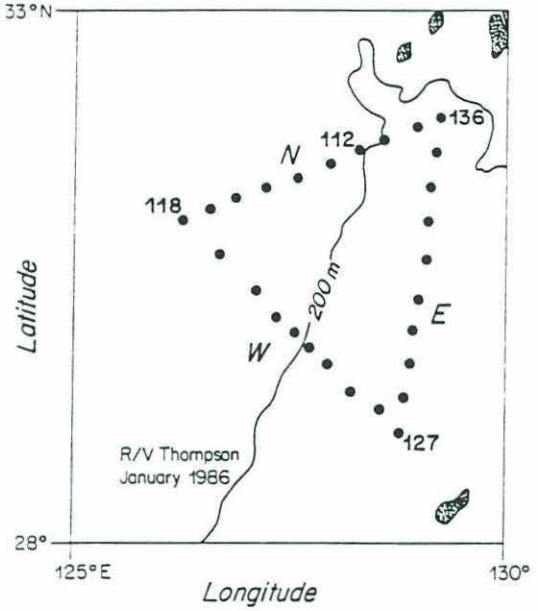

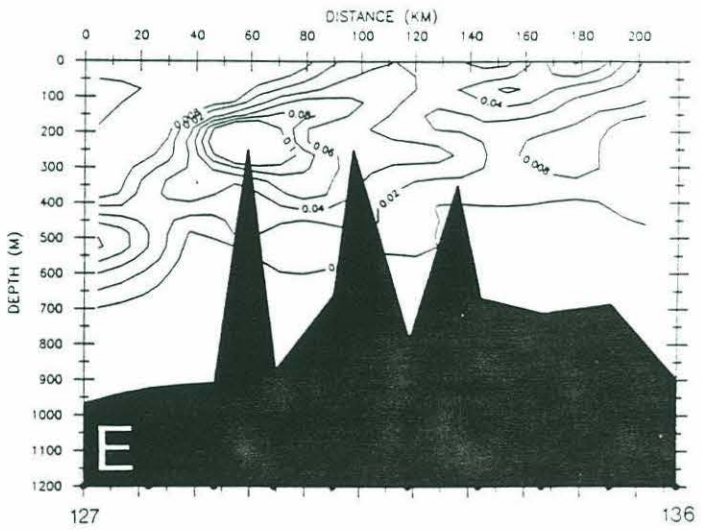

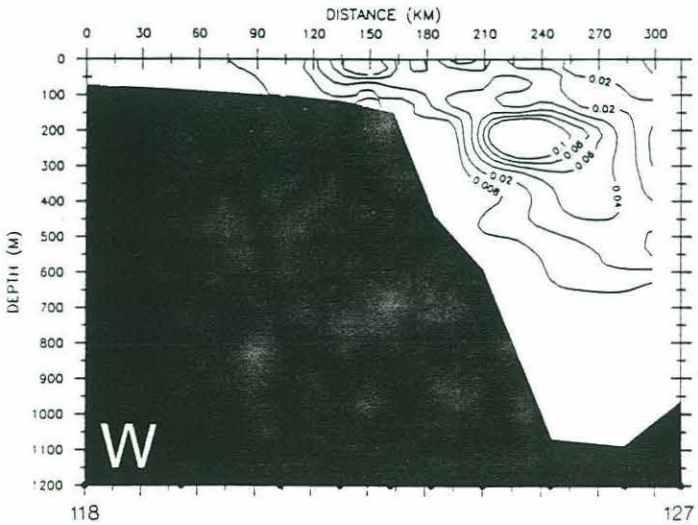

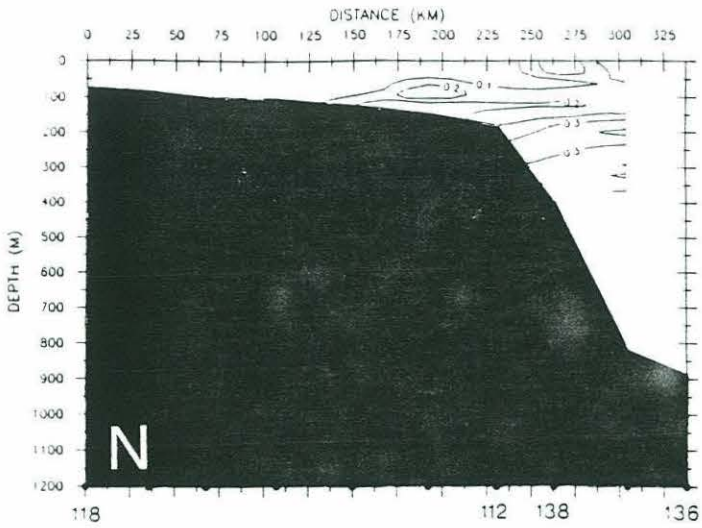

Figure 5.5:

The vertical structure of total potential vorticity $(10^{-9}s^{-1}m^{-1})$.

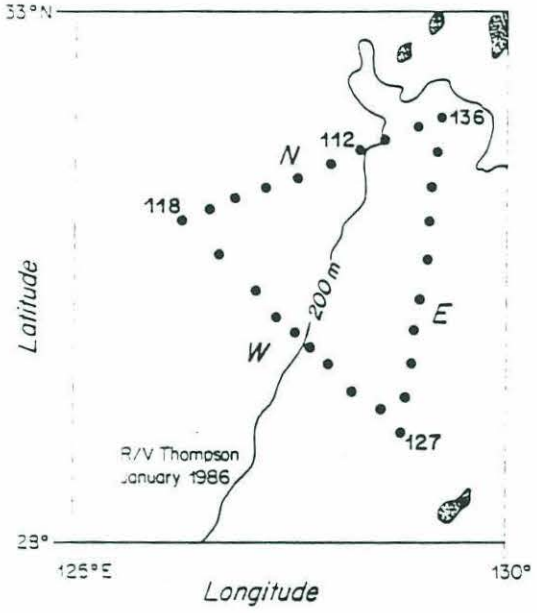

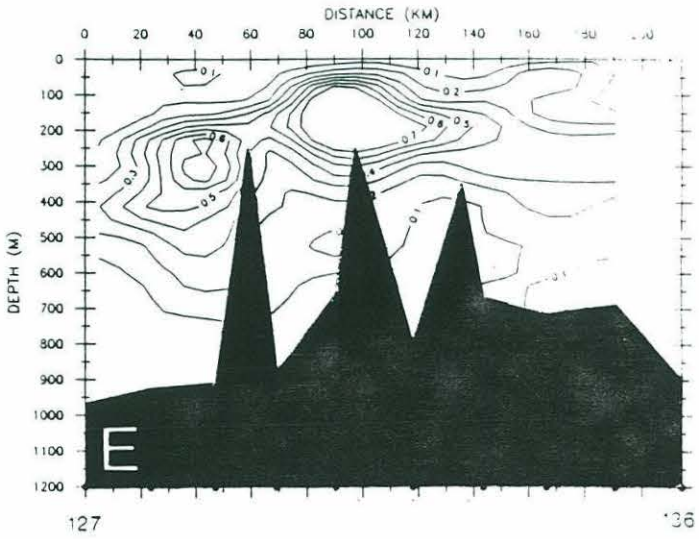

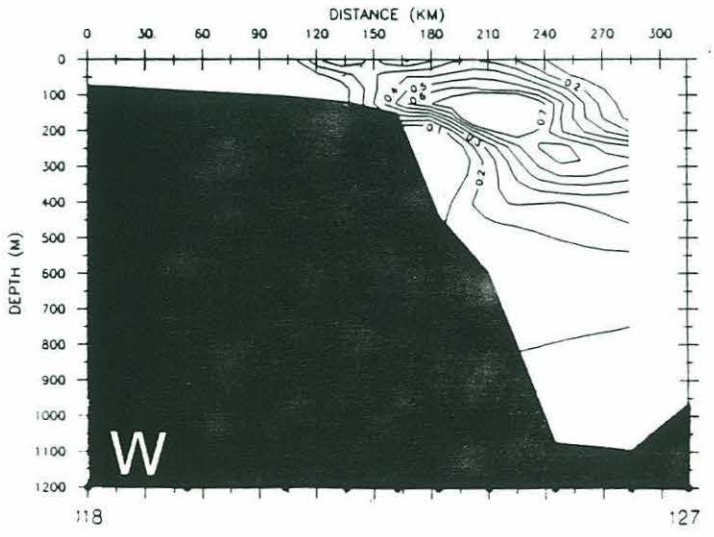

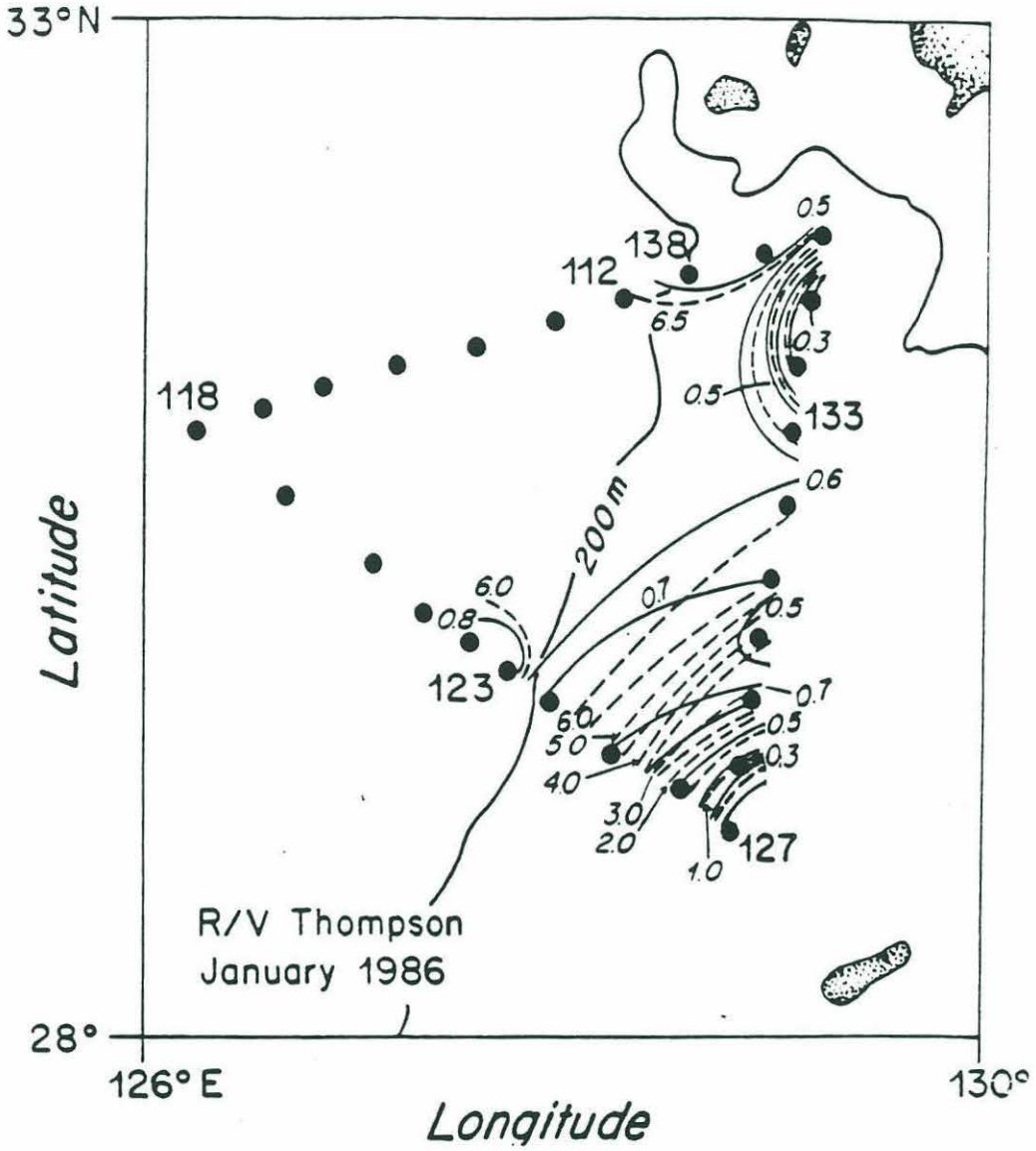

Figure 5.6: The potential vorticity contours (solid line: $10^{-9}s^{-1}m^{-1}$) and streamlines (dash line: $10^{4}m^{2}s^{-1}$) on the potential density surface $\sigma_\theta = 25.7$

Appendix A: Correction of salinity data

An HP85 desktop computer and a Neil Brown CTD were used as the primary data acquisition system on the R/V Thompson. The instrument provided continuous sampling of temperature, conductivity, pressure, dissolved oxygen, and light transmission. Salinity and density were subsequently derived from the measured variables. The HP85 subsampled the raw digital data every 0.4 seconds giving a typical pressure interval of 40 cm between data records. Spurious electronic noise in the conductivity data at some stations (especially the deep stations) was observed in the form of data spikes. A special median filter was used to correct the data spiking. The raw data were then averaged over 2 meter depth intervals. A limited number of water samples were also collected during the hydrographic survey to check the salinity calculation.

During the period of the R/V Thompson CTD survey several independent hydrographic surveys were also conducted in the East China Sea by Jeju National University, the Fisheries Research and Development Agency of Korea, and Nagasaki Marine Observatory of Japan. Comparison of all available data with Korean and Japanese data indicated that salinities from the R/V Thompson CTD survey were about 0.3 - 0.4 $^{\circ}/_{\circ\circ}$ larger . Korean scientists who were collaborating with us in the analysis of this data set suspected that these errors were caused by a systematic offset of the CTD conductivity sensor and suggested a correction for R/V Thompson CTD conductivity data using the synoptic Japanese and Korean hydrographic data obtained over the shelf as the reference.

However, when we started to use these "corrected" CTD data to describe the structure of the Kuroshio west of Kyushu, we still found some scatter in the salinity data due to conductivity noise, and also found that the T/S curves in the Kuroshio deviated from station to station. It is especially difficult to explain why the T/S curves in the deep Kuroshio could shift horizontally because no extra fresh or saline water

sources were found in that region. All concurrent Japanese bottle data west of Kyushu obtained by the R/V Chafu Maru and R/V Royat Maru were plotted and did not show any horizontally shifting of the T/S curves. Therefore, we believe that the deviation of the deep Thompson T/S curves were not real but due to the noise in conductivity data. A least square approximation was then employed to find the best fit to the Japanese bottle data. This approach is described next.

A symmetrical low-pass filter PL30 was first used to smooth the two meter salinity data. The formula of the PL30 filter can be expressed by

$$PL30 = \frac{2\sin(\frac{2\pi z}{n_*}) - (\sin(\frac{\pi z}{n_*}) + \sin(\frac{3\pi z}{n_*}))}{(\frac{1}{n_*})^2 \pi^3 z^3}.$$

The weights of the PL30 filter are shown in Figure A.1, where n_* is taken as 20 m, and the first zero crossing is at 10 m. The corresponding power spectrum for this filter is shown in Figure A.2 in which the signals at frequencies above 0.08 cpm are removed.

As an example, the comparison between the raw salinity data and filtered data for stations 126 and 131 are shown in Figure A.3. Most of the salinity noise with a wave length of less than 10 db was filtered except in the deep region where some noise with a longer wave length still remained. A more smoothed curve can be easily obtained by increasing the weight number of the filter. Additional smoothing, however, reduces the maximum salinity peak near the surface which is believed to be characteristic of Tropical Water. On the other hand, since the results of calculations of geostrophic velocity and the associated transports are not perticularly sensitive to this deep noise, we tend to retain those salinity structures with a longer wave length in the deep region for our present work. In addition, a five-point average was used to filter the raw data which were missed by the symmetrical filter near the surface and bottom.

Next, the horizontal deviation of the salinity data at each station was corrected using a least square approach as follows. Let S_n be the filtered salinity data on a given pressure surface, S_{b_n} be the corresponding bottle sample salinity, and $\triangle S$ be the correction between S_n and S_{b_n}, then,

$$\sigma^2 = \sum_{n=1}^{N} (S_{b_n} - (S_n + \triangle S))^2.$$

The best fit to the bottle data can be found when

$$\frac{\partial \sigma^2}{\partial \triangle S} = 0.$$

Therefore,

$$\triangle S = \sum_{n=1}^{N} \frac{1}{N} (S_{b_n} - S_n)$$

All corrections for salinity at the stations in the Kuroshio are shown in Table A.1. Since water types are mixed in the shelf region, and there exists some fresh water sources there, it is difficult to test whether there were salinity deviations over the shelf. Therefore, no additional correction was employed for the shelf.

TABLE A.1 : SALINITY CORRECTION

station	$\triangle S°/_{oo}$	station	$\triangle S°/_{oo}$	station	$\triangle S°/_{oo}$
122	0.172	128	0.008	134	-0.045
123	0.172	129	0.026	135	0.015
124	1.130	130	0.034	136	0.008
125	0.055	131	0.043	137	0.078
126	0.006	132	-0.075	138	0.01
127	0.016	133	-0.041		

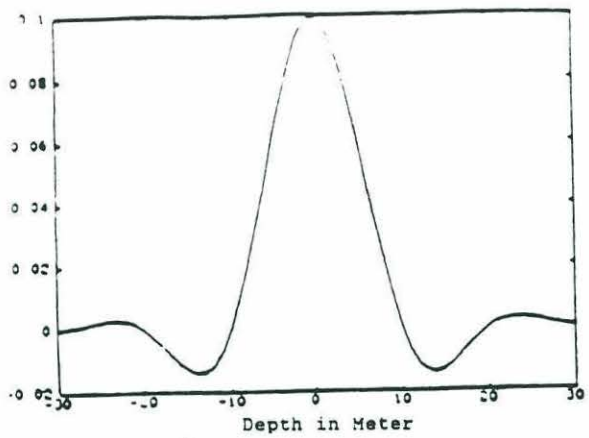

Figure A.1: PL30 filter weight.

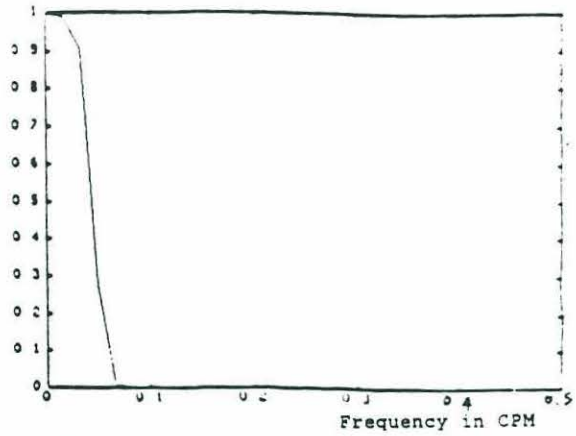

Figure A.2: Power spectrum.

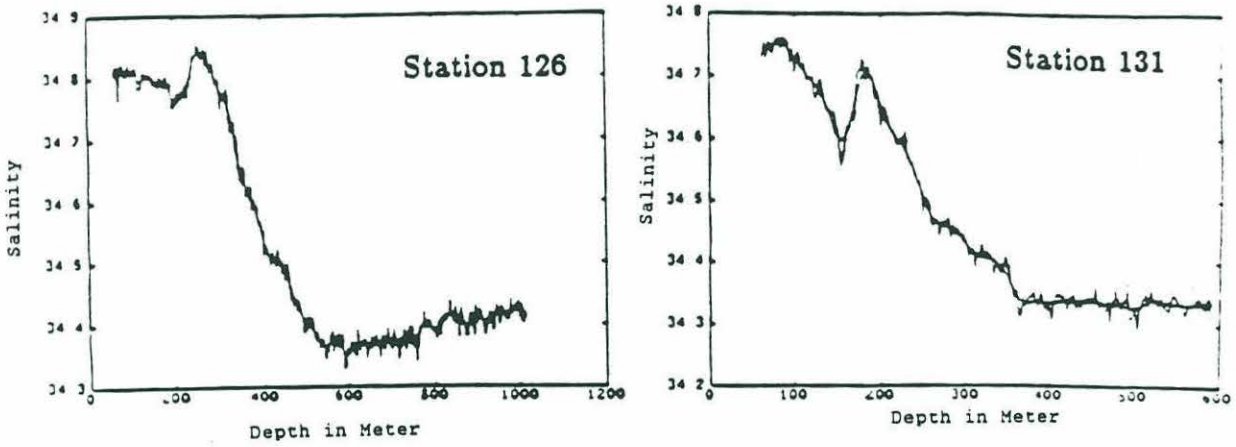

Figure A.3: The comparison between the raw salinity data and filtered data.
Noise curve is the raw data.
Smooth curve is the filtered data.

Appendix B Probability density function of θ'

As mentioned before, θ' can be approximated by

$$\theta' \simeq \frac{Y_{i+1} + Y_i}{L}$$

Let $X_i = Y_i/L$, thus the probability density function of X_i is

$$P_{X_i}(X_i) = P_Y(Y_i)\frac{dY_i}{dx} = \frac{1}{\sigma\sqrt{2\pi}} e^{-\frac{1}{2\sigma^2}(L\,X_i - \bar{Y})^2}.$$

To find the probability density of θ_i, let's first look for its characteristic function $\Phi_{X_i}(q)$ for a random variable X_i, which is equal to

$$\Phi_{X_i}(q) = \int_{-\infty}^{\infty} e^{iX_iq} P_{X_i}(X_i) dX_i$$

$$= \frac{L}{\sigma\sqrt{2\pi}} \int_{-\infty}^{\infty} e^{iX_iq} e^{-\frac{1}{2\sigma^2}(LX_i - \bar{Y})^2} dX_i.$$

Let $LX_i - \bar{Y} = U$, $X_i = U/L + \bar{Y}/L$, $dU = LdX_i$ then,

$$\Phi_{X_i}(q) = \frac{1}{\sigma\sqrt{2\pi}} \int_{-\infty}^{\infty} e^{i(\frac{U}{L} + \frac{\bar{Y}}{L})q} e^{-\frac{1}{2\sigma^2}U^2} dU$$

$$= \frac{1}{\sigma\sqrt{2\pi}} e^{i\frac{\bar{Y}}{L}q} \int_{-\infty}^{\infty} e^{i\frac{U}{L}q - \frac{1}{2\sigma^2}U^2} dU,$$

so that

$$\Phi_{X_i}(q) = e^{i\frac{\bar{Y}}{L}q - \frac{q^2}{2}(\frac{\sigma}{L})^2}.$$

Since θ' is the linear sum of two independent variables X_i and X_{i+1}, $\Phi_{\theta'}(q)$ for θ' is equal to the product of Φ_{X_i} and $\Phi_{X_{i+1}}$, that is,

$$\Phi_{\theta'}(q) = \Phi_{X_i}\Phi_{X_{i+1}}$$

$$= e^{i\frac{2\bar{Y}}{L}q - q^2(\frac{\sigma}{L})^2}$$

Therefore, the probability density function of θ' is

$$P_{\theta'}(\theta') = \frac{1}{2\pi}\int_{-\infty}^{\infty} e^{i\theta' q}\Phi_{\theta'}(q)dq$$

$$= \frac{1}{2\pi}\int_{-\infty}^{\infty} e^{-i(\theta' - \frac{2\Upsilon}{L})q - (\frac{\sigma}{L})^2 q^2} dq \ .$$

Since $\int_{-\infty}^{\infty} e^{ibx-a^2x^2}dx = \frac{\sqrt{\pi}}{a}e^{\frac{-b^2}{4a^2}}$, therefore, the probability density function of θ' is

$$P_{\theta'}(\theta') = \frac{L}{2\sqrt{\pi}\sigma}e^{\frac{-L^2(\theta' - \frac{2\Upsilon}{L})^2}{4\sigma^2}}.$$

REFERENCES

Barth, J. A. and K. H. Brink, 1987. Shipboard Acoustic Doppler Profiler velocity observations near point conception: Spring 1983. *Journal of Geophysical Research*, **92**(C4), 3925–3943.

Beardsley, R. C., R. Limeburner, D. Hu, K. Le, G. A. Cannon and D. J. Pashiuski, 1983. Structure of the Changjiang plume in the East China Sea during June 1980. *In: Proceeding of the International Symposium on Sedimentation on the Continental Shelf with Special Reference to the East China Sea, April 12-16, Hangzhou, P.R. China*, Vol 1, Ocean press, Beijing, 265–284.

Beardsley, R.C., R. Limeburner, H. Yu and G.A. Cannon, 1985. Discharge of the Changjiang (Yangtze River) into the East China Sea. *Continental Shelf Research*, Vol.4, Nos.1/2, 57–76.

Blaha, J. and R. Reed, 1982. Fluctuations of sea level in the Western North Pacific and inferred flow of the Kuroshio. *Journal of Physical Oceanography*, **12**, 669–678.

Brooks, I. H., and P. P. Niiler, 1977. Energetics of the Florida Current. *Journal of Marine Research*, **35**, 163–191.

Bryan, K., 1962. Measurements of meridional heat transport by ocean current. *Journal of Geophysical Research*, **67**, 3403–3413.

Bryan, K., 1963. A numerical investigation of a nonlinear model of a wind–driven ocean. *J. Atmos. Sci* **20**, 594–606.

Bryden H.L., D. H. Roemmich and J. A. Church, 1987. Ocean heat transport across 24°N in the Pacific. Submitted for publication in *Deep-Sea Research.*

Butenko, J., J. D. Milliman and Y. C. Ye, 1985. Geomorphology, shallow structure, and geolopical hazards in the East China Sea. *Continental Shelf Research*, **4**, 121–141.

Chao S. Y., and J. P. McCreary, 1982. A numerical study of the Kuroshio South of Japan. *Journal of Physical Oceanography*, **12**, 680–693.

Chao S. Y., 1984. Bimodality of the Kuroshio. *Journal of Physical Oceanography*, **14**, 92-103.

Charney J. G., and G. R. Flierl, 1981. Ocean analogues of large scale atmospheric motions. *Evolution of Physical Oceanography*, Warren B. and C. Wunsch, eds. The MIT Press, 504–548.

Choi, B. H., 1980. A tidal model of the Yellow Sea and the Eastern China Sea. *Kordi report 80-02*, pp72.

Defant A., 1941 Die absolute topographic des physikalischen meerasniveans und der druckflachen sowie die wasserbewgungen im Raum des atlantischen Ozeans, *Wiss. Ergebn. Dtsch. Atlant Exped. Meteor.*, **6**, 191–260.

Ertel, H., 1942. Ein neuer hydrodynamischer wirbesatz. *Meteorolol. Z.*, **59**, 277–281.

Fofonoff, N. P., 1954. Steady flows in a frictionless homogeneous ocean. *J. Mar. Res.*, **13**, 254-262.

Gill, A. E., 1977. Potential vorticity as a tracer. Appendix to A.F Pearce, some features of upper 500m of the Agulhas current. **J. Mar Res., 35**, 752-753.

Hall, M.M. and H.L. Bryden, 1982. Direct estimates and mechanisms of Ocean heat transport. *Deep Sea Research*, **29**, 339–359.

Hall, M.M., 1985. Horizontal and vertical structure of velocity, potential vorticity and energy in the Gulf Stream. Ph.D Thesis, MIT/Woods Hole Joint Program, pp165.

Hastenrath S., 1980. Heat budget of tropical ocean and atmosphere. *J.Phys. Oceanogr.*, **10**, 159–170.

Hendershott, M. C., 1987. Single layer models of the general circulation. *General Circulation of the Ocean*, Abarbane, H. D.I. and W. R. Young, eds., 203–267.

Ichikawa, H., 1987. Mass and heat transports of the Kuroshio. *Japanese plans for WOCE, Japan–U.S. WOCE Seminar, Seatle, June 8-12, 1987*, 13pp.

Johns, E., 1984. Geostrophic and potential vorticity in the Gulf Stream northeast of Cap Hatteras. Ph.D. thesis, University of Rhode Island.

Joyce, T. M., D. S. Bitterman J_R., and K.E. Prada, 1982. Shipboard acoustic profiling of upper ocean currents, *Deep Sea Research*, **29**, 903-913.

Joyce, T. M., C. Wunsch and S. D. Pierce, 1986. Synoptic Gulf Stream velocity profiles through simultaneous inverson of hydrographic and acoustic Doppler data. *Journal of Geophysical Research*, **91**, 7573– 7585.

Joyce, T,M., 1988. On in-situ" Calibration of shipboard ADCP's". Submitted to *Journal of Atmospheric and Oceanic Technology*, 10pp.

Knauss, J.A., 1969. A note on the transport of the Gulf Stream. *Deep Sea Research*, **16**, 117–123.

Kosro, P.M., 1985. Shipboard acoustic current profiling during the coastal ocean dynamics experiment. Ph.D. thesis, Scripps Institution of Oceanography, University of California, 119pp.

Leaman, K, and R. L. Molinari and P. S. Vertes, 1987. Structure and variability of the Florida Current at 27°N: April 1982–July 1984. *Journal of Physical Oceanography*, **17**, 565–583.

Limeburner, R., R. C. Beardsley and J. Zhao, 1983. Water masses and circulation in the East China Sea. In:*Proceeding of the International Symposium on Sedimentation on the Continental Shelf with Special Reference to the East China Sea, April 12-16; Hongzhou, China*, Vol 1. China Ocean Press, 285–294.

Luyten , J. K., J. Pedlosky and H. Stommel, 1983. The ventilated thermocline. *Journal of Physical Oceanography*, **13**, 292–309.

Masuzawa, J., 1964. Flux and water characteristics of the Pacific north equatorial current. *SO*, (dedicated to Prof.Hidaka in commemoration of his sixtieth birthday),123-128 (in English).

Miyazaki, M. and S. Abe, 1960. On the water masses in the Tsushima current area. *J. Oceanogr. Soc. Japan*, **16**(2), 59–68 (in Japanese with English abstract).

McCartney, M.S., 1982. The subtropical recirculation of Mode Water. *Journal of Marine Research*,**40** supplement, 427–464.

Montogomery R., 1974. Comments on " Seasonal variability of the Florida current.", by Niiler and Richardson. *J.Mar. Res.*,**32**, 533-534.

Muck, W. H., 1950. On the wind-driven Ocean Circulation. *Journal of Meterorology*, **7**, 79-93.

Nagata, Y., 1981. Oceanic conditions in the East China Sea. In: *Proceeding of the Japan–China Oceanic Study Symposium on Physical Oceanography and Marine Engineering in the East China Sea, October 28–29, 1981, Shimizu*, 25–41.

Nakao T., 1977. Oceanic variability in relations to fisheries in the East China Sea and the Yellow Sea. *J. Fac. Mar. Sci. Technol.*, Tokai Univ. Spec. No.11.

Niashisawa et al, 1982. Estimation of the Kuroshio mass transport flowing out of the East China Sea to the North Pacific. *La. Mer.*, **20**, 55–59.

Niiler, P. P., W. J. Schmitz and D. K. Lee, 1985. Geostrophic Volume Transport in High Eddy-Energy Areas of the Kuroshio Extension and Gulf Stream. *Journal of Physical Oceanography*, **15**(7), 825–843.

Nitani, T., 1972. Beginning of the Kuroshio. *Kuroshio, Physical Aspect of the Japan Current*, H. Stommel and K. Yoshida, eds, University of Washington Press, 129-156.

Niiler, P. and W. Richardson, 1973. Seasonal variability of the Florida current. *Journal of Marine Research*, **31**, 144–167.

Oort A., and T. Vonder Haar, 1976. On the observed annual cycle in the ocean-atmosphere heat balance over the northern hemisphere, *J. Phys. Oceanogr.*, **6**, 781-800.

Park, Y. H., 1985. Some important summer oceanographic phenomena in the East China Sea. *J. of the Oceanographic Society of Korea*, **20**(2), 12–21.

Pedlosky, J., 1979. Geophysical Fluid Dynamics. Springer-Verlag, New York, 624pp.

Pickard, G. L., 1979. *Descriptive Physical Oceanography*, 3rd edition. Pregamon Press. pp.

Pinkel, R., 1979. Observation of Strong non-liner internal motion in the open sea using a range-gated Doppler sonar. *J. Phys. Oceanogr.*, **9**, 675-685.

Pond, S., and G. L. Pickard, 1983. *Introductory Dynamical Oceanography* , 2nd edition. Pegamon Press. 329pp.

Pu, Y. X., and X. Y. Xu, 1987. The Kuroshio (on the PN section) in the East China Sea during 1972–1983. *Acta Oceanologica Sinica*, **6**(1)., 37-45.

Qin, Y. S. and F. Li, 1983. Study of influence of sediment loads discharged from the Hanghai river on sedimentation in the Bohai and the Hanghai Sea. In: *Sedimentation on the Continental Shelf with Special REference to the East China Sea, April, 1983, Hongzhou, China*, 83–92.

Regier, L., 1982. Mesoscale current fields observed with a shipboard profiling acoustic current meter. *J. Phys. Oceanogr.*, **12**, 880–886.

Rhines, P.B. and W. K. Young, 1982a: A theory of wind driven ocean circulation, I, Mid ocean gyres. *Journal of Marine Research*, **40**(suppl), 559–596.

Ried, J. L., 1965. Intermediate Water of the Pacific Ocean. *Johns Hopkins Oceanogr. Studies.*, **2**, 85pp.

Roemmich, H., 1984. The application of inverse methods to problems in ocean circulation. Ph.D. Thesis, MIT/Woods Hole Joint Program, 193pp.

Robinson, A. and B. A. Taft, 1972. A numerical experiment for the path of the Kuroshio. *J.Mar.Res.*,**30**, 65–101.

Saiki, M., 1982. Relation between the geostrophic flux of the Kuroshio in the Eastern China Sea and its large meanders in south of Japan. *The Oceanograhical Magazine*, **32**(1–2), 11–18.

Schubel, J. R., H. T. Shen and M. J. Park, 1984. A comparison of some characteristic sedimemtation processes of estuaries entering the Yellow Sea. *Marine Geology and Physical Processes of the Yellow Sea, proceeding of Korea–U.S. seminar and workship, June 19–23, 1984, Seoul, Korea*, 286–308.

Sverdrup, H.V., M.W.Johuson and R.H. Flennig, 1942. *The Oceans.* Drentice-Hall, Inc., N.J., 1087pp.

Stommel, H., 1948. The westward intensification of wind-driven ocean currents. *Trans. Amer. Geophys. Union.* **29**, 202–206.

Stommel, H., 1958. *The Gulf Stream, A Physical and Dynamical Description*, London, Cambridge Univ. Press, 202pp

Stommel, H., 1972. *The Kuroshio.* University of Washington press, 517pp.

Stommel, H. and F. Schott, 1977. The beta spiral and the determination of the absolute velocity field from hydrographic station data. *Deep Sea Res.*, **24**, 325–329.

Taft, B.A., 1972. Characteristic of the flow of the Kuroshio south of Japan. *The Kuroshio*, H. Stommel and K. Yoshida, eds., University of Washington press, 517pp.

Taira, K, 1986. Possible plan to measure heat and fresh water fluxes of the Kuroshio. *U.S.-Japan Symposium of WOCE, Tokyo, March 20–21, 1986.*

Takematsu, M., K. Kawatate, W. Koterayama, T. Suhara and H. Mitsuyasu, 1986. Moored instruments observations in the Kuroshio south of Kyushu. *Journal of The Oceanographical Society of Japan*, **42**, 201–211.

Teramoto, T. 1972. History of The Japanese observation program of the Kuroshio and adjacent regions. *The Kuroshio*, H. Stommel and K. Yoshida Eds, University of Washington press.

Veronis, G., 1966a. Wind-driven ocean circulation–part I, Linear theory and perturbation analysis. *Deep-Sea Research*, **13**, 17–19.

Veronis, G., 1966b. Wind-driven ocean circulation–part II, Numerical solutions of the non-linear problem. *Deep-Sea Research*, **13**, 30–55.

Wade, Y., 1894. A study on the Japan Current. *Tokyo Butsuri Gakko Zasshi*, **3**(33), 241–243 (in Japanese).

Watts, D. R.,1983. Gulf Stream variability. *Eddies in Marine Science*, A.R. Robinson, ed., springer-verlag, 114–144.

Wernstedt, F.L., 1972, *World Climate Data*, climatic data press, 522pp.

White, W. B., and J. P. McCreary, 1976. The Kuroshio meander and its relationship to large scale ocean circulation. *Deep Sea Res.*, **23**, 33–47.

Wunsch, C., 1969. Progressive internal waves on slopes. *Journal of Fluid Mechanics*, **35**, 131–144.

Wunsch, C., 1977. Determining the general circulation of the oceans; A preliminary discussion,*Science*, **196**, 871-875.

Wunsch, C., 1978. The north Atlantic circulation west of 50°W determined by inverse methods. *Rev of Geophys. and Space Phy.*, **16**, 583-620.

Wüst, G., 1935. Schichtung und Zirkulation des Atlantischen Ozeans: Die structosphare des Atlantischer Ozeans. *Wiss Ergeb Deut Atl. Exped. Meteor.*, **6**, 109–228.

Wyrtki, K., 1961. Physical oceanography of the southeast Asia waters, characteristics of the flow of the scientific results of Kuroshio south of Japan, Marine investigations of the South China Sea and Gulf of Thailand, 1959–1961. *Naga. Report*, **2**, 195pp.

Wyrtki, K., 1966. Seasonal variation of heat exchange and surface temperature in the North Pacific Ocean. Hawaii Institute of Geophysics, University of Hawaii, 80pp.

Yang, Z. S., J. D. Milliman and M. G. Fitzgerald, 1983. Transfer of water and sediment from the Yangtze River to the East China Sea, June, 1980. *Canadian Journal of Fisheries and Aquatic Sciences*, **40**, 72–82.